Resonance Line Broadening of Alkali Metals in Pyrotechnic Flames.

BY

David Rogers Dillehay

LONGHORN ARMY AMMUNITION PLANT

MARSHALL, TEXAS 75670

Submitted to the Academic Council
of CLAYTON UNIVERSITY in
Partial Fulfillment of the Requirements for
the Degree of Doctor of Philosophy
in Chemistry

April 15, 1983

ABSTRACT

A mathematical model of a pyrotechnic flame has been developed and validated. The model utilizes a computer program to calculate the relative radiant power of flares containing any of the alkali metals. The computation takes into consideration known system variables such as formulation, candle size, displacement along the plume axis, and atmospheric pressure. These effects were evaluated over a wide range of conditions and the computed spectra follow the established experimental spectra trends. The computer solution is a general solution requiring no ad hoc modifications to the model for any of the metals or conditions tested.

The basis for the model of the flame permits calculation of the effects of mixing of the flare plume with the ambient atmosphere and takes heat loss along the plume axis into consideration. The relative radiant power is determined by solving the radiative transfer equation using parameters calculated from the thermodynamic properties of the flare plume. The individual line dispersion profiles of the resonance lines were replaced with a two-line Voigt function that includes a broadening parameter that considers natural, Lorentz, resonance, quenching and Doppler broadening mechanisms. The solution results in a spectral profile that follows observed experimental spectral variations over a wide range of metals and conditions.

Spectra were computed for lithium, sodium, potassium, rubidium and cesium under a variety of limiting conditions. A comparison of measured spectra with the computed spectra showed good agreement both qualitatively and quantitatively. Cases shown include theoretical and experimental spectra comparing varying ambient pressure, formulations, displacement along the plume axis and candle diameters for sodium and selected cases for the other alkali metals to compare with experimental spectra or show expected trends.

This model should be useful in optimizing flare radiant output using any of the alkali metals as emitters and also as a tool for further study of the radiative transfer system in controlled laboratory conditions.

ACKNOWLEDGEMENTS

The author wishes to thank Dr. Bernard E. Douda, Naval Weapon Support Center - Crane, and Mr. Robert M. Blunt for their valuable guidance and encouragement in this research effort. Their discussions and comments plus the many experimental spectra they furnished were invaluable in completing the work.

The understanding and patience of my wife, Marilyn, and the help of my son, David, in entering some of the computer data is especially appreciated.

Finally, the support and encouragement of Mr. T. M. Davis and Mr. H. C. Havron of Morton-Thiokol Corporation is gratefully acknowledged.

D.R.D.

TABLE OF CONTENTS

INDEX OF TABLES

INDEX OF FIGURES

TABLE OF SYMBOLS

A_{21} - Einstein coefficient for stimulated emission

B_{12} - Einstein absorption coefficient

B_{21} - Einstein induced emission coefficient

$B_\nu(T')$ - Planck function

$C_{21}(T)$ - Rate of collisional deactivation

c - Velocity of light

e - Elementary charge

f - Absorption f-value (oscillator strength)

h - Planck's constant

I - Spectral intensity

k - Boltzman's constant

m - Molecular weight of perturbing specie

m_e - Electron rest mass

M - Molecular weight of emitting specie

N_A - Avagadro's Number

N_1 - Number density of metal atoms (cm^{-3})

N_2 - Number density of perturbing atoms (cm^{-3})

R - Universal Gas Constant

$S_\nu(\tau)$ - Line source function

T - Temperature, $^\circ K$

a - Voigt parameter

β - Cosine of the angle of observation

$\Delta\lambda_D$ - Doppler line broadening half-width

$\Delta\lambda_L$ - Lorentz line broadening half-width

$\Delta\lambda_N$ - Natural line broadening half-width

$\Delta\lambda_Q$ - Quenching line broadening half-width

$\Delta\lambda_R$ - Resonance line broadening half-width

$\Delta\nu_o$ - Doppler half-width

λ_o - Line center wavelength

σ_L - Optical cross section

τ - Optical depth

$\Phi_{\nu a}$ - Normalized spectral profile of the absorption coefficient

μ - Reduced mass

Γ - Optical thickness

INTRODUCTION

Early research in magnesium-sodium nitrate flame spectroscopy has shown that the major component of the visible light emission from these flames is a continuous spectrum called the sodium resonance-line continuum. The resonance-line continuum is much broader than predicted by Doppler or Lorentz effects. Further, many observations of flame spectra seem to differ in the effects noted due to varying test parameters. These incongruities led researchers such as Douda, Blunt and Bair (33,48,49) to consider other mechanisms, such as radiative transfer, to elucidate the origin of the resonance-line continuum. Their early work indicated that radiative transfer was able to yield reasonable agreement in specific cases but required certain ad hoc modification to fit various flame cases. Douda (1) hypothesized that radiative transfer was the major mechanism responsible for this resonance-line continuum. He developed equations for predicting broadening of the sodium D-lines using some simplifying assumptions for temperature and concentration profiles and neglecting the effect of air mixing with the flame. By comparing the spectra of flames at reduced pressure, he demonstrated that the theory produced reasonable agreement with the experiments. The agreement was improved at the lower pressures because the effect of the atmosphere mixing with the flame was reduced. Even with this, however, the coefficient used in the spectral line profile had to be reduced by almost an order of magnitude to get agreement between calculations and experiments. In 1975 and 1976, the model was

expanded by Dillehay (4,5) to take into account the effects of air mixing with the flame. This work improved the calculation of the temperature profile to obtain agreement with experimental observations. The sodium atom concentration was not assumed to be a constant average value in the flame but was approximated as a parabola through the flame cross-section. Using these data, the line broadening profiles were calculated for a number of conditions without making any a priori assumptions. The predicted spectra showed the same broadening features as the experimental data even at atmospheric pressure. These calculations were all done by hand with considerable use of approximations, interpolations and look-up tables. The difficult and time consuming hand calculations in this early model limited the application of this technique for further research.

The purpose of this dissertation will be to develop an improved mathematical flame model that can be used to verify the radiative transfer theory for sodium and add other alkali metal species to the model. By generating a general solution to the equations, the model will allow computation of the broadened line profiles of lithium, sodium, potassium, rubidium and cesium. The solution will be a computer simulation of a pyrotechnic flame and a computer program that will take the predicted combustion species from the simulation, calculate the radiative transfer parameters and generate the spectral profile. The flame model will take into account the effects of varying formulation, mixing of the atmosphere with the flame, heat loss along the flame axis and the effects of pressure on the flame. The equilibrium

compositions and temperatures are calculated using the NASA SP-273 Combustion Equilibrium Program (3). This model will enhance the state-of-the-art of illuminant formulating and improve the understanding of the radiative energy transfers in pyrotechnic flames.

This research will show that the radiative transfer model can be applied to pyrotechnic flames without a priori assumptions or ad hoc modification of the model. The model will then be used to demonstrate that many of the variables noted in previous experiments are predicted by the theory and quantifying rules can be established for the meaningful acquisition and interpretation of pyrotechnic flame spectra. The spectral model will take into account the effects of varying formulation, candle diameter, pressure and position within the flare plume. Data for lithium, sodium, potassium, rubidium and cesium will be included to allow a broader application of the model and increase the confidence in the validation. Experimental data are already available for a variety flare formulations taken under many conditions. These data will be used to compare with the calculated spectral profiles.

THEORETICAL BACKGROUND

The Radiative Transfer Equation

A detailed derivation and discussion of the radiative transfer equation can be obtained from the literature (1,43,50). A brief summary will be presented here to aid in the understanding of the model.

To characterize the mechanisms of luminous energy generation in a flare plume, it is necessary to solve the general radiative transfer equation,

$$I_{\nu 1} = I_{\nu 2}\,EXP\left[-(\tau_2-\tau_1)\,\Phi_{\nu a}/\beta\right] + \int_{\tau=\tau_1}^{\tau=\tau_2}\left[S_\nu(\tau)\Phi_{\nu a}/\beta\right]EXP\left[-(\tau-\tau_1)\,\Phi_{\nu a}/\beta\right]d\tau \quad (1)$$

where τ_1 and τ_2 are the optical depth integration limits from front to rear of the plume respectively, $I_{\nu 1}$ and $I_{\nu 2}$ are the spectral intensities at optical depths τ_1 and τ_2, $S_\nu(\tau)$ is the line source function, β is the cosine of the angle of observation, and $\Phi_{\nu a}$ is the normalized spectral profile of the absorption coefficient. To solve this equation, the plume is constrained by the following boundaries:

1) The plume is a homogeneous gaseous atmosphere with plane-parallel stratification.

2) The gas consists of alkali metal atoms which can be excited to the $^2P_{1/2}$ or $^2P_{3/2}$ level and molecular species which can interact to perturb the metal atom radiation..

3) There is local thermodynamic equilibrium (LTE) governed

by the local temperature.

4) Energy exchange by radiation leads to radiative equilibrium.

5) The refractive index of the medium is unity.

6) The radiation is unpolarized when emitted and remains unpolarized on its interactions with flare species.

7) The temperature gradient can be constructed from the thermodynamic equilibrium temperature calculated for a limited surface penetration of the ambient atmosphere.

8) The absorption profile $\Phi_{\nu a}$ and the number density of sodium atoms are dependent on the calculated thermodynamic equilibrium compositions defined by the limited surface interactions with the ambient atmosphere.

Using these boundary conditions, the radiative transfer equation can be simplified by assuming that the observed flux is emerging normal to the surface ($\beta = 1$) and there is no flux incident on the rear surface of the plume ($I_{\nu 2} = 0$) and for the LTE case $S_\nu(\tau) = B_\nu(T')$ where $B_\nu(T')$ is the Plank function for the flare temperature at optical depth τ . The monochromatic emergent intensity is now

$$I_\nu = \int_{\tau=0}^{\tau=\Gamma} \Phi_{\nu a} B_\nu(T') \, EXP(-\tau \Phi_{\nu a}) \, d\tau \qquad (2)$$

where Γ is the total optical thickness.

A numerical integration of Eq.(2) using Simpson's Rule of 2M intervals (2) yields a theoretical relative spectral radiant power for a given wavelength, proportional to spectral emergent intensity. By calculating values over a spectral frequency range, a theoretical flare spectrum can be generated.

In order to solve the transfer equation simultaneously for both of the sodium D-lines, Douda, Behmenberg, Hoffman and Kohn (1,21,26,27) replaced the individual dispersion profiles, in Eq.(2), with a 2-line Voigt function. This function includes a superposition of broadening mechanisms and is described as

$$V_a(\nu) = \pi^{-3/2} \int_{-\infty}^{\infty} \frac{a \, EXP(-y^2)}{(\nu - y)^2 + a^2} \, dy \qquad (3)$$

where ν is the frequency measured from the line center in units of Doppler half-width and a is the dispersion parameter.

The dispersion parameter, a, is obtained from the equation

$$a = \left[(\Delta\lambda_N + \Delta\lambda_L + \Delta\lambda_R + \Delta\lambda_Q) / \Delta\lambda_D \right] (\ln 2)^{1/2} \qquad (4)$$

where $\Delta\lambda_N$, $\Delta\lambda_L$, $\Delta\lambda_R$, $\Delta\lambda_Q$, and $\Delta\lambda_D$ are the natural, Lorentz (unlike particle), resonance (like particle), quenching, and Doppler line broadening half-widths, respectively.

The Voigt a Parameter

The Voigt a parameter shown in Eq.(3) is the dispersion parameter that takes into account all of the factors considered that contribute to the width of the spectral line. The line broadening mechanisms considered in the pyrotechnic flame spectra are (a) natural broadening (due to the Heisenburg uncertainty

principle (44)), (b) Holtsmark pressure broadening due to collisions with like neutral species, (c) van der Waals pressure broadening due to collisions with unlike neutral species, (d) broadening due to quenching collisions, and (e) Doppler broadening due to the relative motion of the radiating system and the observer. Stark broadening due to charged perturbers was neglected as the concentration of charged metal ions in the flame can be shown to be small (8). As shown in Eq.(4), the effect of all the considered broadening mechanisms is accounted for in the Voigt function a parameter. Each of the line broadening half-widths will be discussed separately below.

The equation for natural line broadening is

$$\Delta\lambda_N(\text{Å}) = 10^8 \lambda_o^2 A_{21}/2\pi c \qquad (5)$$

where λ_o is the line center wavelength and A_{21} is the Einstein coefficient for stimulated emission. The values of A_{21} for the alkali metals are shown in Table 1. along with the calculated natural line broadening for each.

Table 1.
Natural Line Broadening and Einstein Coefficients for the Alkali Metals

Metal	λ_o	A_{21}, sec^{-1}	$\Delta\lambda_N$, Å
Li	6707	.37E+08	0.9E-04
Na	5893	.65E+08	1.2E-04
K	7682	.39E+08	1.2E-04
Rb	7874	.36E+08	1.2E-04

The Doppler broadening half-width for the alkali metals is given by

$$\Delta\lambda_D(\text{Å}) = 2\times10^8[(2R\ln 2)^{1/2}/c]\lambda_o(T_o/M)^{1/2} \quad (6)$$

where M is the molecular weight of the metal in gm./mole. Table 2. shows the values calculated for the Doppler broadening half-width for a temperature of 3000 °K.

Table 2.
Doppler Line Broadening
for the Alkali Metals

Metal	λ_o	M	$\Delta\lambda_D$, Å
Li	6707	6.94	0.0999
Na	5893	22.99	0.0482
K	7682	39.10	0.0482
Rb	7874	85.48	0.0334
Cs	8732	132.91	0.0297

Since the value of $\Delta\lambda_D$ is proportional to the square root of the flame temperature, $\Delta\lambda_D$ for sodium varies from 0.0482 Å at 3000 °K to 0.0387 Å at 1915 °K.

The van der Waals collisional broadening (also known as Lorentz broadening) due to unlike species is given by

$$\Delta\lambda_L(\text{Å}) = 10^8(\lambda_o^2/c)\sigma_L N_2(8kT_oN_A/\pi\mu)^{1/2} \quad (7)$$

where σ_L is the optical cross section (cm^2) of the alkali metal, and N_2 is the number density of perturbing species (cm^{-3}). N_A is Avagadro's number and μ = mM/(m+M), the reduced mass. If the mean relative velocity of colliding species ($cm\cdot sec^{-1}$) is

$$\bar{v}_j = (8kT_oN_A/\pi\mu)^{1/2} \quad (8)$$

where j is the species index, Eq.(7) can be written

$$\Delta\lambda_L(\text{Å}) = 10^8(\lambda_o^2/c)\sigma_L N_2 \bar{v}_j \quad (9)$$

The values for optical cross section at 2500 °K reported by Hoffman and Kohn (21) are shown in Table 3. below, along with typical values for the Lorentz broadening.

Table 3.
Optical Cross Sections and
Lorentz Line Broadening Values
for the Alkali Metals

Metal	$\sigma_L (\times 10^{-15}), cm^2$	$\Delta\lambda_L$, Å
Li	46.5	0.05880
Na	59.3	0.02967
K	59.1	0.04043
Rb	76.3	0.03313
Cs	89.1	0.04355

The values for Lorentz broadening half-width in Table 3. do not take into account the effects of mixing the ambient atmosphere with the plume. These effects will be considered at the end of this section.

The Holtsmark or resonance broadening half-width can be derived from

$$\Delta\lambda_R (\text{Å}) = [(6\times10^8)\underline{e}^2 f N_1 \lambda_o^3]/(4\pi^2 c^2 m_e) \qquad (10)$$

where $\underline{e}$ is the elementary charge ($cm^{3/2}\, gm^{1/2}\, sec^{-1}$), m_e is the electron rest mass (gm), and N_1 = is the number density of the alkali metal atoms. The oscillator strengths, f, of the alkali metals were obtained from several sources (39,40,42). The uncertainty of the determined values is not of sufficient magnitude to cause any significant variation in the calculations. Resonance broadening of the spectral lines is the largest factor in determining the Voigt function a parameter except at very low metal atom concentrations. Again without considering the effects of interactions with the ambient atmosphere, the values of

resonance broadening half-widths and oscillator strengths are shown in Table 4.

Table 4.
Oscillator Strengths and
Resonance Line Broadening Values
of the Alkali Metals

Metal	f_1	f_2	f	$\Delta\lambda_R$, Å
Li	0.502	0.251	0.753	0.52342
Na	0.624	0.312	0.936	0.63442
K	0.682	0.339	1.021	1.30661
Rb	0.675	0.322	0.997	1.19584
Cs	0.732	0.362	1.09	1.88006

The equation for quenching line half-width can be expressed as

$$\Delta\lambda_Q(\text{Å}) = 10^8 \lambda_o^2 \, C_{21}(T)/2\pi c \qquad (11)$$

where $C_{21}(T)$ is the rate of collisional deactivation (i.e., the number of quenching collisions per second). *Hooymayers* (19,20) equates the quenching process to a shortening of the radiative lifetime. He calculates the value of $C_{21}(T)$ as

$$C_{21}(T) \approx Q_{21}(T) = \eta_j \bar{V}_j \sigma_j \qquad (12)$$

where η_j is the density of the quenching flame specie j, $\bar{V}_j$ is the average relative velocity of approach of the colliding specie j, and σ_j is the specific quenching cross section. When the specific alkali metal atoms undergo quenching collisions in a mixture of flame molecules of different species, the quenching frequency $Q_{21}(T)$ is given by

$$C_{21}(T) \approx Q_{21}(T) = \sum_{j=1}^{m} \eta_j \bar{V}_j \sigma_j \qquad (13)$$

where j is the index for the various species of flame molecules. The value for $\bar{V}_j$ is given by

$$\bar{V}_j = \left[(\bar{V}_{metal})^2 + \bar{V}_j^2 \right]^{1/2} \qquad (14)$$

The mean speed of the alkali metal atom and of any specie atom j is given by

$$\bar{v}_{metal} = \bar{v}_j = (8kT_o N_A/\pi M_j)^{\frac{1}{2}} \qquad (15)$$

where N_A is Avagadro's number and M_j is the molecular weight of the metal or specie j. The ideal gas law is used to calculate the number density of the species in the flame by relating the mole fraction of the specie j to the total gas fraction at a given temperature and pressure. Values for the quenching cross section for various species with the different alkali metals were required for the computation of $C_{21}(T)$. Hooymayers and Alkemade (19,20) reported measured values for quenching cross sections of various species with sodium and potassium. It is thought that the apparent quenching cross section of a specie with an alkali metal would be inversely proportional to the atomic weight of the metal. This would be the result of the collisional mass of the metal varying while the mass of the quenching specie remained constant. The quenching cross sections of species in collision with sodium have been examined more extensively than the other alkali metals. The values of quenching cross sections with sodium were divided by the ratio of atomic weights of potassium and sodium (39/23) to predict the values for potassium. The calculated values were compared with the measured values of Hooymayers. The results are shown in Table 5.

Table 5.
Quenching Cross Section Values for
Species with Sodium and Potassium

$\sigma_j (x10^{16}), cm^2$

Specie	Temp	Na Value	Calc. K Value	Meas. K Value
CO	2000	72	42	40
CO2	1670	113	66	80
Ar	2070	2.3	1.35	0.94
H2O	2070	1.0	0.59	0.42
N2	1940	40	23	18
O2	1885	66	39	31.5

The agreement is entirely satisfactory given the uncertainty of the original measurements. Indeed, variations greater than these are noted between results from different researchers. The quenching cross section values of all of the major species in the flare flame were calculated with reference to the sodium quenching cross section values and the atomic weight of the alkali metal. These values are tabulated in Table 6. below for 2000°K.

Table 6.
Quenching Cross Section Values of Species
with the Alkali Metals

$\sigma_j (x10^{16}), cm^2$

Specie	Li	Na	K	Rb	Cs
Ar	7.9	2.4	1.4	.6	.4
CO	239	72	42	19	12
CO2	312	94	55	25	16
H	3.3	1	.6	.3	.2
H2	53	16	9.4	4.3	2.8
H2O	14.6	4.4	2.6	1.2	.8
Mg	3.3	1	.6	.3	.2
N2	139	42	25	11	7.3
O2	205	62	36	17	11

These quenching cross sections were used in the computation of the quenching broadening half-width. Typical values of the quenching broadening half-width calculated for each metal without regard for the interaction with the air are shown in Table 7.

Table 7.
Quenching Line Broadening
of the Alkali Metals

Metal	$\Delta\lambda_q$, Å
Li	4.6954E-03
Na	1.9329E-03
K	1.6166E-03
Rb	1.8645E-03
Cs	6.2197E-04

From Eq.(4), the Voigt function a parameter can be calculated for each metal. Without taking into consideration the effect of the ambient atmosphere, the values for the a parameter for stoichiometric formulations are shown is Table 8.

Table 8.
Voigt Function a Parameter Values
for the Alkali Metals

Metal	a
Li	4.8372
Na	11.3622
K	23.1741
Rb	38.8102
Cs	54.7553

To examine the effect of mixing the ambient atmosphere with the flare plume, thermochemical calculations were made with the admixture of air with the flare composition. Calculations were run in 10% increments from 0% air to 90% air. From these data, new values of the Voigt function parameter were calculated. Table 9. and Figure 1. show the values obtained for sodium over the range of formulations.

Table 9.
Line Broadening and Voigt Function α Parameter Values for Sodium as a Function of % Air Admixed

%Air	T,°K	$\Delta\lambda_N$	$\Delta\lambda_L$	$\Delta\lambda_R$	$\Delta\lambda_Q$	$\Delta\lambda_D$	α
0	3078	.00012	.02967	.63442	.00193	.04881	11.362
10	3064	.00012	.03144	.54871	.00216	.04870	9.957
20	3038	.00012	.03303	.46972	.00238	.04849	8.674
30	2999	.00012	.03453	.39649	.00257	.04818	7.495
40	2938	.00012	.03556	.32874	.00274	.04769	6.410
50	2835	.00012	.03632	.26576	.00288	.04684	5.422
60	2630	.00012	.03632	.20560	.00295	.04512	4.521
70	2246	.00012	.03491	.13779	.00287	.04170	3.508
80	1710	.00012	.03135	.07827	.00260	.03638	2.571
90	1181	.00012	.02662	.00006	.00199	.03023	0.793

From the table, it can be seen that the Doppler half-width is only reflecting changes in the temperature of the mixtures. The natural broadening half-width is only a function of the wavelength and the Einstein coefficient of stimulated emission. The Lorentz, resonance and quenching parameters are influenced not only by the temperature but also by the reduced sodium atom concentration and the change in the perturbing species. It is particularly notable that the nitrogen and oxygen content of the plume mixture increase markedly since they are especially effective in quenching sodium D-line radiation. All of the alkali metal Voigt function α parameters show a similar response to the mixing of air with the flame. Again using sodium as an example, Table 10. and Figure 2. show the effect of varying the formulation of the illuminant on the Voigt function α parameter at the 0% air level.

Table 10.
Line Broadening and Voigt Function Parameter Values for Sodium as a Function of % Magnesium at 8% Binder

%Mg	T,°K	$\Delta\lambda_N$	$\Delta\lambda_L$	$\Delta\lambda_R$	$\Delta\lambda_Q$	$\Delta\lambda_D$	a
30	2948	.00012	.02425	.79960	.00159	.04801	14.317
35	2900	.00012	.02543	.73523	.00144	.04845	13.098
40	2953	.00012	.02761	.65122	.00133	.04824	11.742
45	2815	.00012	.03016	.56543	.00126	.04759	10.443
50	2358	.00012	.03315	.49993	.00123	.04606	9.660
55	1964	.00012	.03817	.48608	.00125	.04201	10.417
60	1938	.00012	.04251	.48479	.00106	.03893	11.303
65	1795	.00012	.04275	.47708	.00051	.03830	11.313

It may be seen that the Voigt function a parameter is sensitive to the changes in formulation. While only sodium values are shown in the table, all of the alkali metals show a similar response to changing formulation.

Optical Thickness

To evaluate Eq.(2), a means is needed to determine the total optical thickness for a given point within the plume. Douda used an equation for optical thickness that assumed that the number density of sodium atoms had an average value inside the flame. With this assumption, the optical thickness can be described as

$$\tau(z) = [h\nu_0/4\pi\Delta\nu_0](N_1 B_{12} - N_2 B_{21})Z \qquad (16)$$

where B_{12} and B_{21} are the Einstein absorption and induced emission coefficients, N_1 is the number density of metal atoms in the lower (^2S) state and N_2 is the number density of metal atoms in the upper (^2P) state and Z is the flame depth (cm.). The Doppler half-width, $\Delta\nu_0$, is in units of frequency. It can be shown that N_2 is negligible compared to N_1 (28,41). Eq.(16) is not adequate for the model described in this research since the metal atom concentration is not assumed constant but allowed to

vary as a function of position within the plume. Accordingly, the model constructs a profile of the metal atom concentration across a section of the plume and calculates the optical thickness by numerical integration using the trapezoidal rule to give the value at any depth in the plume. See Appendix B for a detailed description. The expression for optical thickness may be written as

$$\Gamma = \tau(z) = \frac{h\nu B_{12}}{4\pi \Delta\nu_0} \int_{\tau=1}^{\tau=z} N_1(z)\, dz \qquad (17)$$

where $N_1(z)$ is the metal atom concentration in gram-atoms/cc at depth z. Figure 3. shows the optical thickness as a function of depth in the flame for a typical sodium composition.

THE FLARE FLAME MODEL

Physical and Optical Boundaries

To model the combustion of a flare composition one must take into account several factors that are known to influence the flame both physically and chemically. As the fuel and oxidizer react, the combustion products are expelled from the surface and form a gaseous volume that radiates both line spectra and a continuum due in part to radiative transfer broadening and in part to gray body emission from the solid particles in the plume. This research will consider only the radiative transfer aspects of the resonance-line continuum.

For this model, the burning rate of the composition is assumed to be optimized for the formulation. This is attainable in practice by tailoring the particle size distribution of the magnesium or other fuels. It has been observed that there is an optimum burning rate for a given formulation. If the rate is slower than the optimum, heat losses will be excessive and a low light integral will be recorded. If the rate is faster than the optimum, material will pass through the reaction zone too fast to allow equilibrium combustion and material will be ejected from the plume without contributing to the system resulting in a low light integral. This model assumes that proper adjustment of the burning rate has been accomplished.

The stoichiometric formulation of a composition is the formulation that gives the highest temperature when the equilibrium proceeds to minimize the Gibb's free energy of the system. This is usually a balance point where just sufficient oxidizer is present to oxidize the fuel present. If the reaction products are allowed to mix with the ambient atmosphere, however, and the ambient atmosphere is air, there is a potential to further react excess fuel with the oxygen in the air. This will proceed to a point where there is not sufficient fuel reacting with the air to raise the temperature of the air to the combustion temperature. As the flare formulation is adjusted to be fuel rich, the excess fuel reacts with the air and the reaction proceeds further along the plume axis to give a longer plume. This has been observed experimentally by many investigators (11,12,13,14,15,16,24,29,30,34,35,36). The plume length is also a function of the pressure surrounding the plume. The reduced pressure allows the plume to expand along the plume axis resulting in longer plumes. This is reported by Douda and Blunt (11,15,16). The length of the flare plume is also a function of the diameter of the flare. As the cross section of the plume increases in diameter, it obviously takes longer for the plume to mix with the air and complete the combustion.

To solve the radiative transfer problem requires a mathematical model of the flare plume to permit computation of the temperature and metal atom concentration profiles through the plume at a given height above the flare surface. Figure 4. shows the physical model that was derived. The outer boundaries are

represented by parabolas that are fitted to the edge of the candle and extend to a point above the candle that is defined as a function of the candle diameter and formulation. The parabolas are defined as the 90% air interface and represent the physical boundaries of the plume. The factor F is the fuel fraction that gives a computed temperature of 1800 °K. Lewis and von Elbe (48) reported that sodium D-line emission disappears below 1775 °K. Fristrom and Westenberg (45) reported that emission of additives to flames ceases at about 1700 °K. The thermochemical combustion analysis shows that a limit of 1800 °K agrees well with the disappearance of the metal atoms from the plume due to the formation of the oxides and hydroxides. Brewer and Searcy (6,7) report that the oxides of the various alkali metals are stable at temperatures in the 1500 to 2600 °K range with lithium oxide forming at 2600 °K and cesium oxide forming around 1500 °K. It is assumed that an average temperature of 1800 °K will be suitable for all the alkali metals for the disappearence of emission. The factor F varies as the formulation varies and for a given diameter,(d), the plume lengthens as the composition moves towards a fuel rich composition. Photographs of flare plumes (32,36) show good agreement with the values calculated for plume length. The maximum height of the visible plume above the candle surface is given as

$$L_{max} = d/F \qquad (18)$$

To account for the influence of ambient pressure on the plume length, another term is added to the length calculation to give

$$L_{max} = d/F\,(760/P)^{1/3} \qquad (19)$$

The cube root of the pressure relative to 1 atmosphere gives reasonable agreement with the observed spectra previously cited. The diameter (DL) of the plume at the maximum height above the flare surface is determined as

$$DL = [(760/P)^{1/3}(d^2 + d\,L)]^{1/2} = (760/P)^{1/6}\, d\,(1 + 1/F)^{1/2} \qquad (20)$$

The adjustment of length and diameter for pressure allows the volume of the plume to vary with the pressure according to the Ideal Gas Law relationship $P_1V_1 = P_2V_2$. These two parameters permit the computation of the outer boundaries of the visible plume. To account for the mixing of the ambient atmosphere with the plume, a parabolic inner boundary was established as the 0% boundary for admixture of the atmosphere from one direction into the plume. The parabola used has the same parameters for all diameters of candles. This would be expected as entrainment and diffusion should be independent of the diameter of the candle. This boundary is mirror imaged to account for the admixture of the atmosphere from the other side of the plume. It was felt that the air would be rapidly introduced near the surface due to turbulence and entrainment but that diffusion would be the primary means of transport within the inner regions of the plume. Accordingly, the air is introduced parabolically into the plume as shown in Figure 5. The crossover point defines an envelope within which there is no admixture of the atmosphere. At a given point above the candle surface, the parabolic equations can be solved to give the necessary boundaries to compute the composition of the flame at each point across the plume. Above the crossover point, the per cent of the atmosphere at a given

depth in the plume is given by the sum of the mixing parameters.

The physical boundaries for the flare plume were established as the limit for mixing with 90% air. There is another boundary that must be established for the model also. This is the optical boundary. Since the model is concerned with the resonance-line continuum of an alkali metal, the optical boundary will be defined as a point in the plume where the metal atom concentration has decreased to 1% of its value in the center of the plume. The change in concentration across the radius of the plume is due to dilution with the atmosphere, changes in temperature across the plume, and reaction of the metal atoms with other plume species. It may be seen that the optical boundary is very close to the physical boundary but the distinction is important, especially with the lithium flames. The temperature at the physical boundary is generally around 1200 °K which is close to the value chosen by Douda(1). The temperature at the optical boundary is around 1800 °K for all the metals except lithium where it is around 2000 °K. These temperatures are considered reasonable for both disappearance of the metal atoms and the cessation of emission.

Heat Loss Correction

One other factor must be accounted for to allow the flame model to simulate processes occurring in the flame. This factor is heat loss along the flare axis. There are losses of the heat of combustion due to convective, conductive and radiative processes occurring in the plume. Hamrick, Tanner, and Douda

(1,29,30,34,35) have made calculations and measurements along the plume axis to estimate the temperature along the axis. Using their values and combining this with the assumption that the visible radiation limit is 1800°K at d/F, a correction profile for temperature can be calculated. A parabola is fit with the computed adiabatic temperature as the vertex on the y-axis and the height above the candle surface along the x-axis. The flame temperature is set at 1800°K at d/F on the x-axis. The flame temperature along the centerline can then be computed as a function of distance above the candle surface. The maximum temperature in any cross section is determined by thermochemical calculation with the admixture of ambient atmosphere. This value includes excess heat of combustion that is stored in the magnesium oxide and this tends to hold the maximum temperature to less temperature drop than along the axis. It is assumed that the maximum temperature will drop parabolically by a factor of $555(d)^{1/3}$ °K along the length of the visible plume axis. The factor includes a term for $d^{1/3}$ since mixing with the atmosphere in the plume is not complete as the diameter increases. Using these fixed parameters for the rate of temperature drop along the axis, a correction factor is calculated for each incremental step in the plume cross section to adjust the temperature for heat loss. All modes of heat loss are included in the correction factor. The values chosen are related to the observed and calculated temperatures of other researchers and will be shown in later sections to give good agreement between calculated and measured spectral profiles. The actual equations used for the temperature correction are given in Appendix B.

THE COMPUTER PROGRAM

All of the parameters required to solve the radiative transfer equation may now be computed from the mathematical model described. To enable the solution to be run on a microcomputer, several tables of values were calculated and stored as disk files. When the desired metal and formulation have been selected, the appropriate tables of values are loaded into memory. Complete listings of the main program and the special programs used to construct the tables are given in Appendix C. The Voigt function values were computed using a set of parameter values in a Fortran program written by G. Rybicki and included in Douda's program. It was found that the log of the Voigt function at any given wavelength is linear with respect to the log of the Voigt function a parameter. By using the slope and intercept of the log function line, the Voigt function can be readily calculated for any Voigt function a parameter using the microcomputer program. The Voigt functions were taken for five different a parameter values and the slope and intercept of the log values computed by the method of least squares. The tables for use in the new model were constructed for each metal by selecting representative wavelengths, calculating the slope and intercept of the log values and storing the values in a disk file. The actual tables used are shown in Appendix C as Tables C-1 through C-5. Plots of the slope and intercept as a function of wavelength are shown in Figures C-1 through C-5. The discontinuity of the functions at the resonance wavelengths is apparent.

To enable the calculation of temperature and specie concentration through a cross section of the plume, a depth index, Z, is used. The plume is divided into 0.1 cm. segments and the position at the plume surface is identified as Z=1. At each step into the plume of 0.1 cm., the Z value is incremented so that Z times 0.1 will give the depth of the plume in cm. The per cent air that has mixed with the combustion products is calculated and the temperature, Voigt function a parameter, total gas concentration, and metal gas concentration are calculated by interpolation from the appropriate look-up table. The gas concentrations and the Voigt function a parameter are adjusted for the chosen pressure. The temperature profile is next corrected for heat loss and the Voigt function a parameter is corrected for the temperature change at each point in the plume. Once the temperature, concentration and Voigt a parameter functions have been calculated for each position up to the centerline of the plume, a mirror image is constructed for the back half of the plume. The optical thickness is computed for each of the Z index positions by a numerical integration using the trapezoidal rule. See Appendix B. for details. All of the parameters are now available for a numerical integration of Eq.(2) by Simpson's Rule (2). The values computed for each wavelength are stored as a disk file to be recalled and plotted by a special plotting routine.

EXPERIMENTAL RESULTS

Computed Radiation and Temperature Profiles

The mathematical model of the flare plume results in a predicted double peak in the temperature profile of fuel rich compositions. See Figure 6. This is due to the reaction of the excess fuel with the oxygen in the air to maximize the temperature at a radial distance that is a function of the formulation. This double peak has been determined to be a real feature of flames similar to these pyrotechnic flares (9,22,37,38). This is considered additional justification for the selection of the mathematical model as representing the average flame processes.

In the solution of Eq.(2) for the radiant power output, the radiant power at each point in the flare plume is calculated. The curves shown in Figures 7 through 11 show the calculated radiant power for five different wavelengths of a sodium spectrum. In the wings of the spectral profile where the resonance is weak, the radiant power is proportional to the temperature profile. Little of the radiation from the back of the plume is absorbed as it traverses the plume. As the wavelength moves closer to the resonance wavelength, the radiant power output becomes highly distorted as the radiant energy from the deeper areas of the plume is strongly absorbed by the cooler sodium near the front surface. Very near the resonance wavelengths, only the radiant energy from the outer few tenths of a centimeter can escape from the plume. This is the reason that

the early models had to adjust the spectral line profile coefficient to a much lower value to get agreement with experiments. The Voigt function a parameter is only about 1.4 near the surface where all the radiant power is derived in the wavelength regions near resonance. This is in good agreement with the value of 1.2 used by Douda as the best empirical fit to his data.

Computed Spectra

The computer program has generated spectra for each of the alkali metals at 760 Torr for each of three formulations representing near stoichiometry and two cases of increasing fuel rich compositions. These spectra are shown as Figures A-1 through A-15 in Appendix A. All of the spectra were computed at a point one flare diameter above the candle surface with a 3 cm. diameter candle. The computed radiant power values were normalized to give a maximum value of 1.0 for the spectra and show the shape of the curves. Figures A-16 through A-25 are experimental spectra taken by Blunt (36) and reproduced here for purposes of comparison.

Since a large volume of sodium spectra are available from a wide range of experimental conditions, an extensive comparison of calculated sodium spectra has been made. Figure A-26 shows the computed spectra for several heights above the candle surface. Experimental spectra taken by Blunt (15,16) show a similar trend of decreasing power and broadening as the position moves up the plume axis. A typical set of experimental spectra is shown in

Figure A-27 for comparison. This variation is due mainly to the drop in plume temperature and the change in cross-section concentrations due to additional mixing with air. The differences noted in these spectra point out how essential the definition of spatial resolution is when taking spectra of pyrotechnic flames.

Figures A-28 through A-41 show the computed spectra at different ambient pressures. These spectra are compared with the experimental spectra of Douda and Blunt taken at different ambient pressures (8,11,17). The agreement of the computed spectra with the experimental spectra demonstrates that the model is predicting observed spectral changes with reasonable accuracy.

Figure A-42 shows a comparison of the radiant power output of two formulations integrated over the full length of their plumes at each wavelength. These integrals compare the total power output without correction for the response of the human eye to radiation. The areas under the curves for the range of wavelengths calculated are 0.006667 and 0.01616 watts/steradian. These are in the proper relationship for observed candlepower variations with increasing magnesium content.

The diameter of the candle has an effect on the spectral profile of the metal also. Figures A-43 through A-46 show the computed spectra for four different diameter candles with each computed at two candle diameters above the surface. The half-width and the peak-to-peak separation increase with diameter. The changes are proportional to the square root of the diameter

of the candle. This is in accord with experimental evidence reported by Douda (49) and in a private communication from D. C. A. Izod, Royal Armament Research and Development Establishment, Fort Halstead, U.K.

The computation of the spectral profile of lithium has been made with comparison to the results reported by Douda (10) and by Taylor and Farnell (31). The results are shown in Figures A-47 through A-52. The agreement with both the shape and peak half-widths is very good without making any special adjustment of parameters.

For general comparison purposes, the spectra of potassium, rubidium and cesium were computed for the cases of 300 Torr, 76 Torr and 6 Torr. The peak separation and self-absorption are shown clearly in Figures A-53 through A-61.

DISCUSSION

One of the important features of the computer model is the simpification of the computation of the Voigt function for the alkali metals. The method used by Rybicki (1) gives a solution for the Voigt function at a large number of wavelengths for a single value of the a parameter but at the expense of requiring a very large computer and considerable computing time. This does not easily lend itself to the calculation of the Voigt function for varying a parameters through the plume cross-section. The microcomputer solution uses a limited but significant number of wavelengths to cover both the broad spectral region and a high resolution region. By using a correlation of Voigt function with the Voigt function a parameter, the computation can be rapidly effected on a microcomputer over a wide range of formulations and conditions even though the a parameter varies at each point in the plume.

The broad range of cases that has been examined strongly supports the theoretical model that has been developed. Many of the computed spectral phenomena have been observed experimentally without a clear understanding of the mechanisms producing the results. It is well established, for instance, that an increase in percent magnesium above the stoichiometric level will produce an increase in candlepower from an illuminant. It had been noted, however, that the stoichiometric formulation produced the highest theoretical temperature and spectral measurements showed that the output per unit area was highest for the stoichiometric

formulation. It can be seen from the theoretical model that this is the predicted mode for these cases. The increase in magnesium causes an increase in the total surface area of the flare plume so that, even with a decrease in the output per unit area, the overall result is a net increase in candlepower. The changes in radiant power output and the half-width of the metal resonance lines with changes in ambient pressure or metal atom concentration are accounted for in the model, also.

The model accounts for a very wide range of parameters in the computation of the resonance broadening of all the alkali metals. The unique variability of lithium atom concentration with temperature has caused difficulties with previous models. The present model adequately predicts both the half-width and the spectral profile for lithium over a wide range. This uniqueness is not handled as a special case, however, but is a part of the general solution.

In some cases the experimental spectra do not always vary in a systematic and consistent manner. This variation from the predicted mode is not viewed as a failure of the model to predict properly but is a measure of the difficulties in obtaining reproducible spectra from a variable source such as a pyrotechnic flame. Combustion irregularities and plume distortion due to such things as uneven case burning can cause the flare plume to fluctuate and the region of interest will be displaced from the slit of the spectrograph. The spectral profile is sensitive to the height above the candle surface and also to radial

displacement from the plume centerline at a fixed height above the surface. Many of the spectra reported in the literature were taken under less than ideal conditions and on a variety of instruments. Much of the spectral variability is due to the experimental techniques used. The overall response of the model to known shifts in performance correlates well with all of the observed trends that have been established by years of testing. The quantitative agreement with spectra that have been taken recently with closely documented parameters is remarkable in that no ad hoc assumptions are made across the entire range of alkali metals.

In summary, it has been shown that a mathematical representation of a pyrotechnic flame can be used to describe the temperature and concentration profiles of any of the alkali metals in the flame. The computed values can then be used in a two-line radiative transfer model to compute the spectral radiant power distribution for that metal. The model has been developed to be useful on a microcomputer by using techniques to generate the two-line Voigt function from simplified slope and intercept values with the Voigt function a parameter.

REFERENCES

1) B. E. Douda, *Radiative Transfer Model of a Pyrotechnic Flame,* RDTR No. 253, Naval Weapon Support Center, Crane, Indiana, Sept. 1973. AD-769 237.

2) D. G. Moursund and C. S. Duris, Elementary Theory and Application of Numerical Analysis, McGraw-Hill Book Co., New York, 1967, p. 191.

3) S. Gordon and B. J. McBride, Computer Program for Calculation of Complex Chemical Equilibrium Compositions, Rocket Performance, Incident and Reflected Shocks, and Chapman-Jouguet Detonations, NASA-SP-273. Lewis Research Center, 1971.

4) D. R. Dillehay, *Pyrotechnic Flame Modeling,* Proceedings of Pyrochem International 1975, Univ. of Surrey, Guildford, UK. DDC No. AD-B006 100L.

5) D. R. Dillehay, *Pyrotechnic Flame Modeling for Sodium D-Line Emissions,* Proceedings of the Fifth International Pyrotechnics Seminar, 1976.

6) L. Brewer and A. W. Searcy, High Temperature Chemistry, Dept. of Chemistry and Chemical Engineering and Division of Mineral Technology, University of California, Berkeley, California. 1957.

7) L. Brewer, The Thermodynamic Properties of the Oxides and Their Vaporization Processes, Dept. of Chemistry and Chemical Engineering, University of California, Berkeley, California. 1952.

8) N. Ozaki, *Resonance Radiations from High-Pressure Sodium Plasma,* J. Quant. Spectros. Radiat. Transfer, Vol. 11, pp. 1463-1473. (1971).

9) H. Haraguchi and J. D. Winefordner, *Flame Diagnostics: Local Temperature Profiles and Atomic Fluorescence Intensity Profiles in Air-Acetylene Flames,* Applied Specroscopy, Vol. 31, pp. 195-199. (1977).

10) B. E. Douda, *Prediction of Line Shapes in Pyrotechnic Flares Containing Lithium,* Proceedings of the Fifth International Pyrotechnics Seminar, 1976.

11) B. E. Douda, *Atlas of Radiant Power Spectra of Four Flare Formulas at 8 Levels of Ambient Pressure,* Naval Weapon Support Center, Crane, Indiana, RDTR No. 205. June, 1972.

12) R. M. Blunt, *Flare Flame Phenomena,* Naval Weapon Support Center, Crane, Indiana, RDTR No. 186, June, 1971.

13) R. M. Blunt, *Relation of Flame Luminance to Flame Area Measured,* Naval Weapon Support Center, Crane, Indiana, RDTR No. 184, May, 1971.

14) B. E. Douda, *Illuminating Flame Size Comparisons,* Naval Weapon Support Center, Crane, Indiana, RDTR No. 150, April, 1969.

15) R. M. Blunt, *Spectral Distribution of Different Regions of Illuminating Flare Flames*, Naval Weapon Support Center, Crane, Indiana, RDTR No. 220, Dec. 1972.

16) R. M. Blunt, *Spectral Distribution of Different Regions of Illuminating Flare Flames II*, Naval Weapon Support Center, Crane, Indiana, RDTR No. 292, Jan. 1975.

17) B. E. Douda and R. J. Exton, *Optically Thick Line Widths in Pyrotechnic Flares*, Proceedings of Pyrochem International 1975, Univ. of Surrey, Guildford, UK. DDC No. AD-B006 100L.

18) H. A. Webster III, *Alkali Metal Emitters II. Identification of Diatomic Features*, Naval Weapon Support Center, Crane, Indiana, RDTR No. 30, May, 1976.

19) H. P. Hooymayers and C. Th. J. Alkemade, *Quenching of Excited Alkali Atoms and Related Effects in Flames: Part I. Theoretical Analysis*, J. Quant. Spectrosc. Radiat. Transfer, Vol. 6, pp. 501-526 (1966).

20) H. P. Hooymayers and C. Th. J. Alkemade, *Quenching of Excited Alkali Atoms and Related Effects in Flames: Part II. Measurements and Discussion*, J. Quant. Spectrosc. Radiat. Transfer, Vol. 6, pp. 847-874 (1966).

21) F. W. Hoffman and H. Kohn, *Optical Cross Section of Resonance Lines Emitted by Flames Under Conditions of Partial Thermal Ionization*, J. Optical Soc. Amer., Vol. 51, No. 5, pp. 512-521. (1961).

22) M. E. Britske, Yu. S. Sukach and A. N. Savel'eva, *Structure and Physical Properties of Flames*, Zavodskaya Laboratorya, Vol. 39, No. 4, pp. 423-428, (1973).

23) H. A. Webster III, *Spectral Characteristics of Flares Containing Sodium Iodate as an Oxidizer*, Naval Weapon Support Center, Crane, Indiana, RDTR No. 276, June, 1974.

24) C. A. Dinerman, *An Attempt to Increase the Luminous Output of Magnesium-Sodium Nitrate Flares by the Introduction of Nitrogen-Containing Compounds*, Naval Weapon Support Center, Crane, Indiana, RDTR No. 278, June, 1974.

25) W. Behmenburg, H. Kohn and M. Mailander, *An Acetylene Oxygen Flame Using Various Diluents for the Study of Broadening and Shift of Spectral Lines*, J. Quant. Spectrosc. Radiat. Transfer, Vol. 4, pp. 149-161, (1964).

26) W. Behmenburg and H. Kohn, *Broadening of Resonance Lines by Various Perturbing Gases Under Flame Conditions*, J. Quant. Spectrosc. Radiat. Transfer, Vol. 4, pp. 163-176, (1964).

27) W. Behmenburg, *Broadening and Shift of the Sodium D2 Line by Various Perturbing Gases Under Flame Conditions*, J. Quant. Spectrosc. Radiat. Transfer, Vol. 4, pp. 177 -193 (1964).

28) J. Pomerantz and R. Piacesi, *The Equilibrium Compositon and Thermodynamic Properties of Sodium Vapor from 400 to 10,000 K*, US Naval Ordnance Laboratory, White Oak, Maryland, NOLTR No. 62-170. April, 1963, AD-420 172.

29) J. T. Hamrick, J. D. Stanitz and P. L. Blackshear, Jr. et al, *Exploratory Development of Illuminating Flares,* Air Force Armament Laboratory, Eglin AFB, Florida, AFATL–TR–68–91, Aug. 1968, AD- 840 086.

30) J. T. Hamrick, P. L. Blackshear, Jr. and J. D. Stanitz et al, *Exploratory Development of Illuminating Flares – Phase II,* Air Force Armament Laboratory, Eglin AFB, Florida, AFATL–TR–69–107, Aug. 1969.

31) P. L. Farnell and F. R. Taylor, *The Energetics and Spectra of Various Illuminating Flare Systems,* ARRADCOM, LCWSL, Dover, NJ. Paper presented at the Eighth International Pyrotechnic Seminar, 1982.

32) R. M. Blunt, *Evaluation of Processes Occurring in Pyrotechnic Flames,* Naval Weapon Support Center, Crane, Indiana, RDTR No. 91, March 1967, AD–655–820.

33) E. J. Bair, *Pyrotechnic Flare Mechanisms,* Naval Air Systems Command, Dept. of the Navy, 1977, AD–B025 621.

34) J. E. Tanner, Jr., *A Mathematical Model of Flare Plume Combustion and Radiation,* Naval Weapon Support Center, Crane, Indiana, RDTR No. 9, June 1975.

35) J. E. Tanner, Jr., *Thermodynamics of Combustion of Various Pyrotechnic Compositions,* Naval Weapon Support Center, Crane, Indiana, RDTR No. 277, June 1974.

36) R. M. Blunt, *Study of Illuminating Flames from Solid Reactants,* Naval Weapon Support Center, Crane, Indiana, RDTR No. 77, June 1970.

37) N. A. Chigier and V. Strokin, *Mixing Processes in a Free Turbulent Diffusion Flame,* Combustion Science and Technology, Vol. 9, pp. 111–118, Science Publishers, Ltd., London, 1974.

38) R. South and B. M. Hayward, *Temperature Measurement in Conical Flames by Laser Interferometry,* Combustion Science and Technology, Vol. 12, pp. 183–195, Science Publishers, Ltd., London, 1976.

39) J. K. Link, *Measurement of the Radiative Lifetimes of the First Excited States of Na, K, Rb, and Cs by Means of the Phase Shift Method,* Opt. Soc. of Am. J., Vol. 56, No. 9, 1966.

40) G. V. Marr and D. M. Creek, *The Absorption Oscillator Strengths in Alkali Metal Vapours,* Proceedings of the Royal Society of London, A 304 pp. 245–254. (1968).

41) R. N. Newman, *The Vapour Phase Combustion of Sodium,* Berkeley Nuclear Laboratories, RD/B/M–2965, April 1974.

42) W. L. Wiese, M. W. Smith and B. M. Glennon, *Atomic Transition Probalities, Vols. I and II,* NSRDS–NBS 4 and 22, National Bureau of Standards, 1966.

43) M. N. Ozisik, Radiative Transfer and Interactions with Conduction and Convection, John Wiley and Sons, New York, 1973.

44) G. Herzburg, Atomic Spectra and Atomic Structure, Dover Publications, New York, 1944.

45) R. M. Fristrom and A. A. Westenberg, Flame Structure, McGraw-Hill, New York, 1965.

46) J. N. Friend, The Chemistry of Combustion, Gurney and Jackson, London, 1922.

47) A. G. Gaydon, Spectroscopy and Combustion Theory, Chapman and Hall, London, 1948.

48) B. E. Douda, R. M. Blunt and E. J. Bair, *Visible Radiation from Illuminating-Flare Flames: Strong Emission Features*, Jour. Optic. Soc. Am., Vol. 60, No. 8, pp. 1116–1119, August, 1970.

49) B. E. Douda and E. J. Bair, *Visible Radiation from Illuminating–Flare Flames. II. Formation of the Sodium Resonance Continuum*, Jour. Optic. Soc. Am., Vol. 60, No. 9, pp. 1257–1261, September, 1970.

50) J. T. Jefferies, Spectral Line Formation, Blaisdell Publishing Co., Waltham, Mass., 1968.

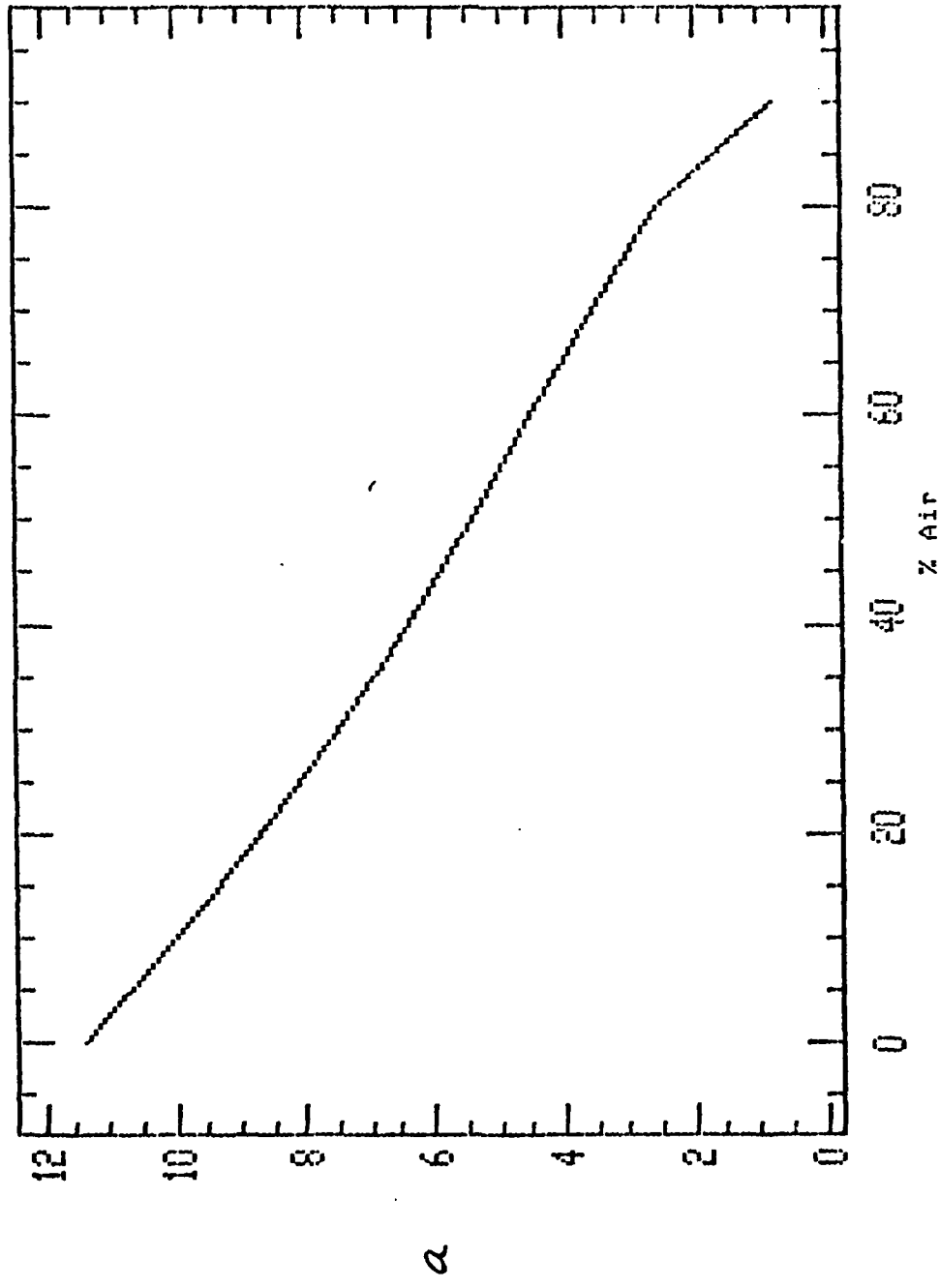

Figure 1.
Voigt Function a Parameter
versus % Air Mixed in the Plume

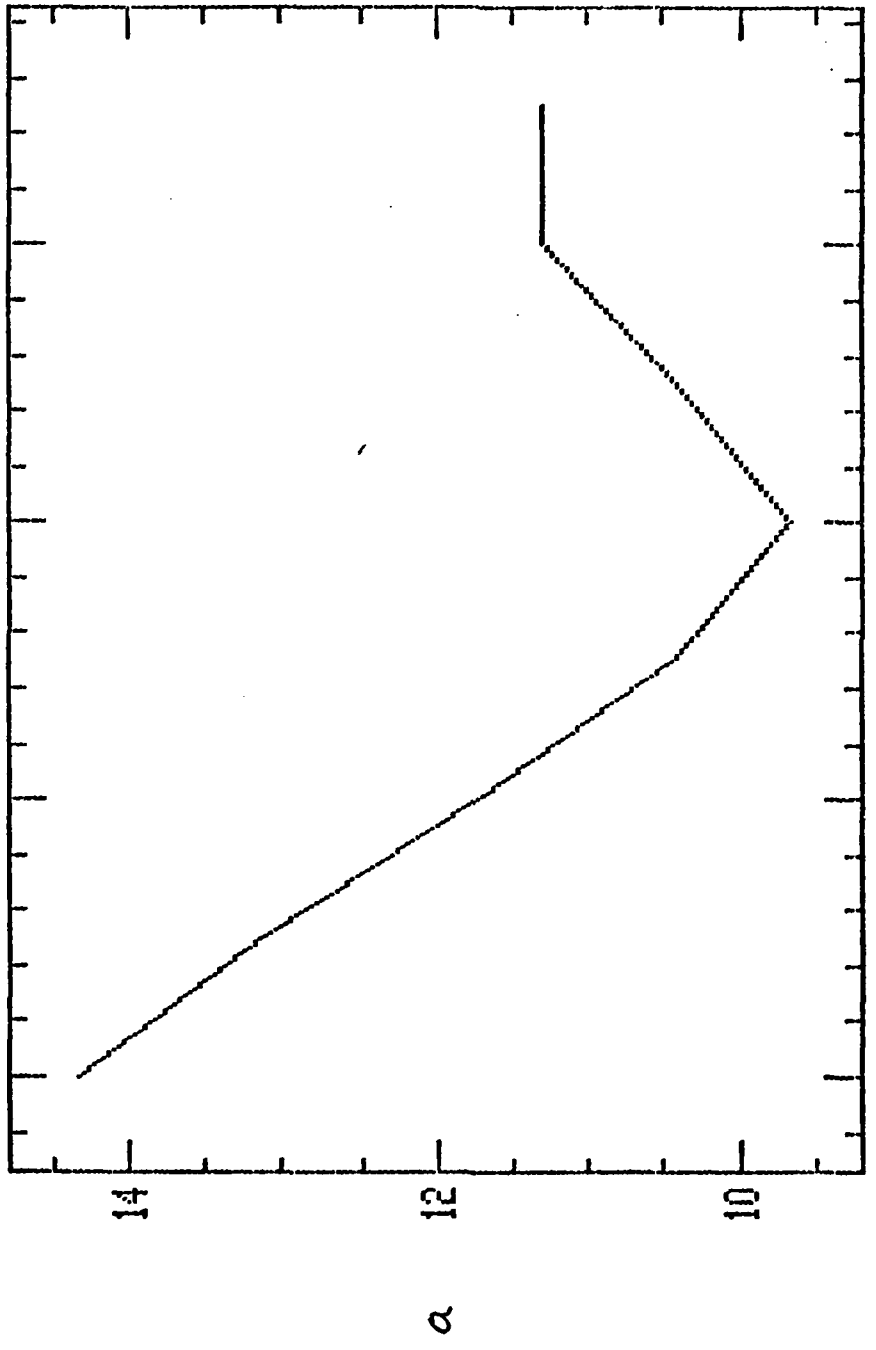

Figure 2.
Voigt Function α Parameter
versus % Magnesium at 8% Binder

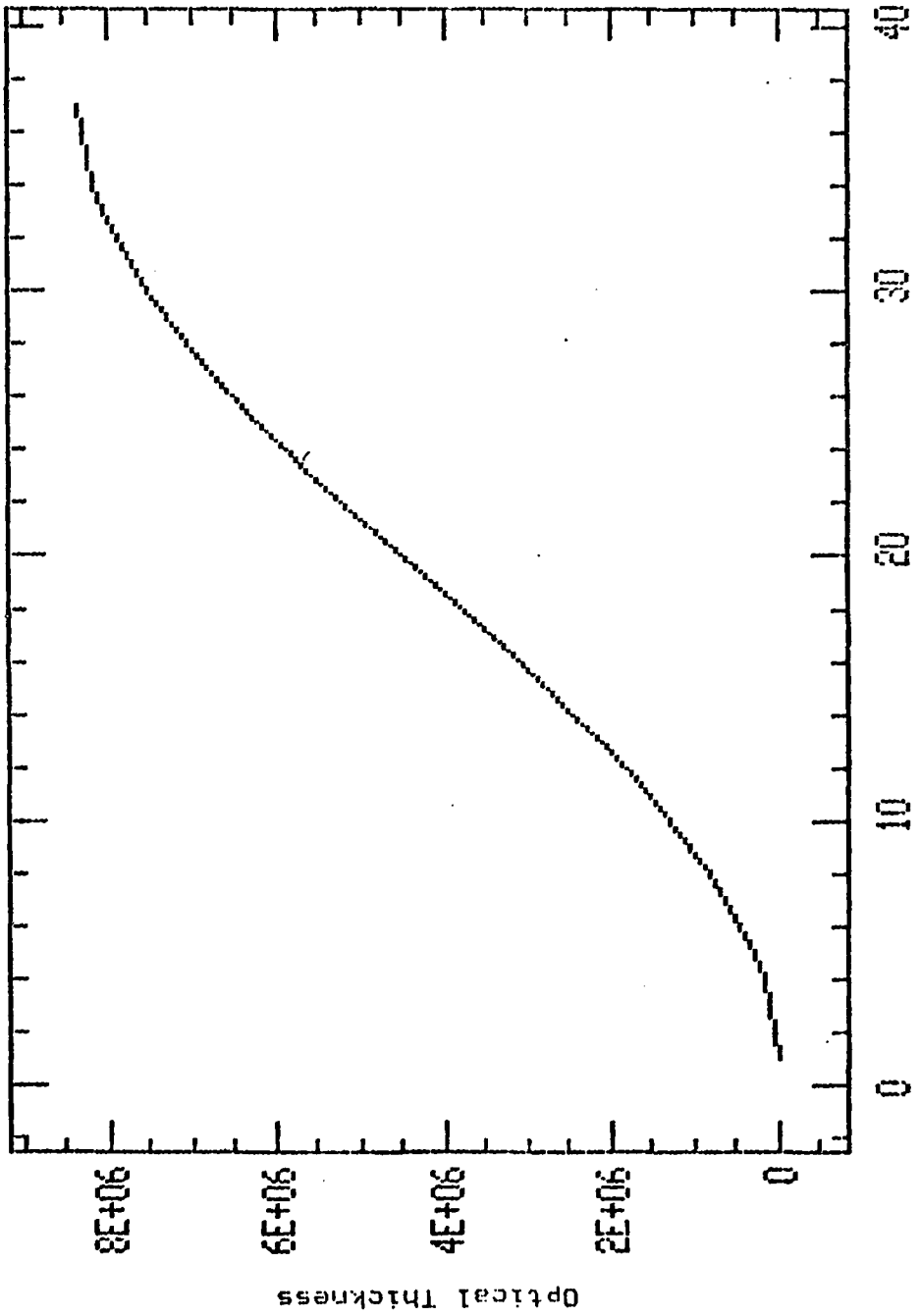

Figure 3.
Optical Thickness versus Distance Across Plume

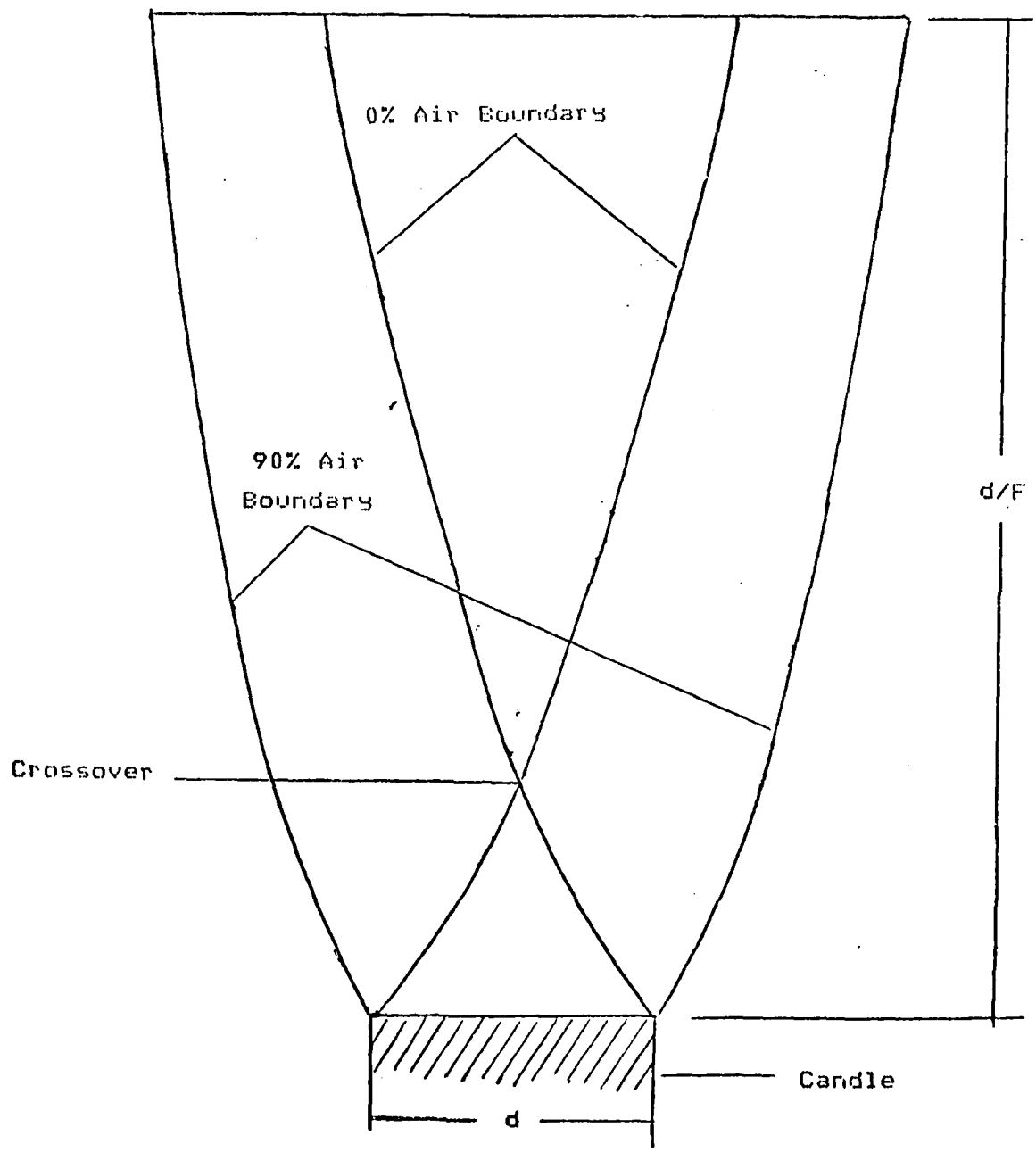

Figure 4.
Physical Flame Model

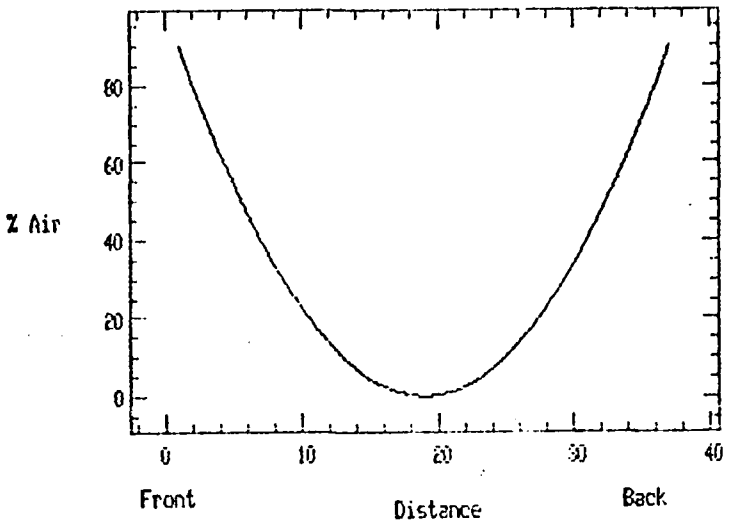

Figure 5.
Mixing of Air at the Crossover
of the 0% Air Boundaries

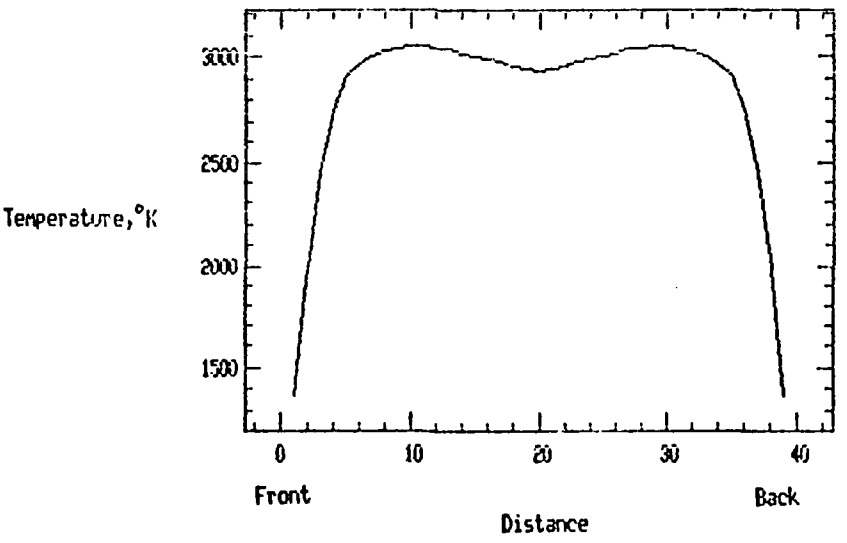

Figure 6.
Temperature Profile of the Flare Plume

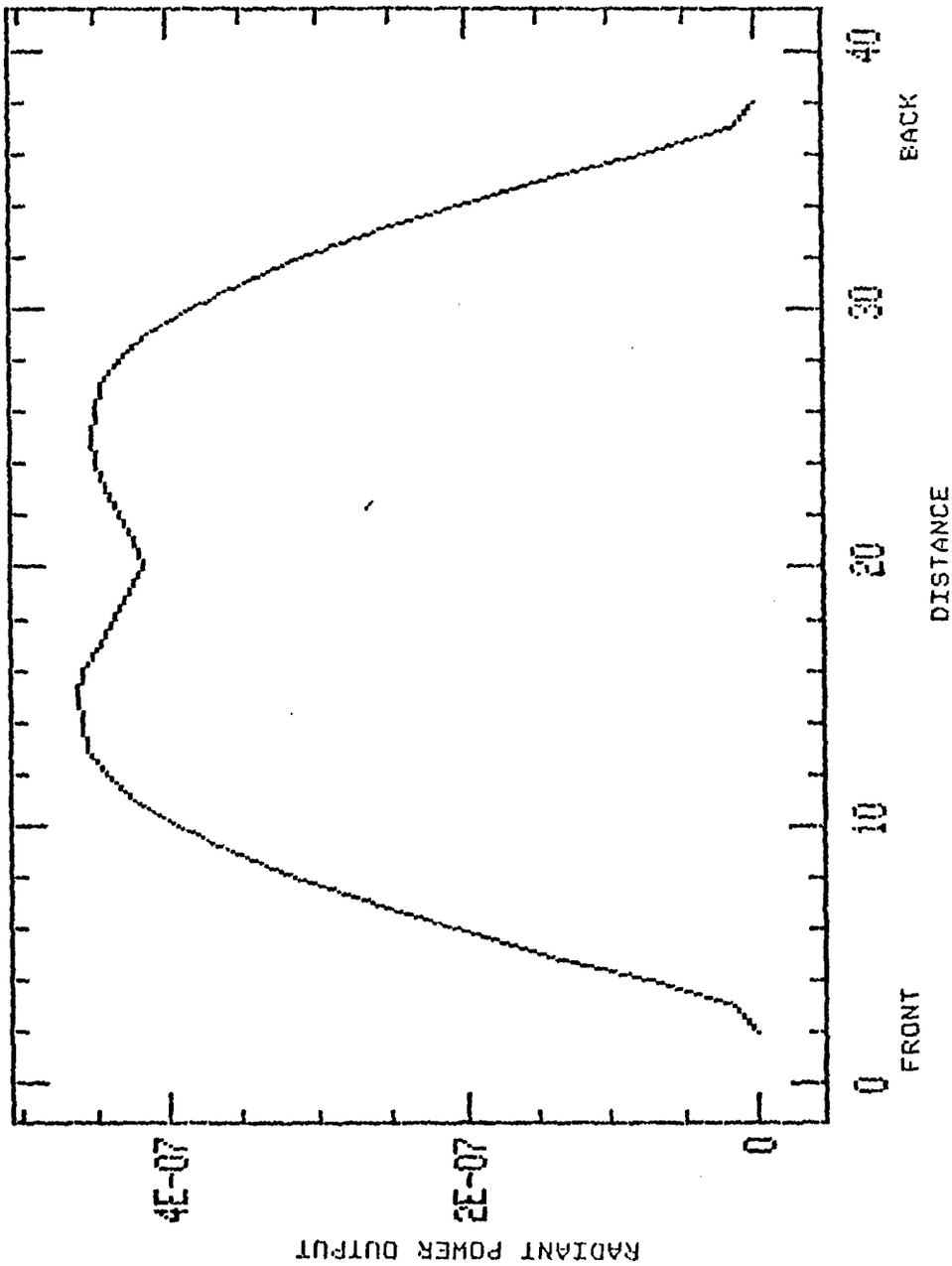

Figure 7.
Radiant Power Output at 5000 Å

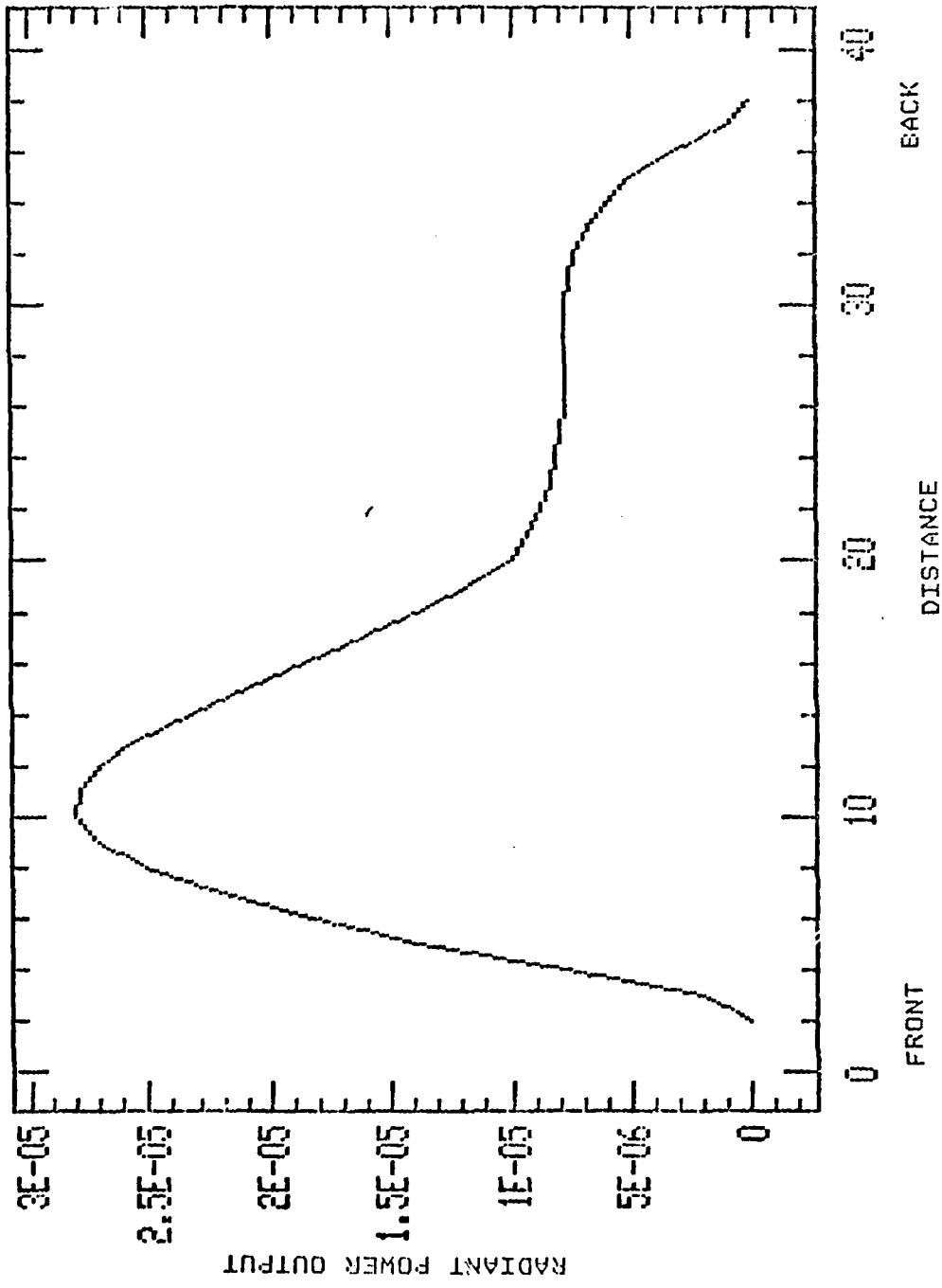

Figure 8.
Radiant Power Output at 5750 Å

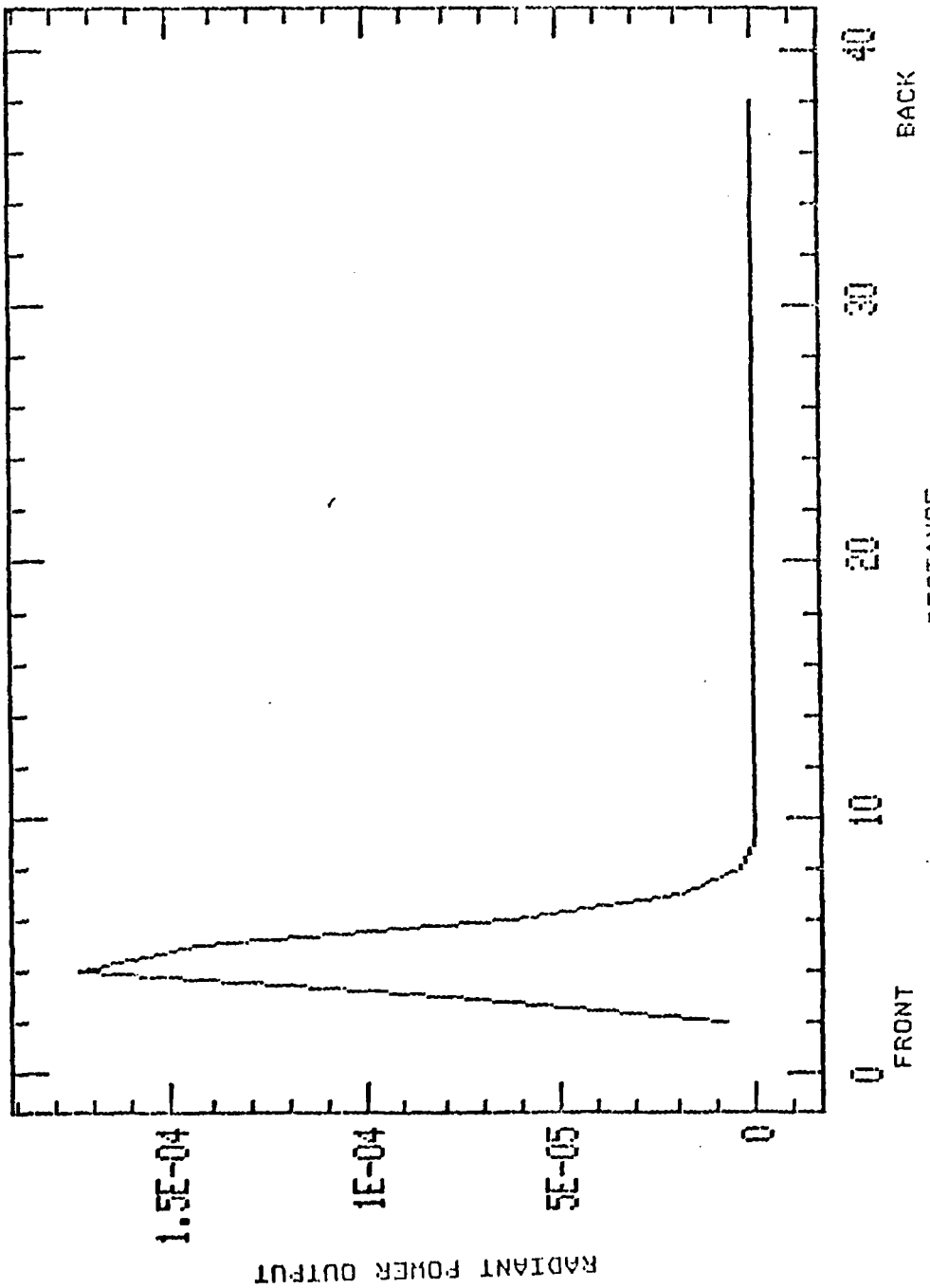

Figure 9.
Radiant Power Output at 5870 Å

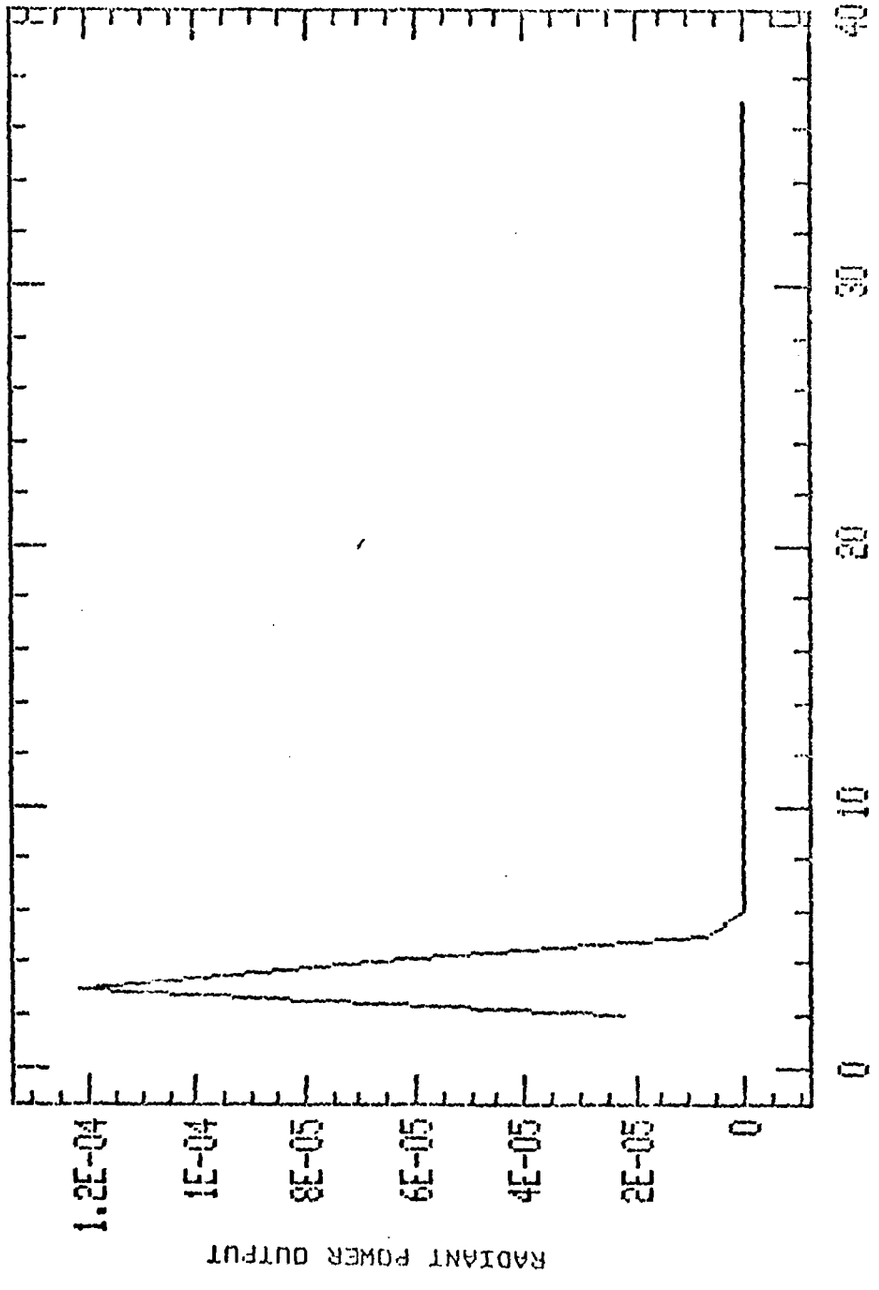

Figure 10.
Radiant Power Output at 5880 Å

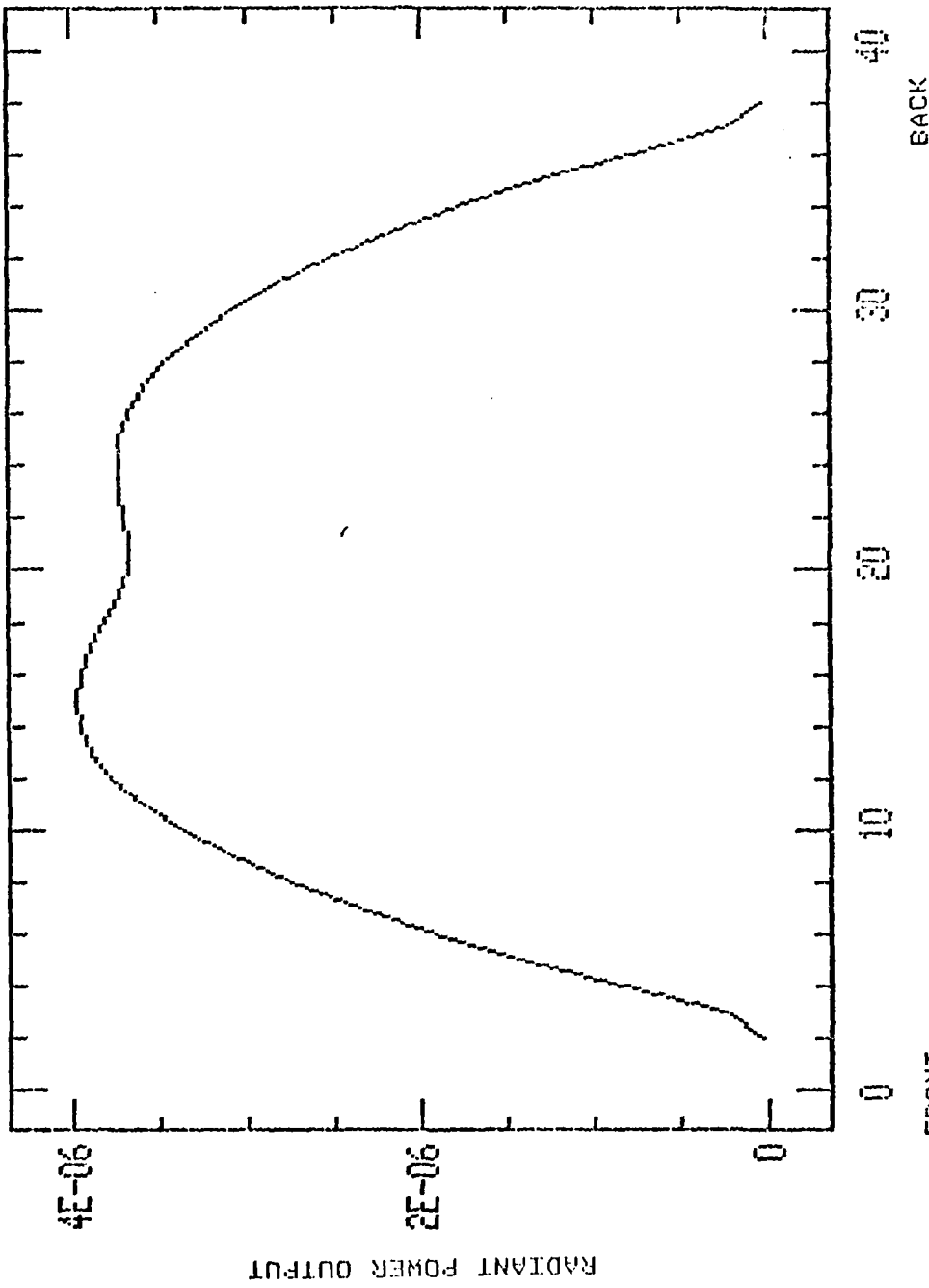

Figure 11.
Radiant Power Output at 6500 Å

APPENDIX A

Theoretical and Experimental Spectra

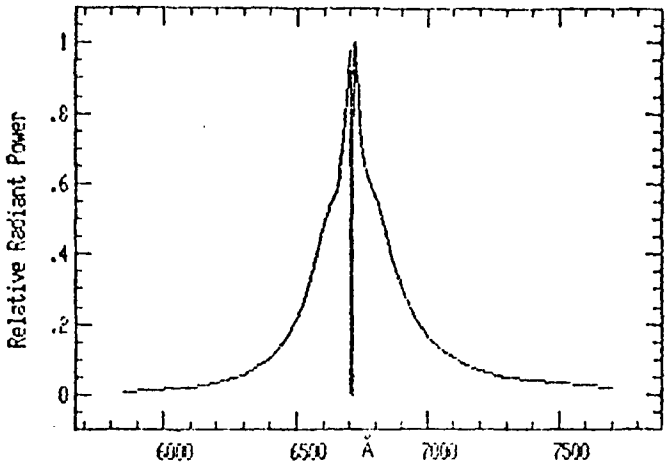

Figure A-1
Lithium at 760 Torr
40% Mg, 55% LiNO3, 5% Binder

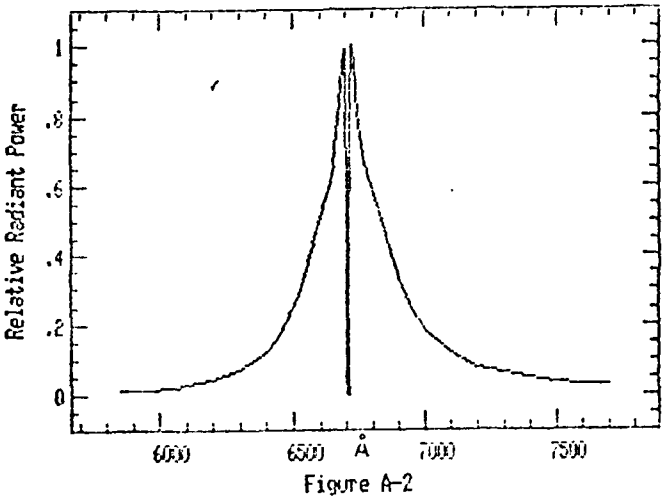

Figure A-2
Lithium at 760 Torr
50% Mg, 45% LiNO3, 5% Binder

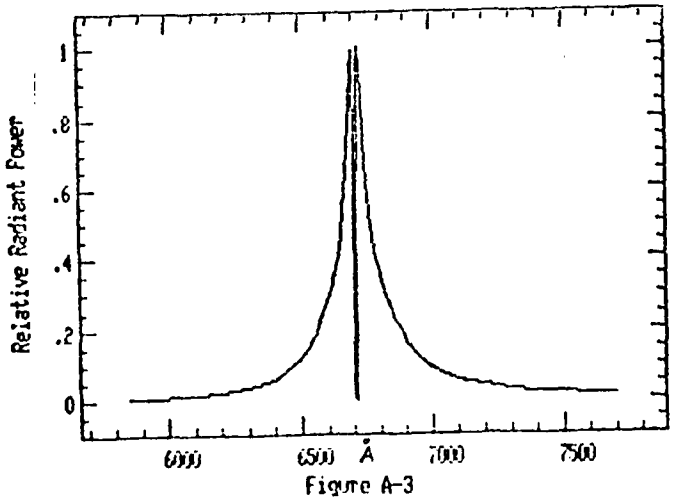

Figure A-3
Lithium at 760 Torr
60% Mg, 35% LiNO3, 5% Binder

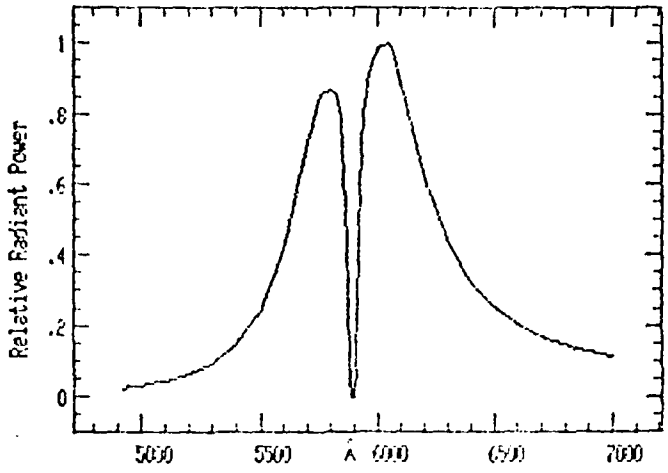

Figure 4.
Sodium at 760 Torr
40% Mg, 55% NaNO3, 5% Binder

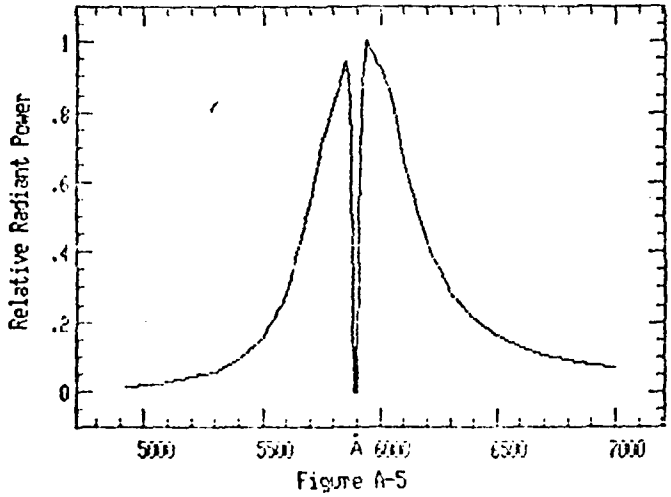

Figure A-5
Sodium at 760 Torr
50% Mg, 45% NaNO3, 5% Binder

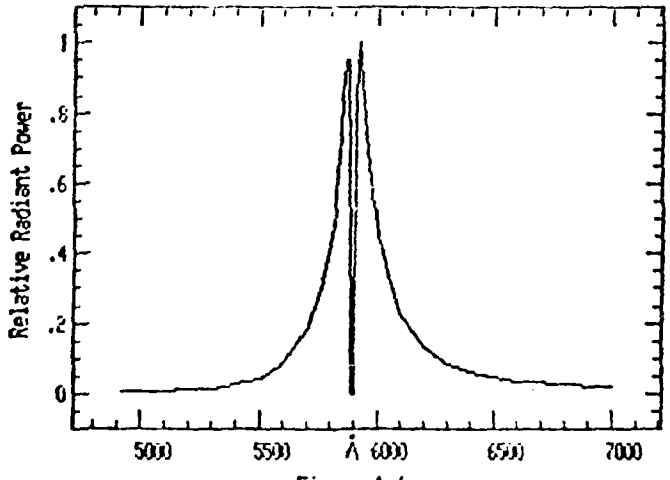

Figure A-6
Sodium at 760 Torr
60% Mg, 35% NaNO3, 5% Binder

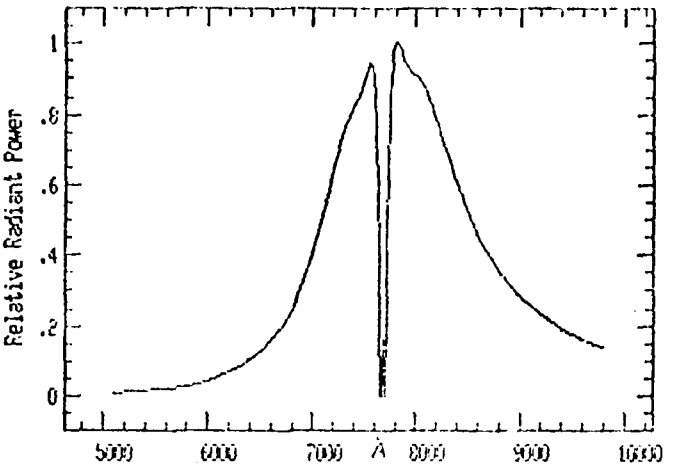

Figure A-7
Potassium at 760 Torr
40% Mg, 55% KNO3, 5% Binder

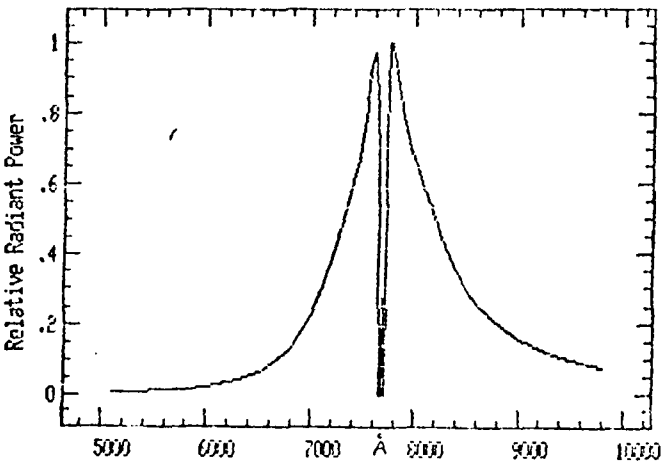

Figure A-8
Potassium at 760 Torr
50% Mg, 45% KNO3, 5% Binder

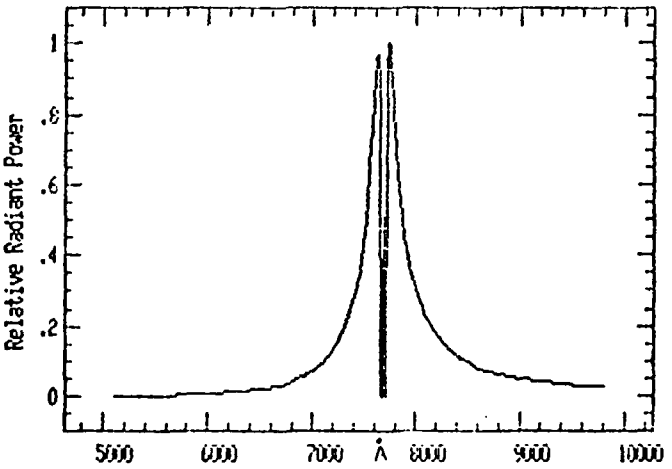

Figure A-9
Potassium at 760 Torr
60% Mg, 35% KNO3, 5% Binder

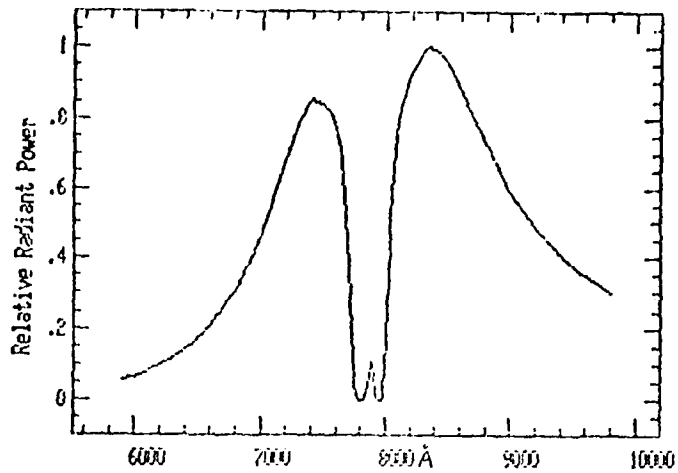

Figure A-10
Rubidium at 760 Torr
35% Mg, 60% RbNO3, 5% Binder

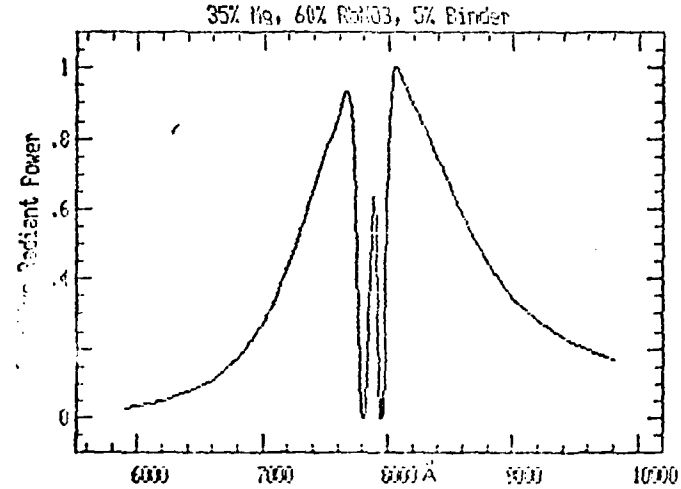

Figure A-11
Rubidium at 760 Torr
45% Mg, 50% RbNO3, 5% Binder

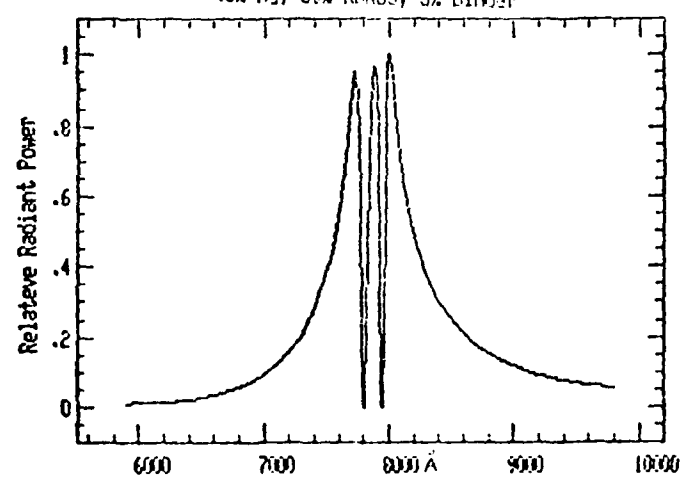

Figure A-12
Rubidium at 760 Torr
55% Mg, 40% RbNO3, 5% Binder

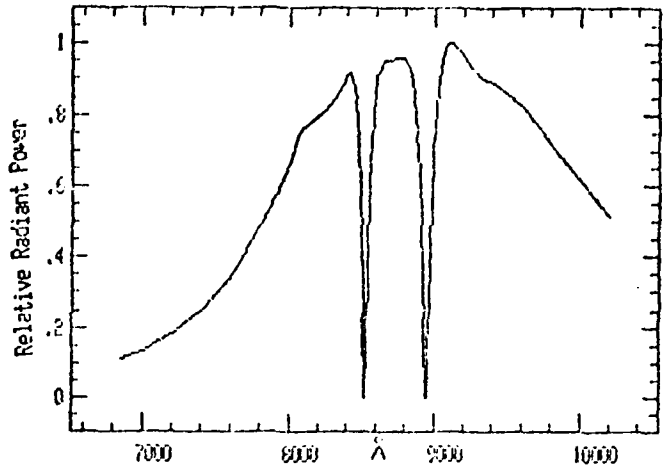

Figure A-13
Cesium at 760 Torr
25% Mg, 70% CsNO3, 5% Binder

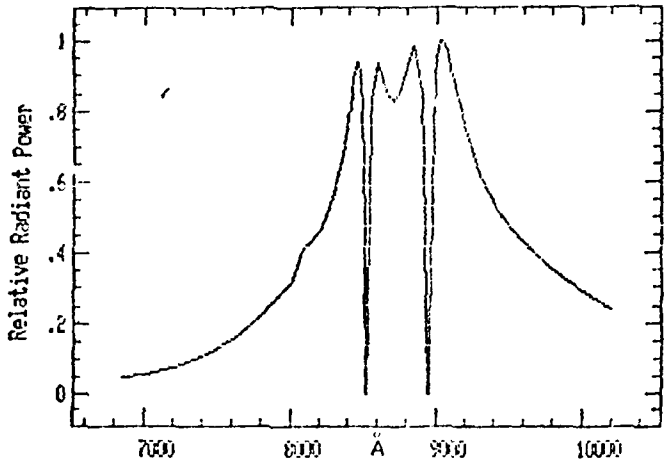

Figure A-14
Cesium at 760 Torr
35% Mg, 60% CsNO3, 5% Binder

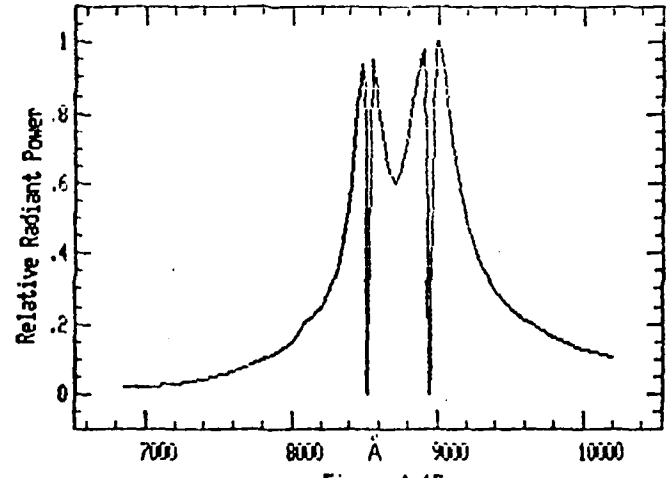

Figure A-15
Cesium at 760 Torr
45% Mg, 50% CsNO3, 5% Binder

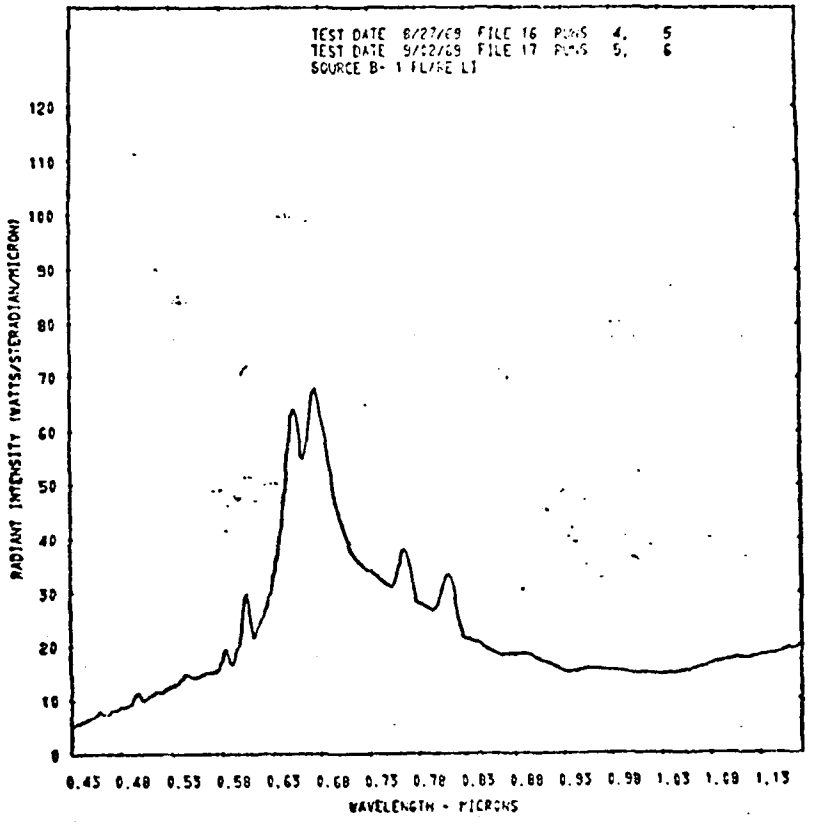

Figure A-16
Lithium at 630 Torr
48.8% Mg, 46.2% LiNO3, 5% Binder
Reproduced by Permission from Ref.(36)

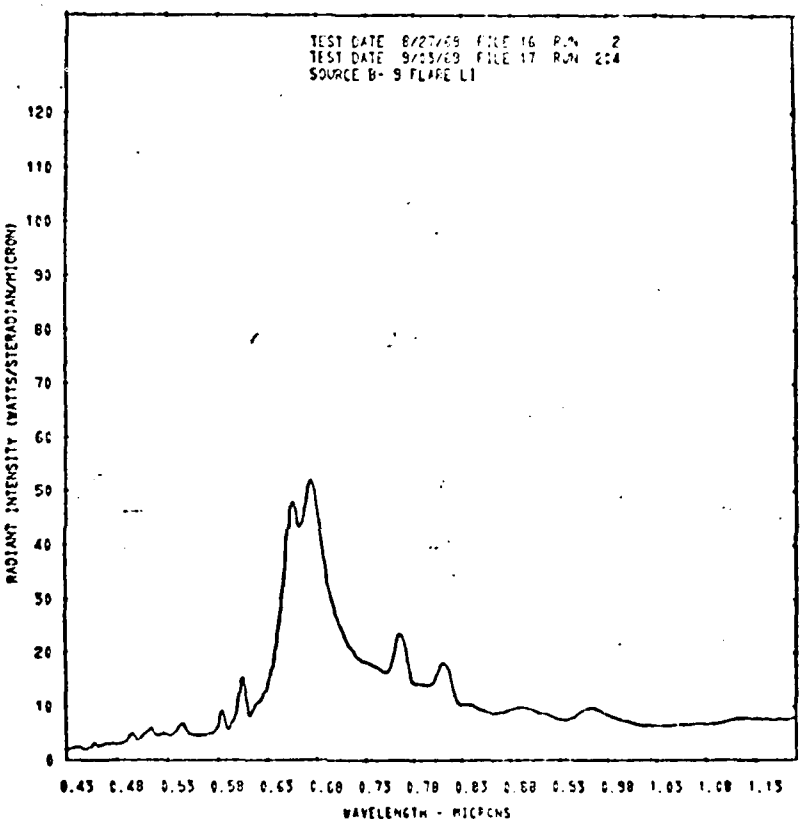

Figure A-17
Lithium at 630 Torr
61.6% Mg, 33.4% LiNO3, 5% Binder
Reproduced by Permission from Ref.(36)

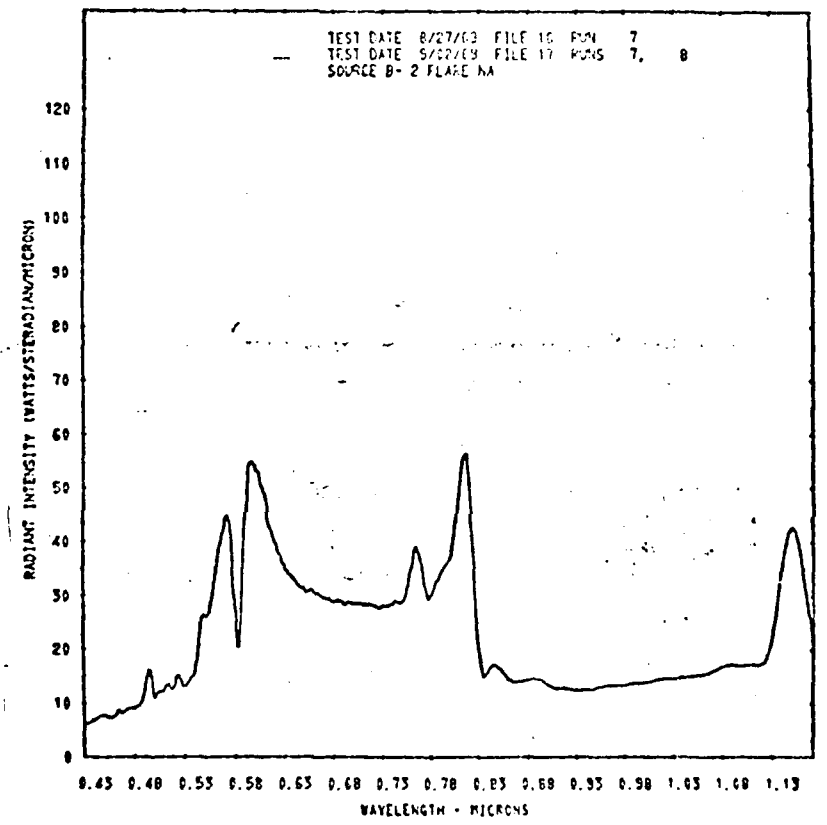

Figure A-18
Sodium at 630 Torr
43.8% Mg, 51.2% $NaNO_3$, 5% Binder
Reproduced by Permission from Ref.(36)

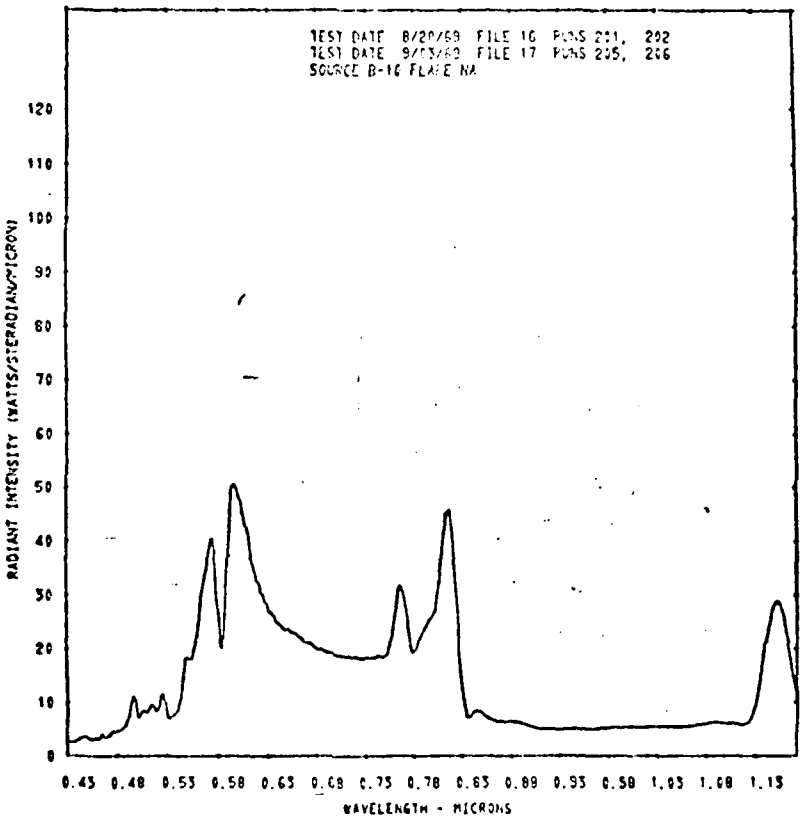

Figure A-19
Sodium at 630 Torr
57.0% Mg, 38.0% NaNO3, 5% Binder
Reproduced by Permission from Ref.(36)

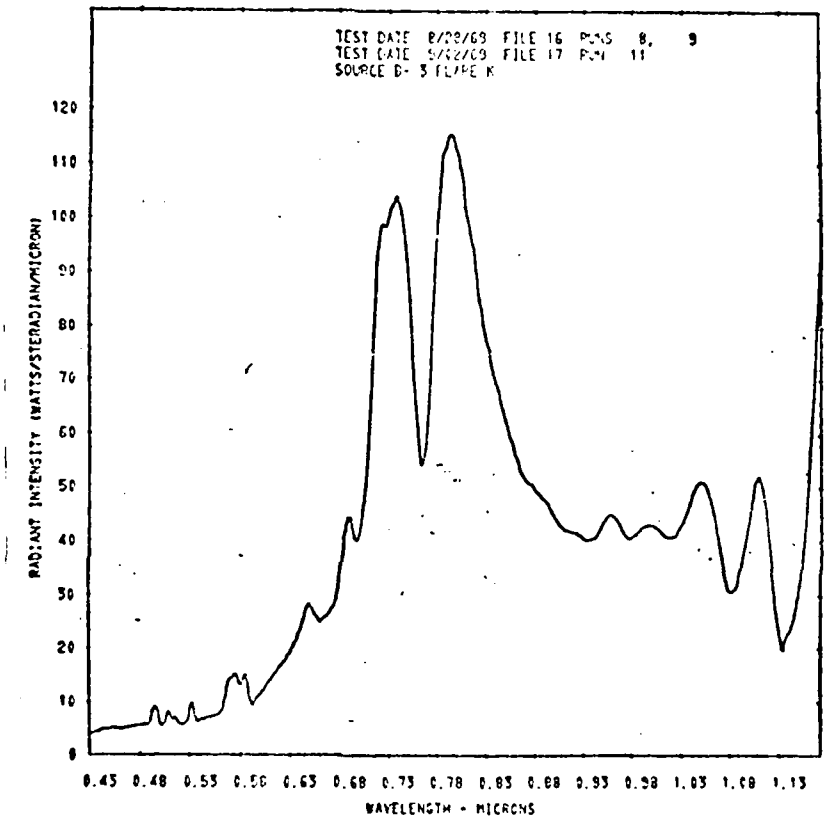

Figure A-20
Potassium at 630 Torr
39.8% Mg, 55.2% KNO3, 5% Binder
Reproduced by Permission from Ref.(36)

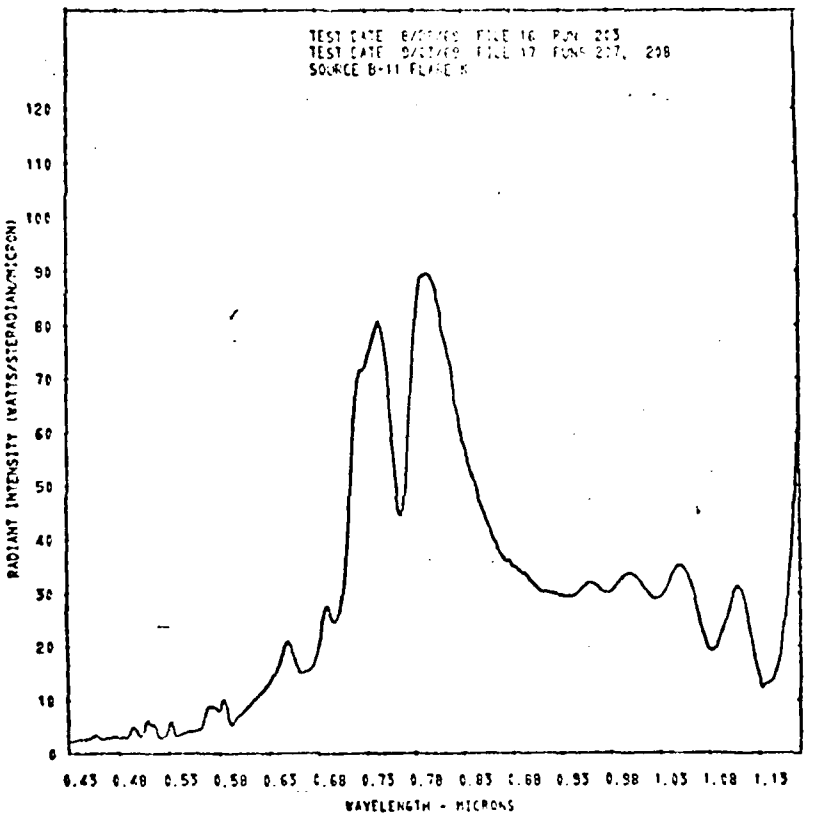

Figure A-21
Potassium at 630 Torr
53.0% Mg, 42.0% KNO3, 5% Binder
Reproduced by Permission from Ref.(36)

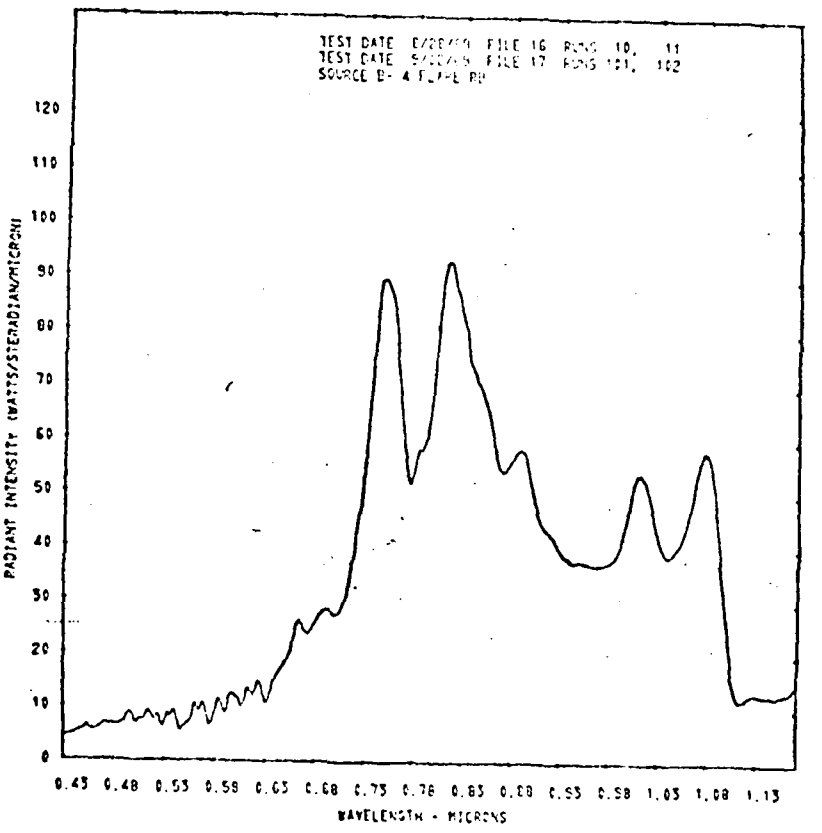

Figure A-22
Rubidium at 630 Torr
31.4% Mg, 63.6% RbNO3, 5% Binder
Reproduced by Permission from Ref.(36)

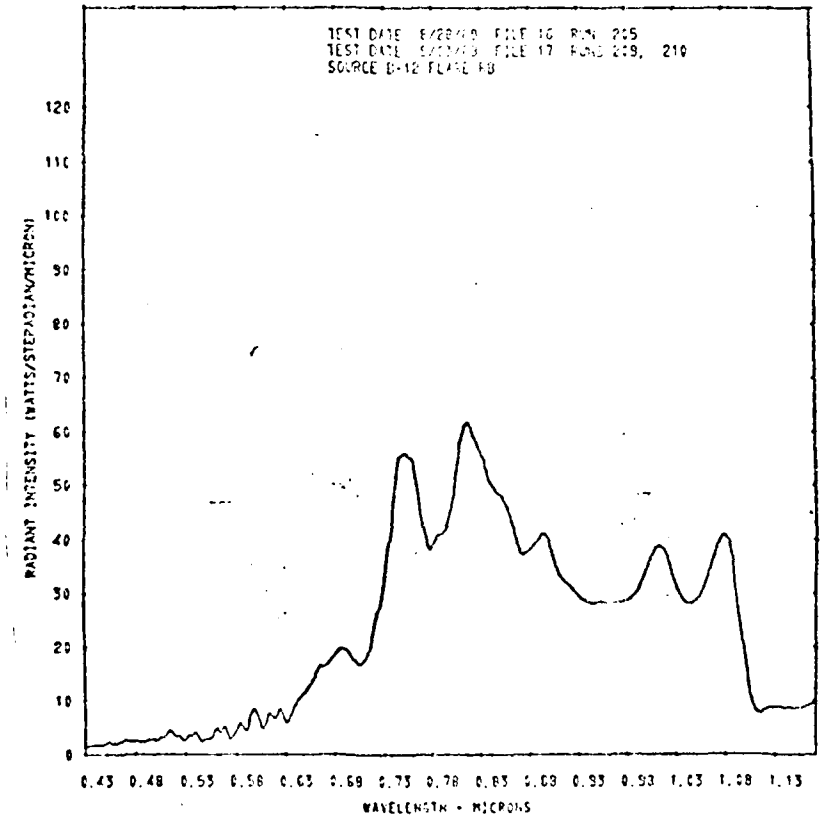

Figure A-23
Rubidium at 630 Torr
44.0% Mg, 51.0% $RbNO_3$, 5% Binder
Reproduced by Permission from Ref.(36)

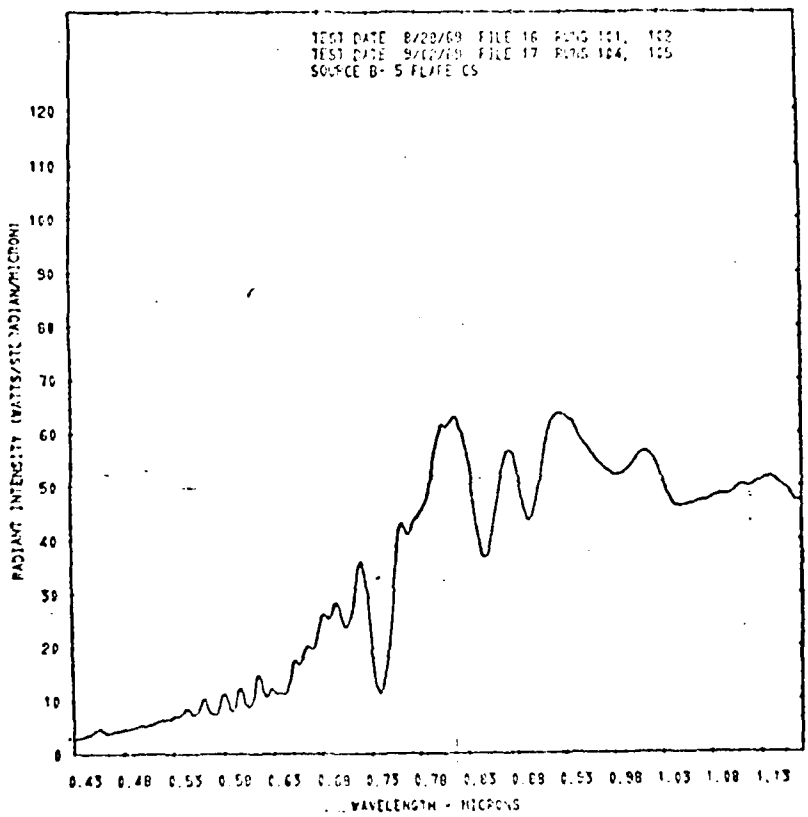

Figure A-24
Cesium at 630 Torr
25.9% Mg, 69.1% CsNO3, 5% Binder
Reproduced by Permission from Ref.(36)

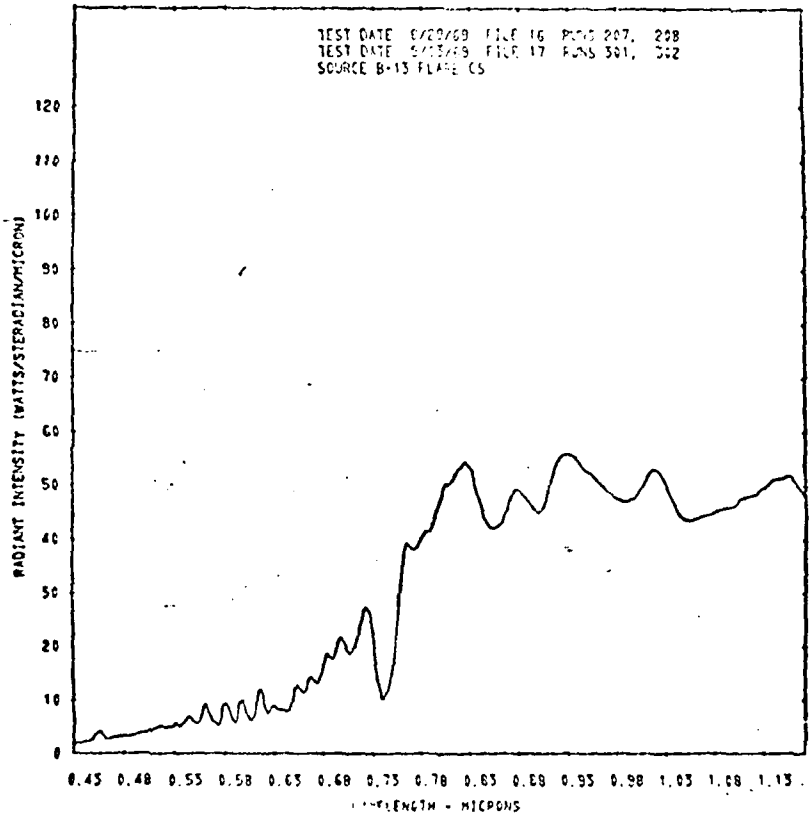

Figure A-25
Cesium at 630 Torr
37.6% Mg, 57.4% CsNO3, 5% Binder
Reproduced by Permission from Ref.(36)

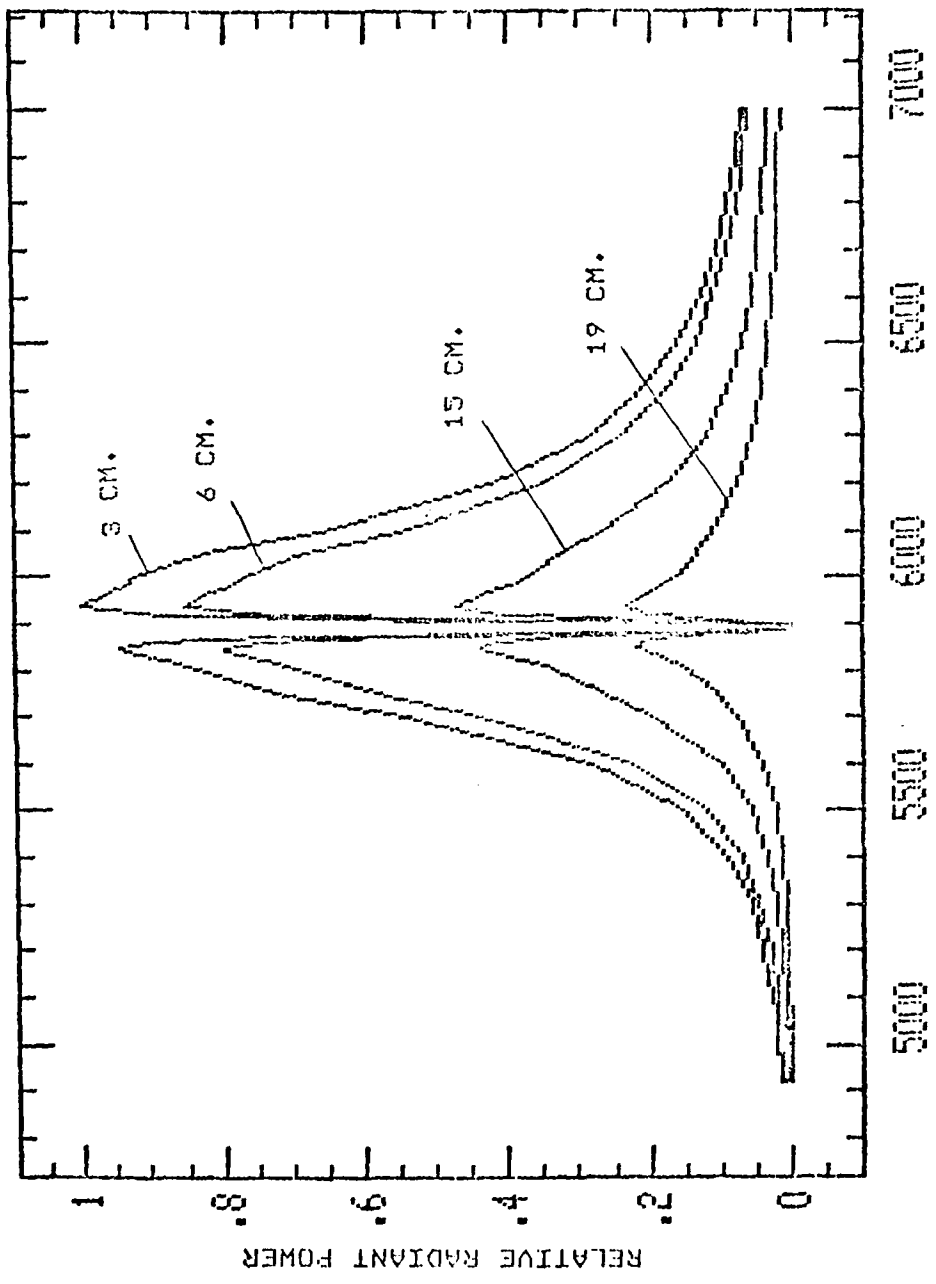

Figure A-26
Sodium at 760 Torr
Effect of Height Above Candle on Spectra
Calculated Values for 3,6,15 and 19 cm.
Above a 3 cm. Diameter Candle

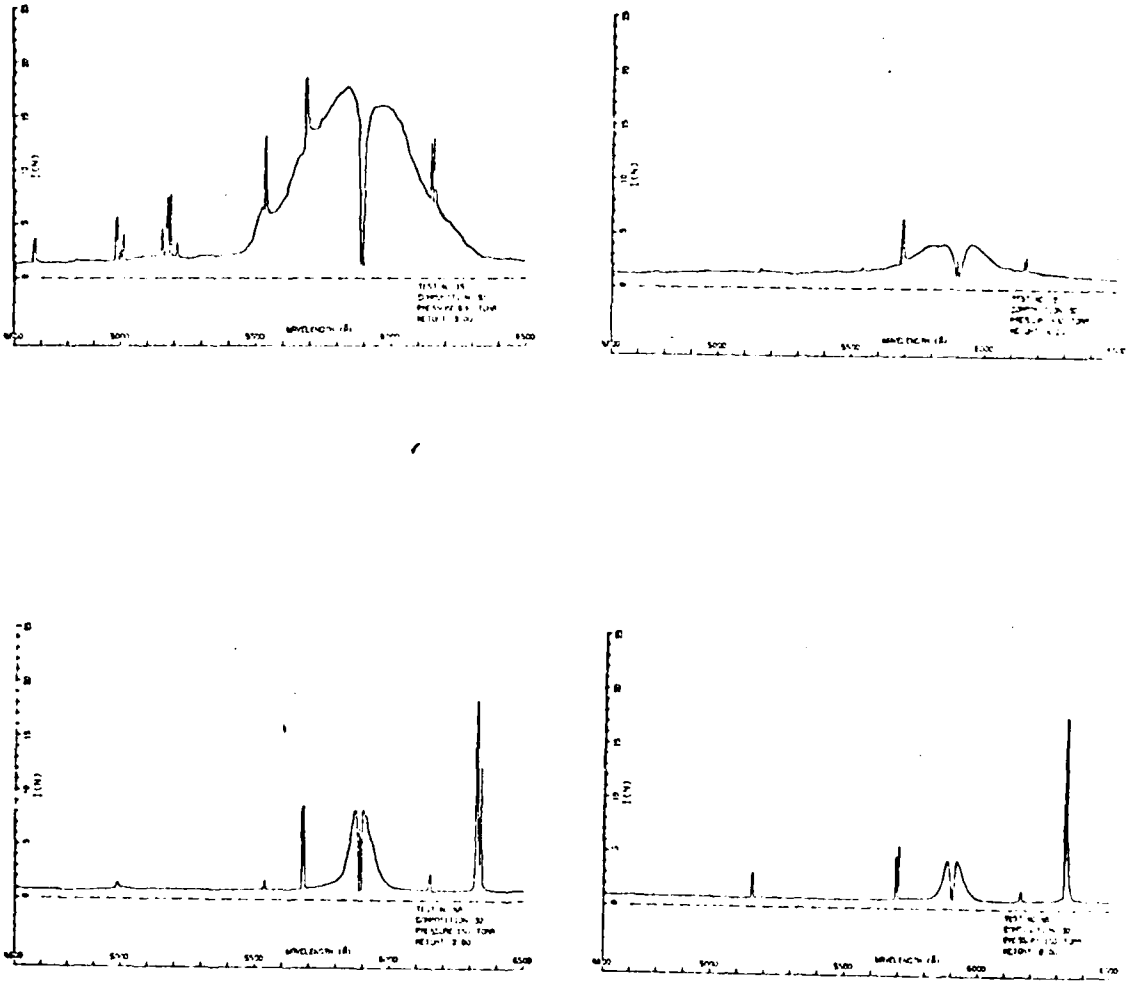

Figure A-27
Sodium
Experimental Spectra at Two Pressures
Showing Trend of Reduced Output Above Candle
Reproduced by Permission from Ref.(16)

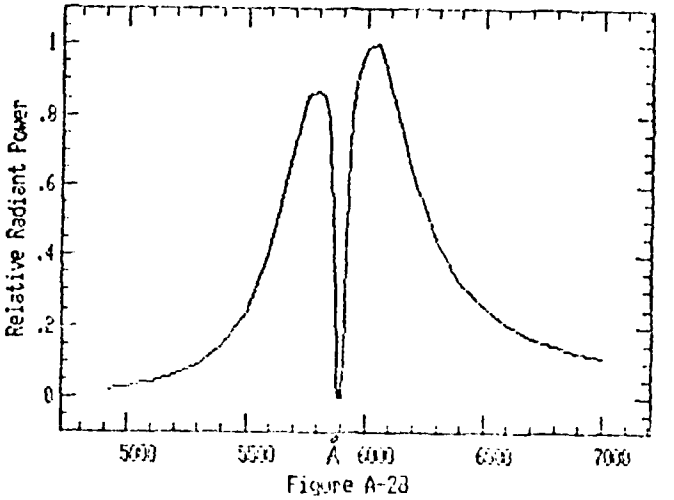

Figure A-28
Sodium at 760 Torr
Calculated Spectrum

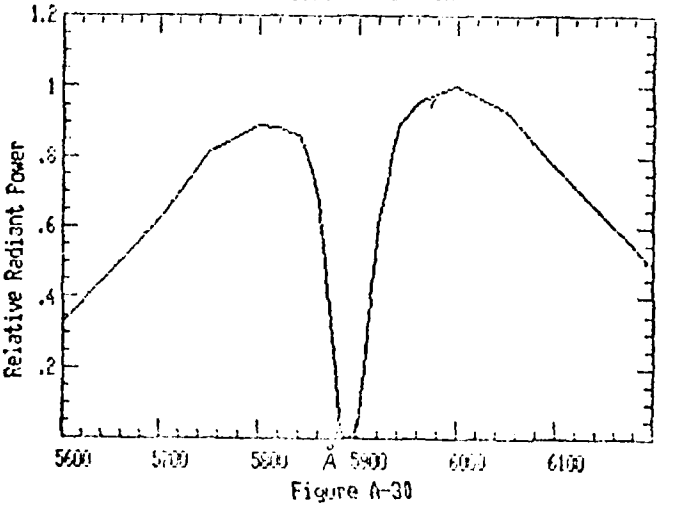

Figure A-30
Sodium at 630 Torr
Calculated Spectrum

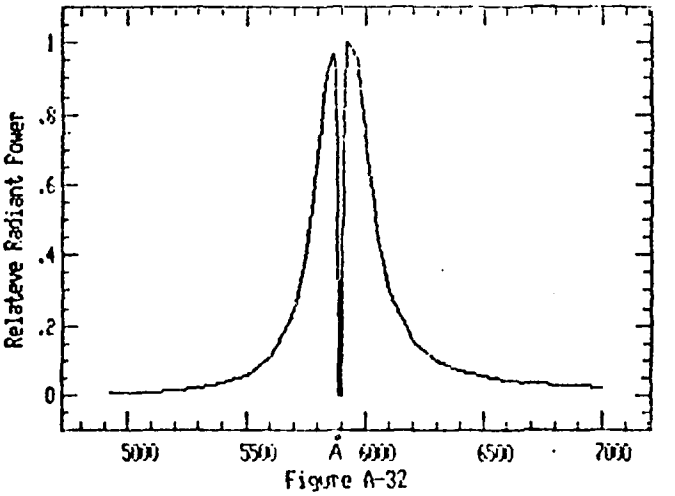

Figure A-32
Sodium at 300 Torr
Calculated Spectrum

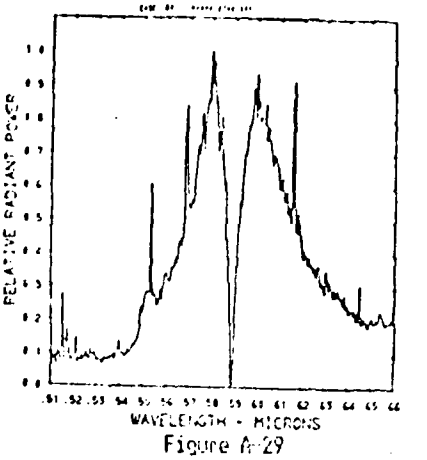

Figure A-29
Sodium at 760 Torr
Experimental Spectrum
Reproduced by Permission from Ref.(1)

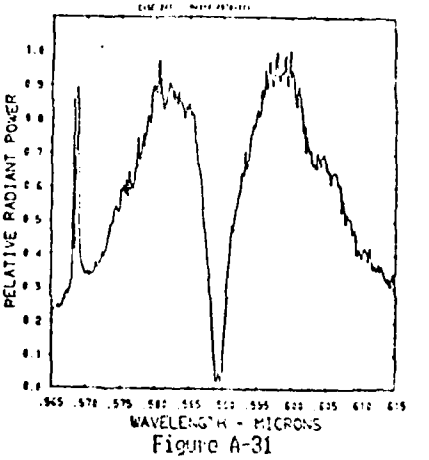

Figure A-31
Sodium at 630 Torr
Experimental Spectrum
Reproduced by Permission from Ref.(1)

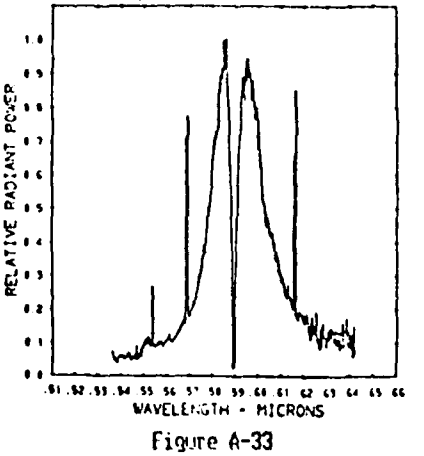

Figure A-33
Sodium at 300 Torr
Experimental Spectrum
Reproduced by Permission from Ref.(1)

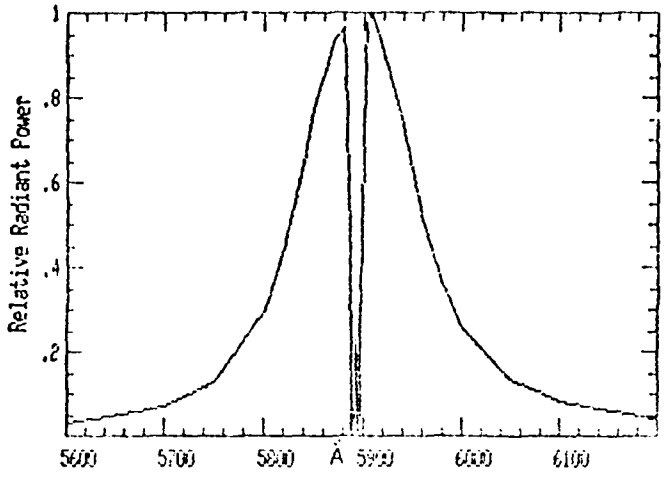

Figure A-34
Sodium at 150 Torr
Calculated Spectrum

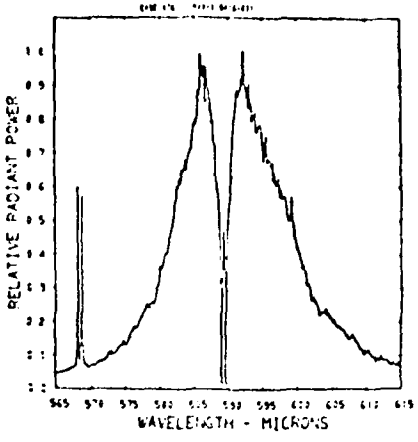

Figure A-35
Sodium at 150 Torr
Experimental Spectrum
Reproduced by Permission from Ref.(1)

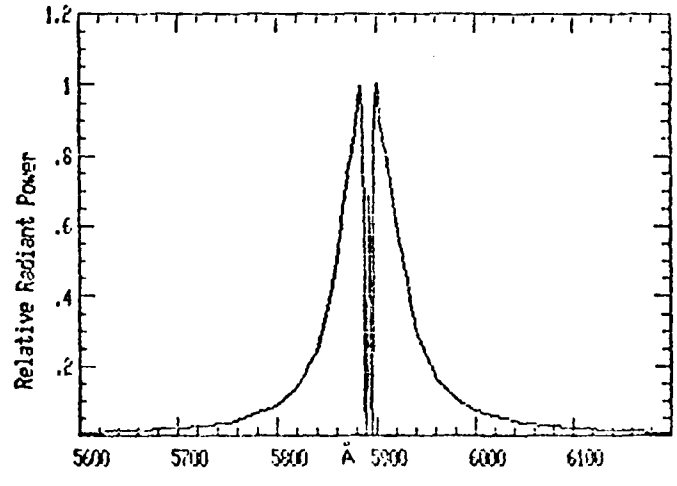

Figure A-36
Sodium at 75 Torr
Calculated Spectrum

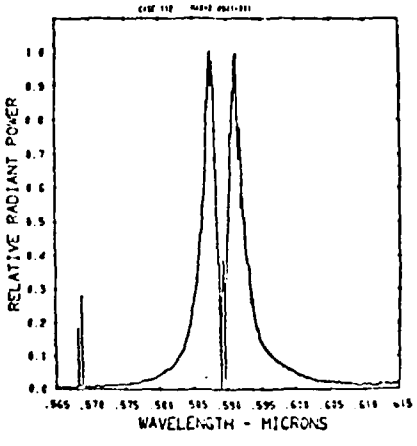

Figure A-37
Sodium at 75 Torr
Experimental Spectrum
Reproduced by Permission from Ref.(1)

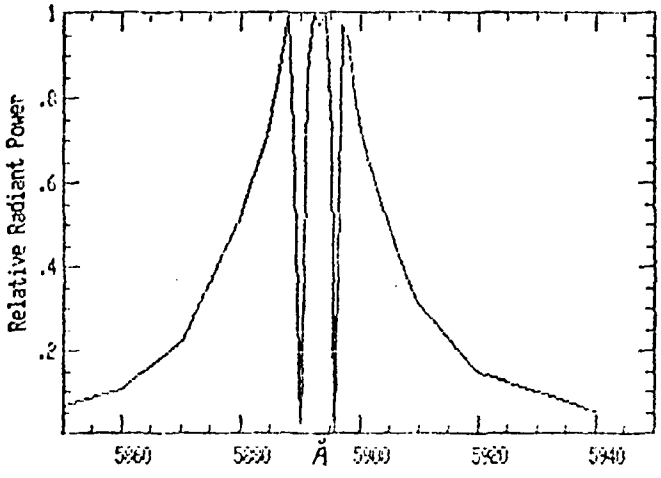

Figure A-38
Sodium at 30 Torr
Calculated Spectrum

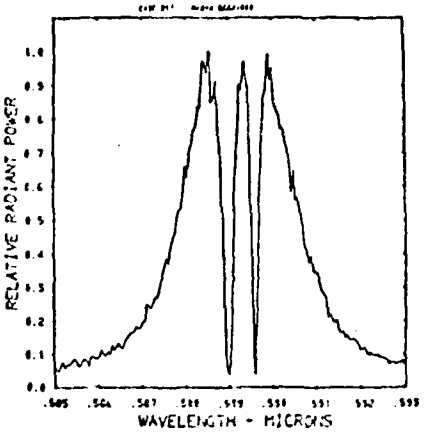

Figure A-39
Sodium at 30 Torr
Experimental Spectrum
Reproduced by Permission from Ref.(1)

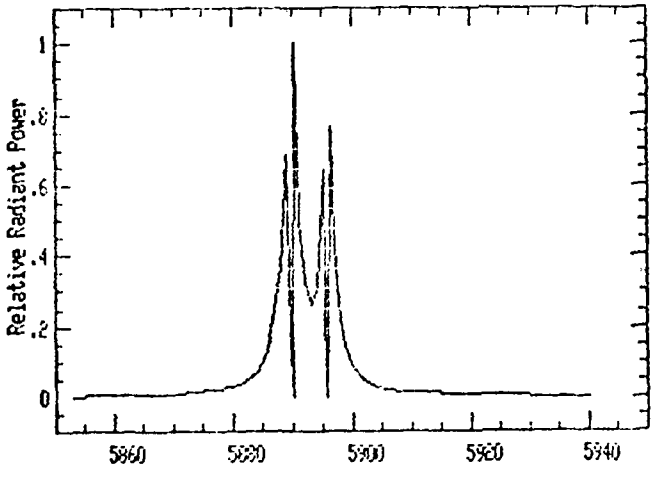

Figure A-40
Sodium at 6 Torr
Calculated Spectrum

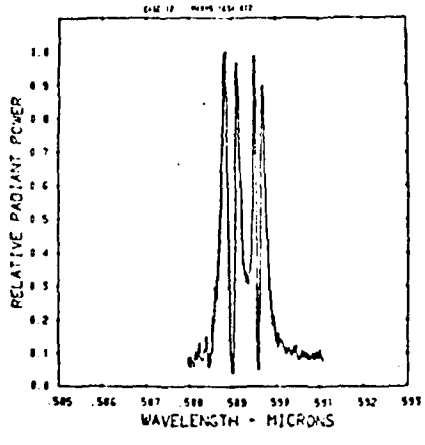

Figure A-41
Sodium at 6 Torr
Experimental Spectrum
Reproduced by Permission from Ref.(1)

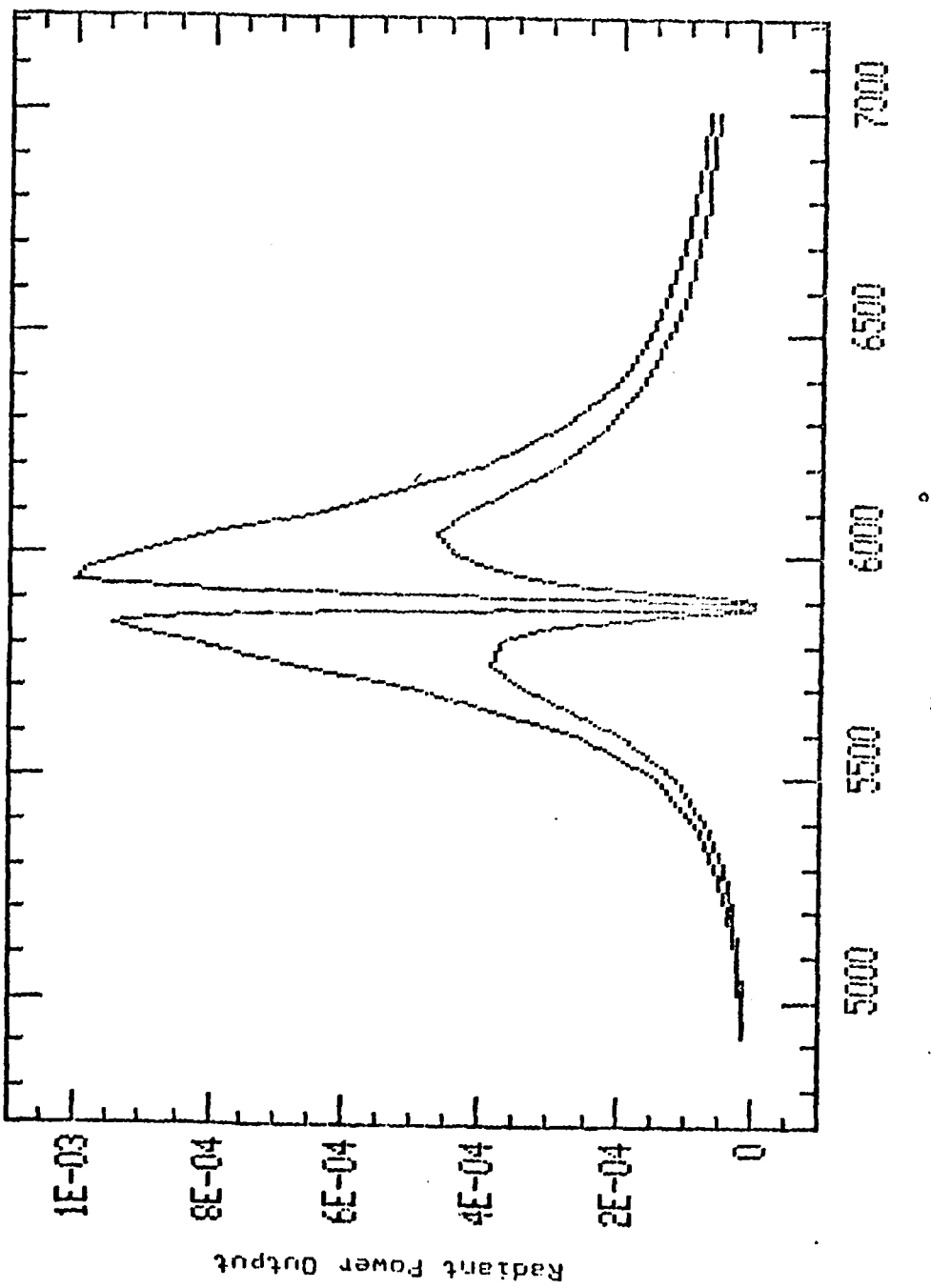

Figure A-42
Sodium at 760 Torr
Integrated Spectra for 40% and 50% Mg and 5% Binder

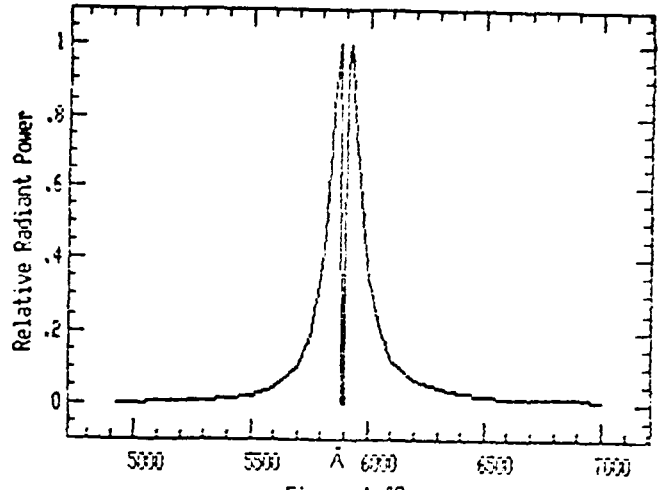

Figure A-43
Sodium at 760 Torr
50% Mg, 45% NaNO3, 5% Binder
Calculated at 2.4 cm. Above a 1.2 cm. Candle

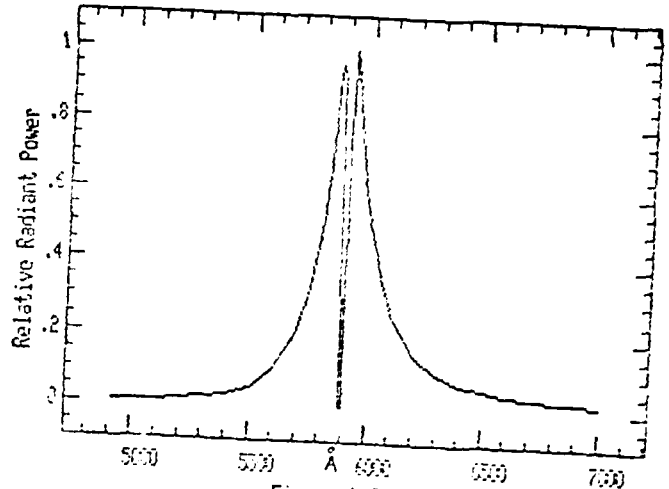

Figure A-44
Sodium at 760 Torr
50% Mg, 45% NaNO3, 5% Binder
Calculated at 6.6 cm. Above a 3.3 cm. Candle

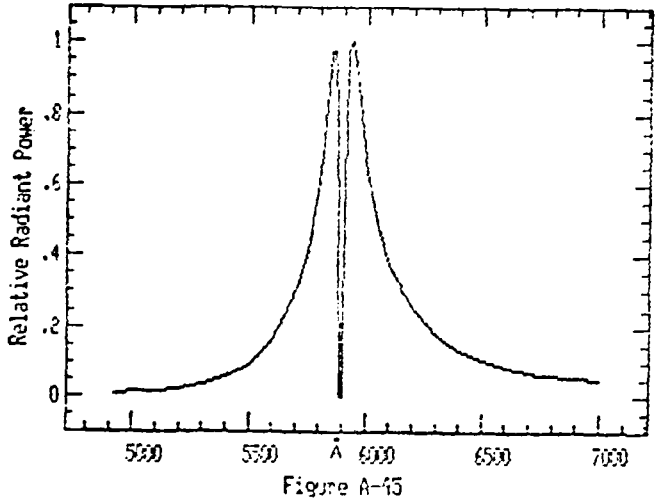

Figure A-45
Sodium at 760 Torr
50% Mg, 45% NaNO3, 5% Binder
Calculated at 12 cm. Above a 6.0 cm. Candle

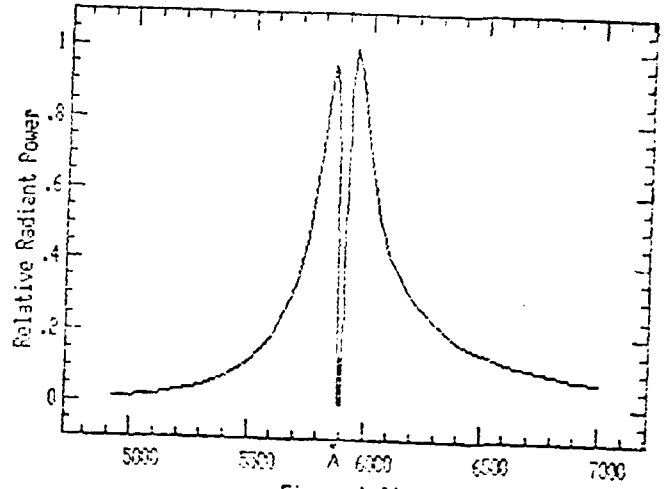

Figure A-46
Sodium at 760 Torr
50% Mg, 45% NaNO3, 5% Binder
Calculated at 21.6 cm. Above a 10.8 cm. Candle

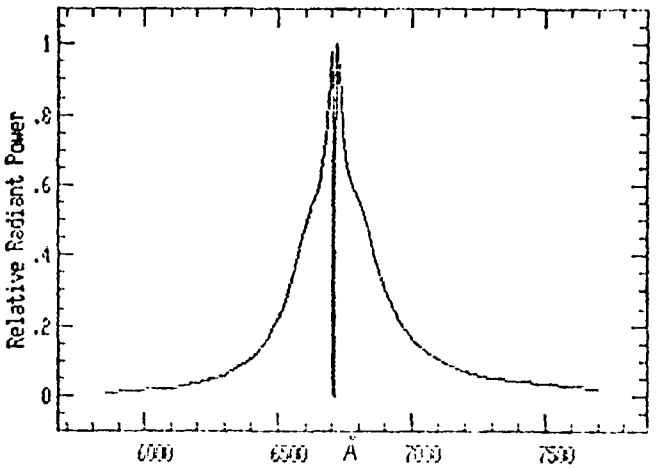

Figure A-47
Lithium at 760 Torr
Calculated Spectrum

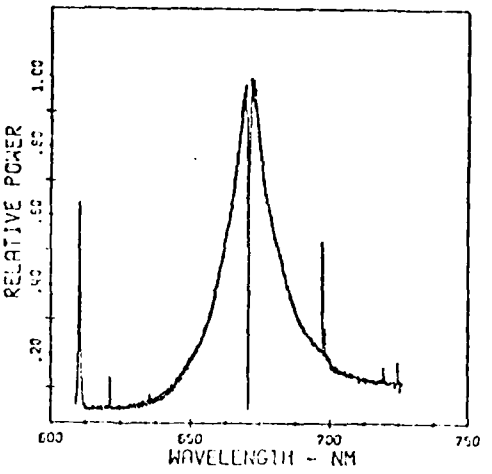

Figure A-48
Lithium at 760 Torr
Experimental Spectrum
Reproduced by Permission from Ref.(10)

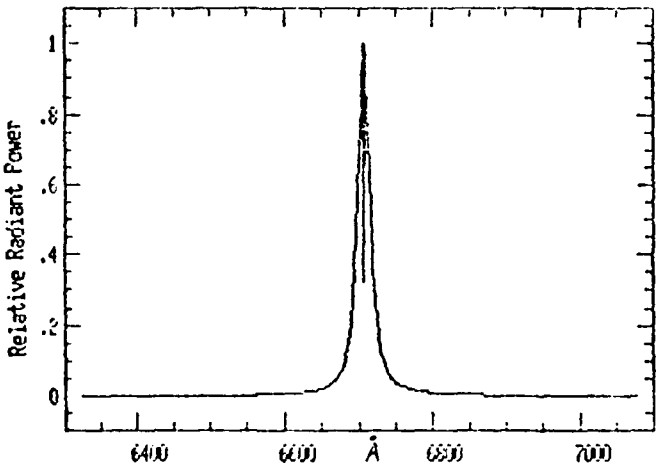

Figure A-49
Lithium at 760 Torr
Low Lithium Concentration
Calculated Spectrum

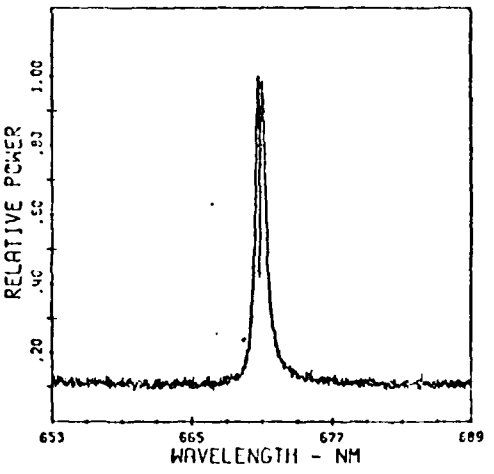

Figure A-50
Lithium at 760 Torr
Low Lithium Concentration
Experimental Spectrum
Reproduced by Permission from Ref.(10)

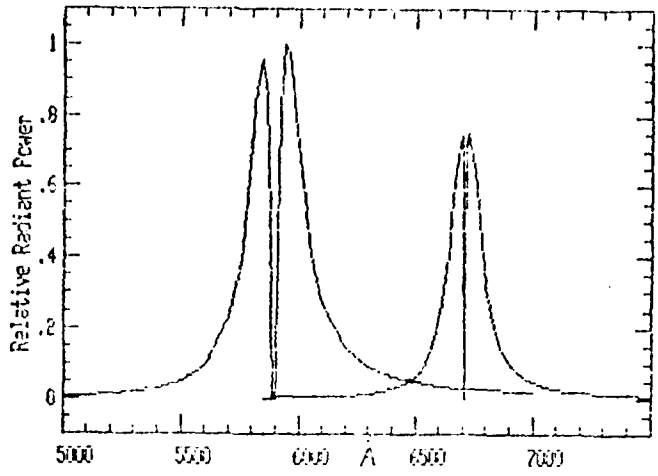

Figure A-51
Sodium and Lithium at 760 Torr
Calculated Spectra

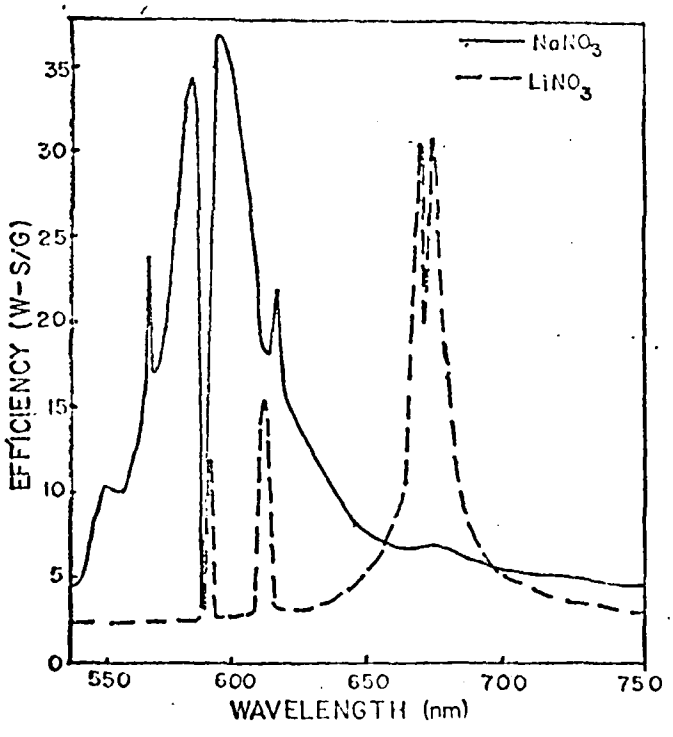

Figure A-52
Sodium and Lithium at 760 Torr
Experimental Spectra
Reproduced from Ref.(31)

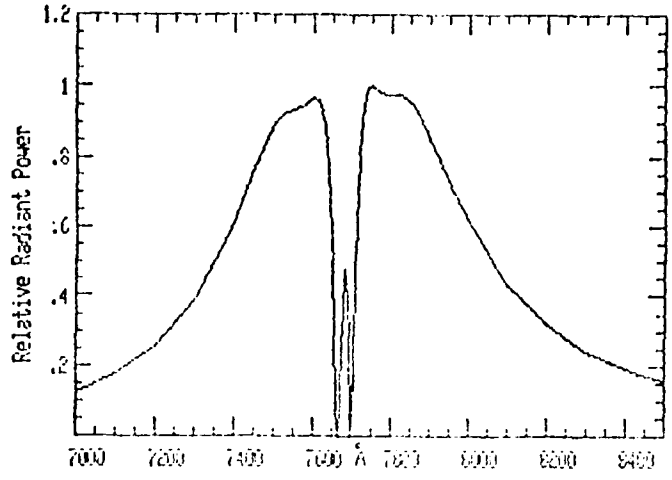

Figure A-53
Potassium at 380 Torr
40% Mg, 55% KNO3, 5% Binder

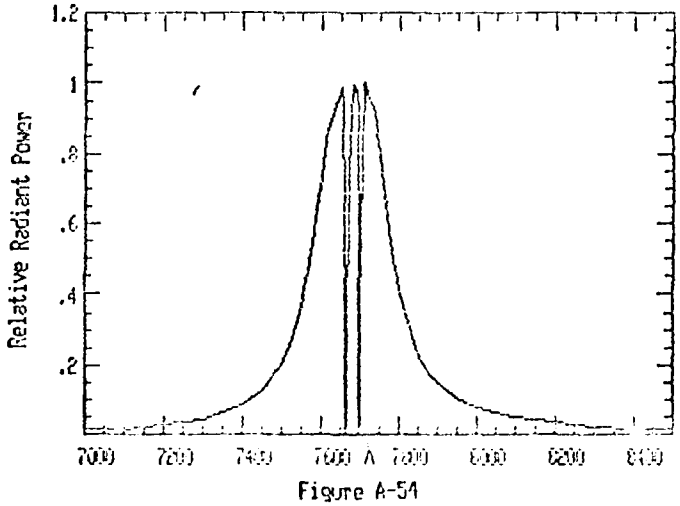

Figure A-54
Potassium at 76 Torr
40% Mg, 55% KNO3, 5% Binder

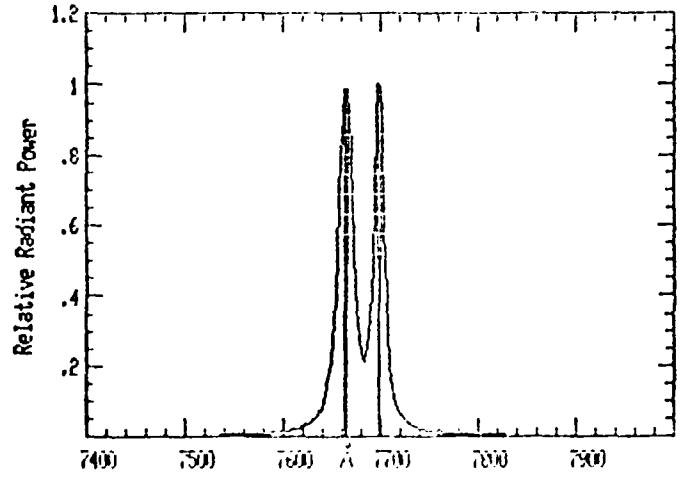

Figure A-55
Potassium at 6 Torr
40% Mg, 55% KNO3, 5% Binder

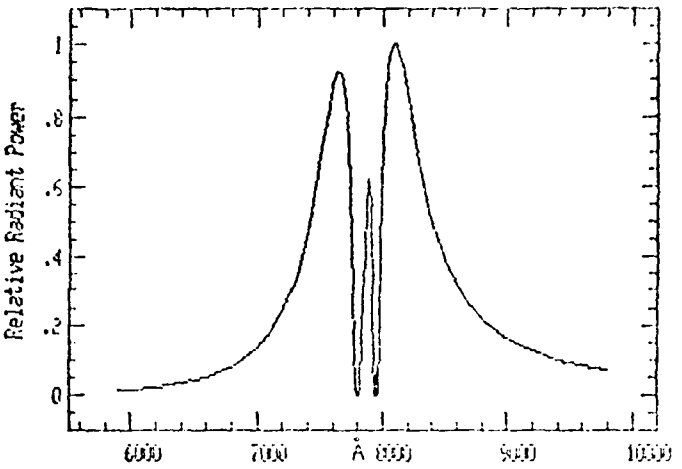

Figure A-56
Rubidium at 300 Torr
35% Mg, 60% RbNO3, 5% Binder

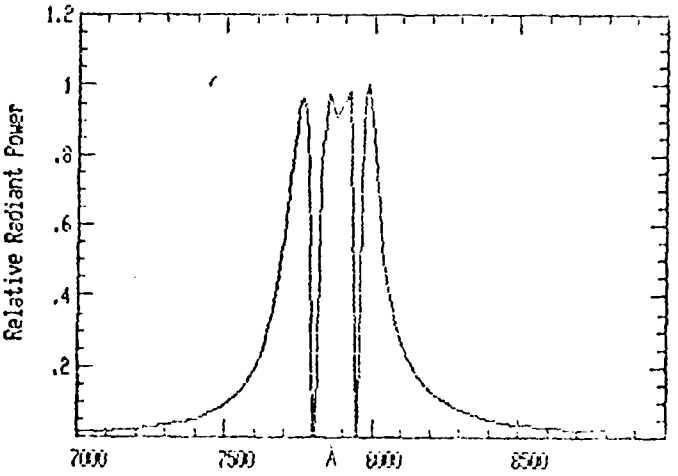

Figure A-57
Rubidium at 76 Torr
35% Mg, 60% RbNO3, 5% Binder

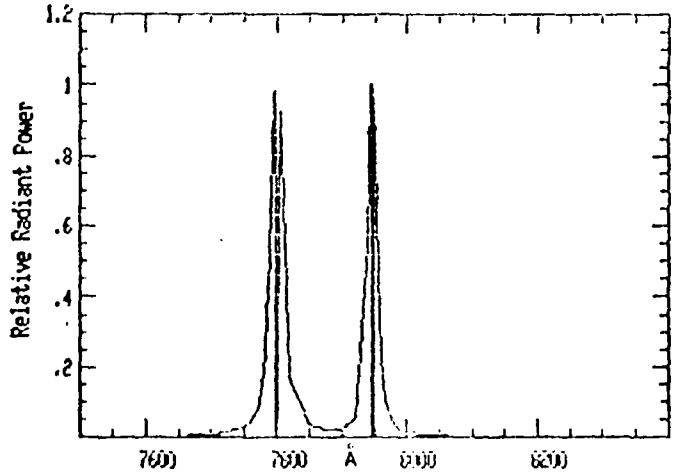

Figure A-58
Rubidium at 6 Torr
35% Mg, 60% RbNO3, 5% Binder

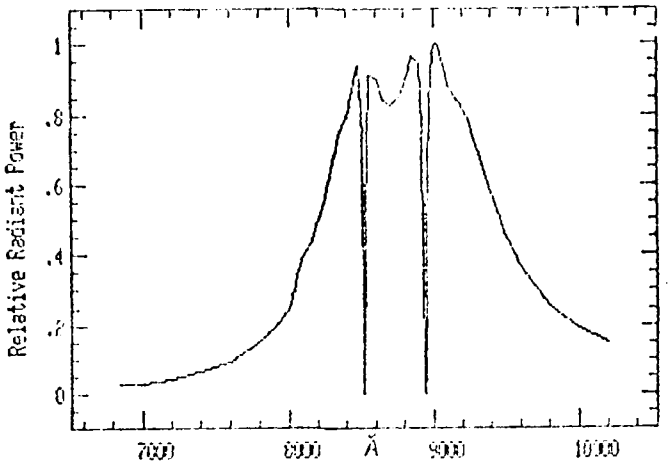

Figure A-59
Cesium at 360 Torr
25% Mg, 70% CsNO3, 5% Binder

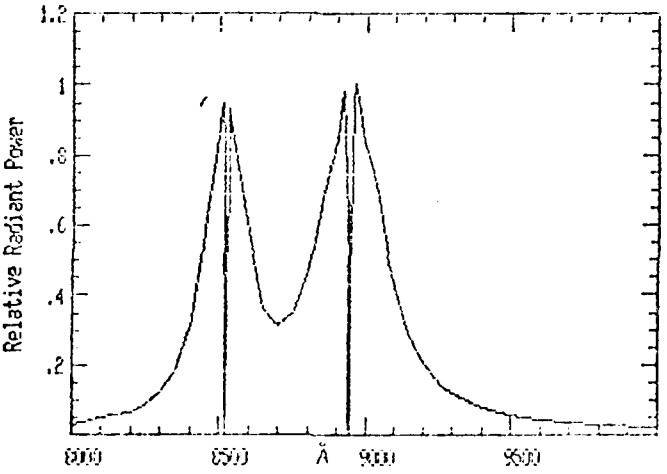

Figure A-60
Cesium at 76 Torr
25% Mg, 70% CsNO3, 5% Binder

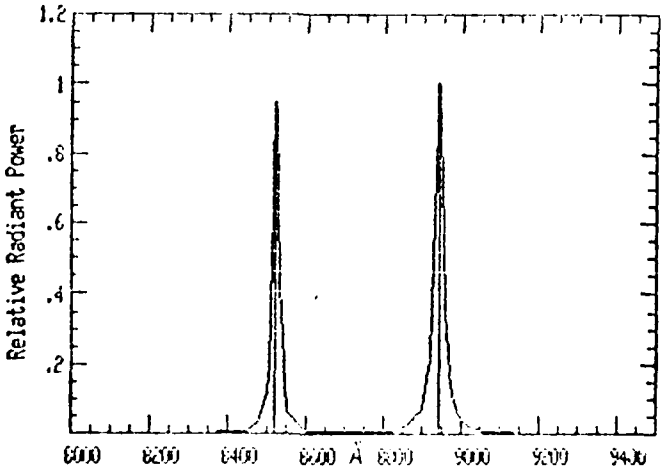

Figure A-61
Cesium at 6 Torr
25% Mg, 70% CsNO3, 5% Binder

APPENDIX B

Temperature Correction and Optical Thickness

APPENDIX B

Temperature Correction Calculations

The correction of temperature loss is an important factor in the use of the flame model. Figures B-1 and B-2 show graphically the assumptions made concerning heat loss along the axis and radially across the plume. The temperature along the centerline of the flare plume axis is defined by the equation:

$$TCL = \frac{(1800 - T_o)}{(d/F)^2} L^2 + T_o \qquad (1)$$

where L is the height above the candle surface and T_o is the adiabatic temperature at 0% air. The definitions of d and F are the same as discussed in the text. A general solution for the maximum temperature is defined as:

$$TMAX = TB - 555(FL/d)^2 D^{1/3} \qquad (2)$$

where TB is the maximum temperature calculated for the stoichiometric mixture with air. This temperature will always be near 3000 °K, the melting point of magnesium oxide.

TPRIME is the calculated temperature at the centerline determined from the interpolated values in the table of values for each Z index position. TJ is the interpolated maximum temperature at the stoichiometric air ratio for the given composition. Now, to compute the temperature correction factors, the following equations are used:

For 1 <= Z <= ZMAX,

$$TCORR = T(Z)\left[1 + (TMAX/TJ - 1)\left(\frac{Z-1}{ZMAX-1}\right)^2\right] \qquad (3)$$

where ZMAX is the index value where the stoichiometric temperature occurs.

For ZMAX < Z <= (I+1)/2

$$TCORR = T(Z)\left\{\left[\frac{Z-ZMAX}{\left(\frac{I+1}{2}\right)-ZMAX}\right]\left[\frac{TCL}{TFINAL} - \frac{TMAX}{TJ}\right] + \frac{TMAX}{TJ}\right\} \qquad (4)$$

where I is the Z index value for the back of the plume. The corrected values for T(Z) are then mirror-imaged from the centerline to I.

The Voigt function α parameter values are corrected by dividing each indexed value by the same computed correction factors and mirror-imaging the values from the centerline to I also.

Optical Thickness Calculation

The values for the optical thickness are determined by calculating the optical density at each index point and storing it in an array. The optical density is

$$\tau_Z = \tau_{Z-1} + HZ\left\{\left[\frac{N_1}{ng\,T_0}\right]_{Z-1} + \frac{1}{2}\left[\left(\frac{N_1}{ng\,T_0}\right)_Z - \left(\frac{N_1}{ng\,T_0}\right)_{Z-1}\right]\right\} \qquad (5)$$

for Z = 2,3,4.....I where $\tau_1 = 0$ and HZ is defined as

$$HZ = 1.33266 \times 10^{-24}(M\lambda_0^3 OS) \qquad (6)$$

where M is the molecular weight of the metal, λ_0 is the resonance wavelength, and OS is the oscillator strength. Now, optical

thickness is

$$OP(z) = OP(z-1) + \frac{DE}{2}\left[\sigma(z) + \sigma(z-1)\right] \qquad (7)$$

where OP(1)=0 and DE is the depth increment. The values for optical thickness are stored in the computer program as an array for use in the calculation of the radiant energy profile.

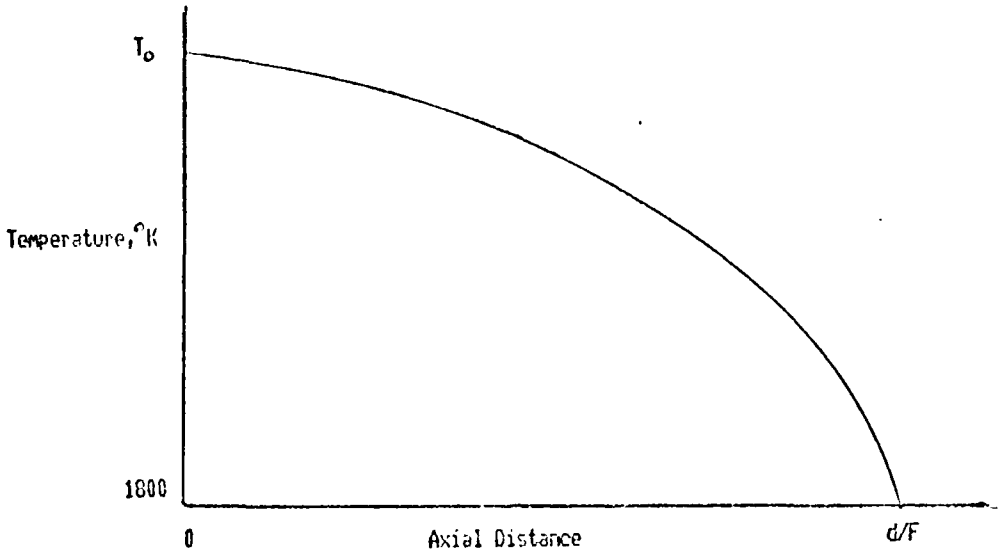

Figure B-1
Temperature Loss Along the Plume Axis

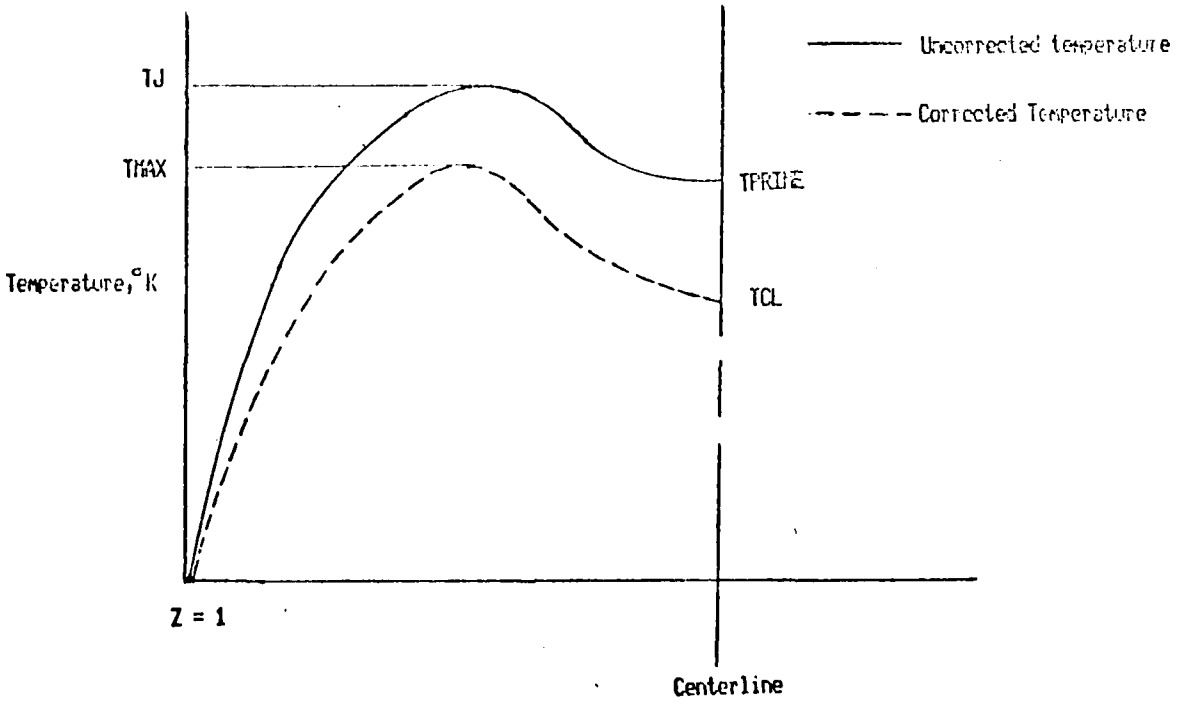

Figure B-2
Radial Temperature Correction Profile

APPENDIX C

Program Listings

```
5 REM:RADTRANS
10 DIMA(400),PA(10,3),TT(400),TAU(400,3),VO(75,2),OP(400),RV
(75),IV(75)
     :DEFINTJ,K,Z
15 NA=6.024E23
     :C1=3.71415E24
     :C2=1.4388E8
     :REM C1=2*PI*h*c*c* TO GIVE BT IN WATTS/CM**2/MICRON
16 GOSUB4000
20 REM A(400) IS THE ARRAY FOR %AIR AT EACH Z INDEX
21 REM PA(9,4) IS THE ARRAY FOR THE TABLE OF VALUES
22 REM THE 1st TERM REPRESENTS THE % AIR
23 REM THE 2nd TERM REPRESENTS TEMP,VOIGT a,MOLES GAS,MOLES
METAL
24 REM TAU(400,3) IS AN ARRAY HOLDING THE INTERPOLATED VALUE
S
25 REM TT(400) IS AN ARRAY OF CALCULATED OPTICAL DENSITY VAL
UES
26 REM OP(400) IS THE OPTICAL THICKNESS FOR EACH Z INDEX
27 REM VO(75,2) IS AN ARRAY FOR WAVELENGTH,SLOPE AND INTERCE
PT
28 REM THE VOIGT FUNCTION PHI IS CALCULATED FROM VO(75,2)
35 CLS
     :INPUT"ENTER CANDLE DIAMETER IN CM.";D
42 PRINT
     :PRINT"FUEL FRACTION AT TEMP. ";TF;" = ";F
     :PRINT
45 DE=.1
     :REM DE IS THE DELTA D FOR DEPTH IN THE PLUME (CM)
50 INPUT"ENTER HEIGHT ABOVE CANDLE IN CM.";L
55 DY=D/2
     :F1=SQR(1+1/F)
     :PC=(760/PR)[.333333
56 REM DY IS THE REFERENCE X COORDINATE FOR THE CANDLE EDGE
60 LM=(D/F)*PC
     :LX=LM/(F1*SQR(PC)+1)[2
61 REM LM IS THE MAXIMUM LENGTH OF THE PLUME
62 REM LX IS THE CROSS-OVER HEIGHT FOR THE 0% AIR LINES
63 REM PR IS THE PRESSURE IN TORR
65 DM=SQR(PC*(D*L+D*D))
     :D1=-(DM/2)
     :D2=DY*(F1*SQR(PC)+1)*SQR(F*L/D/PC)-DY
66 REM DM IS THE DIAMETER OF THE PLUME AT HEIGHT L
67 REM D1 IS THE OUTSIDE BOUNDARY FOR 90% AIR
68 REM D2 IS THE INSIDE BOUNDARY FOR 0% AIR
70 I=INT(DM/DE+.5)
71 REM I IS THE NUMBER OF STEPS THE PLUME IS DIVIDED INTO
75 IFI=INT(I/2)*2THENI=I+1
80 IM=(I+1)/2
```

```
     :K=INT(D2/DE)
81 REM IM IS THE MIDPOINT INDEX VALUE
82 REM K IS THE INDEX VALUE FOR THE 0% AIR LINE
85 IFL<=LXTHENGOSUB1000ELSEGOSUB2000
90 FORZ=1TOIM
91 REM ZMAX IS THE INDEX VALUE FOR THE MAXIMUM TEMPERATURE
95 IFTAU(Z,0)>TAU(Z-1,0)THENZMAX=Z
100 NEXTZ
112 TPRIME=TAU(IM,0)
     :TJ=TAU(ZMAX,0)
115 TCL=((TF-PA(0,0))*(L/LM)[2)+PA(0,0)
116 REM TCL IS THE CENTERLINE TEMP CORRECTED FOR HEAT LOSS
117 REM TF IS THE TEMPERATURE LIMIT FOR EXCITATION
120 TMAX=TB-555*(D[.333333)*(L/LM)[2
     :Q=INT(A(IM)/10)
     :Q1=(A(IM)-Q*10)/10
     :TPRIME=(PA(Q+1,0)-PA(Q,0))*Q1+PA(Q,0)
121 REM TMAX IS THE MAX TEMP CORRECTED FOR HEAT LOSS
122 REM TB IS THE MAXIMUM FLAME TEMPERATURE
123 REM TPRIME IS THE CENTERLINE TEMP WITHOUT HEAT LOSS CORR
ECTION
125 T1=TMAX/TJ
     :T2=TCL/TPRIME
130 FORZ=2TOZMAX
     :TAU(Z,0)=TAU(Z,0)*(1+(T1-1)*((Z-1)/(ZMAX-1))[2)
132 TAU(Z,1)=TAU(Z,1)/(1+(T1-1)*((Z-1)/(ZMAX-1))[2)
     :NEXTZ
135 IFZMAX=IMTHEN150
140 IFL<LXTHENIX=(IM+K)ELSEIX=IM
145 FORZ=(ZMAX+1)TOIM
     :TAU(Z,0)=TAU(Z,0)*((Z-ZMAX)[2/(IM-ZMAX)[2*(T2-T1)+T1)
148 TAU(Z,1)=TAU(Z,1)/((Z-ZMAX)[2/(IM-ZMAX)[2*(T2-T1)+T1)
     :NEXTZ
149 IFIX<IMTHENFORZ=IXTOIM
     :TAU(Z,0)=TAU(Z,0)*T2
     :TAU(Z,1)=TAU(Z,1)/T2
     :NEXTZ
150 FORZ=(IM+1)TOI
     :FORX=0TO3
     :TAU(Z,X)=TAU(I-Z+1,X)
     :NEXTX,Z
155 HZ=1.33266E-24*MW*(XLAM[3)*OS
160 TT(0)=0
     :FORZ=2TOI
     :TT(Z)=HZ*(TAU(Z,3))
     :NEXTZ
165 OP(1)=0
     :FORZ=2TOI
```

```
     :OP(Z)=OP(Z-1)+DE/2*(TT(Z-1)+TT(Z))
     :NEXTZ
170 GOSUB3000
171 RE=TAU(IM,3)/100
172 FORZ=2TO10
     :IFTAU(Z,3)>=RETHENRJ=Z
     :Z=11
     :NEXTELSENEXT
173 LPRINT"CASE NO. ";CN$;" FOR ";ID$;" WITH PRESSURE = ";PR
;" TORR AND HEIGHT ABOVE CANDLE = ";L
175 FORR=1TONR
     :WL=VO(R,0)
     :SL=VO(R,1)
     :IN=VO(R,2)
176 PRINT@512,"WAVELENGTH NO. = ";R
180 Z=RJ
     :GOSUB2100
     :E=OP(Z)*PHI
181 IFE>60THENE=60
182 IFE<-60THENE=60
183 TERM(1)=BT*PHI/EXP(E)
185 Z=I-RJ+1
     :GOSUB2100
     :E=OP(Z)*PHI
186 IFE>60THENTERM(2)=0
     :GOTO190
187 TERM(2)=PHI*BT/EXP(OP(Z)*PHI)
190 SUM=0
     :FORZ=(RJ+1)TO(I-RJ)STEP2
     :GOSUB2100
     :E=OP(Z)*PHI
191 IFE>60THENE=60
192 IFE<-60THENE=60
195 SUM=SUM+PHI*BT/EXP(E)
     :NEXTZ
200 TERM(3)=2*SUM
     :SUM=0
210 FORZ=(RJ+2)TO(I-RJ-1)STEP2
     :GOSUB2100
     :E=OP(Z)*PHI
211 IFE>60THENE=60
212 IFE<-60THENE=60
215 SUM=SUM+PHI*BT/EXP(E)
     :NEXTZ
220 TERM(4)=4*SUM
230 IV(R)=DE/3*(TERM(1)+TERM(2)+TERM(3)+TERM(4))
240 PRINT@832,VO(R,0),IV(R)
250 NEXTR
```

```
260     (0)=0
         RR=1TONN
          IV(R)>IV(0)THENIV(0)=IV(R)
265      R
270     R=1TONN
       :RV(R)=IV(R)/IV(0)
272 LPRINTVO(R,0),IV(R),RV(R)
275 NEXTR
       :CLOSE3
280 LINEINPUT"ENTER THE NAME OF THE FILE";NM$
281 OPEN"O",3,NM$
       :PRINT#3,NN
285 FORQ=1TONN
       :PRINT#3,VO(Q,0),IV(Q),RV(Q)
       :NEXTQ
       :CLOSE3
300 RUN"AUTOPLOT
1000 J=IM+K
1010 FORZ=1TOJ
       :A(Z)=(1-.1)*100*((Z-J)[2/(1-J)[2)
       :NEXT
1020 FORX=ZTOIM
       :A(X)=0
       :NEXT
1030 FORZ=1TO(IM-1)
       :A(1M+Z)=A(IM-Z)
       :NEXT
1035 FORZ=1TOIM
       :FORX=0TO3
       :Q=INT(A(Z)/10)
       :Q1=(A(Z)-Q*10)/10
1040 TAU(Z,X)=PA(Q,X)-(PA(Q,X)-PA(Q+1,X))*Q1
       :NEXTX,Z
1045 FORZ=1TO(IM-1)
       :FORX=0TO3
       :TAU(IM+Z,X)=TAU(IM-Z,X)
       :NEXTX,Z
1050 RETURN
2000 J=IM+K
2010 FORZ=1TOJ
       :A(Z)=(1-.1)*100*((Z-J)[2/(1-J)[2)
       :NEXT
2020 P=0
       :FORZ=(2*IM-K)TOIM
       :A(Z)=A(Z)+A(J-P)
       :P=P+1
       :NEXT
2025 FORZ=1TO(IM-1)
```

```
     :A(IM+Z)=A(IM-Z)
     :NEXT
2035 FORZ=1TOIM
     :FORX=0TO3
     :Q=INT(A(Z)/10)
     :Q1=(A(Z)-Q*10)/10
2040 TAU(Z,X)=PA(Q,X)-(PA(Q,X)-PA(Q+1,X))*Q1
     :NEXTX,Z
2045 FORZ=1TO(IM-1)
     :FORX=0TO3
     :TAU(IM+Z,X)=TAU(IM-Z,X)
     :NEXT
2050 RETURN
2099 REM ROUTINE TO CALCULATE PLANK FUNCTION BT
2100 E=EXP(C2/(WL*TAU(Z,0)))
2110 BT=C1/(WL[5*(E-1))
2199 REM ROUTINE TO CALCULATE PHI FOR A GIVEN VOIGT a
2200 PHI=EXP(SLOPE*LOG(TAU(Z,1))+IN)
2220 RETURN
2999 REM ROUTINE TO LOAD ARRAY WITH WAVELENGTH, SLOPE AND IN
TERCEPT
3000 FI$="PHI"+ID$
3005 OPEN"I",3,FI$
     :INPUT#3,NN
3015 FORQ=1TONN
3020 INPUT#3,VO(Q,0)
     :INPUT#3,VO(Q,1)
     :INPUT#3,VO(Q,2)
     :INPUT#3,CC
     :NEXT
3025 CLOSE
     :RETURN
4000 CLS
     :PRINT"SELECT THE METAL FROM THE LIST BELOW:"
4005 PRINT
     :PRINT"    1 - SODIUM"
4010 PRINT"    2 - POTASSIUM"
4015 PRINT"    3 - LITHIUM"
4020 PRINT"    4 - RUBIDIUM"
4025 PRINT"    5 - CESIUM"
4030 PRINT
     :PRINT"ENTER THE NUMBER OF YOUR CHOICE";
4035 A$=INKEY$
     :IFVAL(A$)<1ORVAL(A$)>5THEN4035ELSEIFA$=""THEN4035
4040 ID=VAL(A$)
4042 PRINT
     :PRINT"ENTER ATMOSPHERIC PRESSURE IN TORR";
     :INPUTPR
```

```
4045 ONIDGOTO4100,4200,4300,4400,4500
4100 ID$="NA"
     :OS=.936
     :OS(1)=.312
     :OS(2)=.624
     :MW=22.9898
4105 XL(1)=5895.92
     :XL(2)=5889.95
     :XLAM=5892.94
4110 TF=1800
4120 GOSUB5000
4130 RETURN
4200 ID$="K"
     :OS=1.021
     :OS(1)=.339
     :OS(2)=.682
     :MW=39.100
4205 XL(1)=7699.0
     :XL(2)=7664.9
     :XLAM=7681.95
4210 TF=1800
4215 GOSUB5000
4220 RETURN
4300 ID$="LI"
     :OS=.753
     :OS(1)=.251
     :OS(2)=.502
     :MW=6.939
4305 XL(1)=6707.912
     :XL(2)=6707.761
     :XLAM=6707.837
4310 TF=1900
4320 GOSUB5000
4330 RETURN
4400 ID$="RB"
     :OS=.997
     :OS(1)=.322
     :OS(2)=.675
     :MW=85.48
4405 XL(1)=7947.6
     :XL(2)=7800.3
     :XLAM=7873.95
4410 TF=1800
4415 GOSUB6000
4420 RETURN
4500 ID$="CS"
     :OS=1.09
     :OS(1)=.362
```

```
     :OS(2)=.732
     :MW=132.91
4505 XL(1)=8521.1
     :XL(2)=8943.5
     :XLAM=8732.3
4510 TF=1800
4520 GOSUB7000
     :RETURN
5000 CLS
     :PRINT"SELECT A FORMULATION FROM THE MENU BELOW:"
5002 J$=ID$+"NO3"
     :PRINT
5005 PRINT"   1 - 40% MG   55% ";J$;" 5% BINDER"
5010 PRINT"   2 - 50% MG   45% ";J$;" 5% BINDER"
5015 PRINT"   3 - 60% MG   35% ";J$;" 5% BINDER"
5017 PRINT"   4 - SPECIAL CASE"
5020 PRINT
     :PRINT"ENTER THE NUMBER BY YOUR CHOICE";
5025 CN$=INKEY$
     :IFVAL(CN$)<1OR VAL(CN$)>4THEN5025ELSEIFCN$=""THEN5025
5030 IFVAL(CN$)=4THEN5050ELSE5100
5050 LINEINPUT"ENTER THE SPECIAL MIX IDENTIFIER FOR THE VOIG
T FUNCTION";NF$
5060 GOTO5105
5100 NF$="VOIGT"+ID$+CN$
5105 OPEN"I",1,NF$
5110 FORX=0TO9
     :FORY=0TO3
     :INPUT#1,PA(X,Y)
     :NEXTY,X
5111 TB=0
     :   X=0TO9
     : IFPA(X,0)>TFTHENTB=PA(X,0)
     :NEXTXELSENEXTX
5115 FORX=0TO9
     :V=PA(X,2)*.08205*PA(X,0)*1000
5120 PA(X,2)=(PR/760)*PA(X,2)*NA/V
5121 PA(X,3)=(PR/760)*PA(X,3)*NA/V
5122 NEXTX
5123 FORX=0TO9
     :PA(X,1)=PA(X,1)*(PR/760)
5124 NEXTX
5125 FORX=0TO9
     :IFPA(X,0)<TFTHENY=X
     :X=10
5126 NEXTX
5130 X=Y-1
     :F=1-0.10*(Y-(TF-PA(Y,0))/(PA(X,0)-PA(Y,0)))
```

```
5200 CLOSE
     :RETURN
6000 CLS
     :PRINT"SELECT A FORMULATION FROM THE MENU BELOW:"
6002 J$=ID$+"NO3"
     :PRINT
6005 PRINT"   1 - 35% MG   60% ";J$;" 5% BINDER"
6010 PRINT"   2 - 45% MG   50% ";J$;" 5% BINDER"
6015 PRINT"   3 - 55% MG   40% ";J$;" 5% BINDER"
6017 PRINT"   4 - SPECIAL CASE"
6020 PRINT
     :PRINT"ENTER THE NUMBER BY YOUR CHOICE";
6025 CN$=INKEY$
     :IFVAL(CN$)<1ORVAL(CN$)>4THEN6025ELSEIFCN$=""THEN6025
6030 IFVAL(CN$)=4THEN6050ELSE6100
6050 LINEINPUT"ENTER THE SPECIAL MIX IDENTIFIER FOR THE VOIG
T FUNCTION";NF$
6060 GOTO6105
6100 NF$="VOIGT"+ID$+CN$
6105 OPEN"I",1,NF$
6110 FORX=0TO9
     :FORY=0TO3
     :INPUT#1,PA(X,Y)
     :NEXTY,X
6111 TB=0
     :FORX=0TO9
     :IFPA(X,0)>TBTHENTB=PA(X,0)
     :NEXTXELSENEXTX
6115 FORX=0TO9
     :V=PA(X,2)*.08205*PA(X,0)*1000
6120 PA(X,2)=(PR/760)*PA(X,2)*NA/V
6121 PA(X,3)=(PR/760)*PA(X,3)*NA/V
6122 NEXTX
6123 FORX=0TO9
     :PA(X,1)=PA(X,1)*(PR/760)
6124 NEXTX
6125 FORX=0TO9
     :IFPA(X,0)<TFTHENY=X
     :X=10
6126 NEXTX
6130 X=Y-1
     :F=1-0.10*(Y-(TF-PA(Y,0))/(PA(X,0)-PA(Y,0)))
6200 CLOSE
     :RETURN
7000 CLS
     :PRINT"SELECT A FORMULATION FROM THE MENU BELOW:"
7002 J$=ID$+"NO3"
     :PRINT
```

```
7005 PRINT"   1 - 25% MG   70% ";J$;" 5% BINDER"
7010 PRINT"   2 - 35% MG   60% ";J$;" 5% BINDER"
7015 PRINT"   3 - 45% MG   50% ";J$;" 5% BINDER"
7017 PRINT"   4 - SPECIAL CASE"
7020 PRINT
     :PRINT"ENTER THE NUMBER BY YOUR CHOICE";
7025 CN$=INKEY$
     :IFVAL(CN$)<1ORVAL(CN$)>4THEN7025ELSEIFCN$=""THEN7025
7030 IFVAL(CN$)=4THEN7050ELSE7100
7050 LINEINPUT"ENTER THE SPECIAL MIX IDENTIFIER FOR THE VOIG
T FUNCTION";NF$
7060 GOTO6105
7100 NF$="VOIGT"+ID$+CN$
7105 OPEN"I",1,NF$
7110 FORX=0TO9
     :FORY=0TO3
     :INPUT#1,PA(X,Y)
     :NEXTY,X
7111 TB=0
     :FORX=0TO9
     :IFPA(X,0)>TBTHENTB=PA(X,0)
     :NEXTXELSENEXTX
7115 FORX=0TO9
     :V=PA(X,2)*.08205*PA(X,0)*1000
7120 PA(X,2)=(PR/760)*PA(X,2)*NA/V
7121 PA(X,3)=(PR/760)*PA(X,3)*NA/V
7122 NEXTX
7123 FORX=0TO9
     :PA(X,1)=PA(X,1)*(PR/760)
7124 NEXTX
7125 FORX=0TO9
     :IFPA(X,0)<TFTHENY=X
     :X=10
7126 NEXTX
7130 X=Y-1
     :F=1-0.10*(Y-(TF-PA(Y,0))/(PA(X,0)-PA(Y,0)))
7200 CLOSE
     :RETURN
```

```
10 REM:PROGRAM TO CALCULATE VOIGT PARAMETERS FROM EQUILIBRIUM
 CONSTANTS
20 CLS
     :DIMVO(9,14),N$(14),N(14),SI(13),Q1(13),M(13)
30 PI=3.1416
     :NA=6.024E23
     :K=1.3804E-16
     :C=2.99793E18
40 K1=3.13786E-08
     :K2=7.15844E-07
     :K3=5.66584E+06
50 FORY=0TO14
     :READN$(Y)
     :NEXT
60 DATA "TEMP","VOIGT A","TOTAL GAS","METAL","AR","CO","CO2",
"H","H2","H2O","MG","N2","O2","OTHER","SOLIDS"
70 FORY=4TO13
     :READN(Y),SIGMA(Y)
     :NEXT
80 DATA 39.94,1E-16,28.01,41E-16,44.01,50E-16,1.008,1E-16,2.0
16,8E-16
90 DATA 18.016,2.2E-16,24.32,1E-16,28.02,21E-16,32.00,34E-16,
30,10E-16
100 CLS
     :INPUT"ENTER THE CHEMICAL SYMBOL OF THE METAL";CS$
110 IFCS$="NA"THENX=1ELSEIFCS$="K"THENX=2ELSEIFCS$="LI"THENX=
3ELSEIFCS$="RB"THENX=4ELSEIFCS$="CS"THENX=5ELSEGOTO
100
120 ONXGOSUB1000,1010,1020,1030,1040
130 N(3)=MW
140 FORY=4TO13
     :Q1(Y)=SIGMA(Y)*SQR(1/N(3)+1/N(Y))/MU
     :PRINTN$(Y),Q1(Y)
     :NEXT
150 FORX=1TO2000
     :NEXTX
160 CLS
     :FORX=0TO9
     :FORY=3TO12
170 PRINT@64,"THE VALUES ARE TO BE ENTERED FOR ";X*10;"% AIR"

180 POKE16916,3
190 PRINT@256,"ENTER THE VALUE FOR ";N$(Y);
200 INPUTVO(X,Y)
     :CLS
     :NEXTY
210 CLS
     :INPUT"ENTER THE VALUE FOR SOLIDS";VO(X,14)
220 CLS
```

```
    :INPUT"ENTER THE COMBUSTION TEMPERATURE";VO(X,0)
232 SIGMA(0)=SIGMA(3)*VO(X,0)/2000
240 FORQ=3TO12
    :VO(X,2)=VO(X,2)+VO(X,Q)
    :NEXTQ
    :CLS
250 VO(X,13)=1-VO(X,2)-VO(X,14)
260 VO(X,2)=1-VO(X,14)
270 CLS
    :INPUT"ENTER THE TOTAL MOLES/KG OF ANY SPECIE";TS
280 PRINT
    :INPUT"ENTER THE TOTAL MOLE FRACTIONS OF THAT SPECIE";TF
290 TM=TS/TF
    :M=1000/TM
300 POKE16916,0
    :CLS
310 REM ENTER THE ROUTINES TO CALCULATE THE VARIOUS BROADENIN
G PARAMETERS
320 MU=(M*MW)/(M+MW)
330 LN=XLAM[2*A2/(2*PI*C)
340 LL=(XLAMBDA[2*SIGMA(0)/C)*(8*K*NA*VO(X,0)/PI/MU)[.5*(NA*(
VO(X,2)-VO(X,3))/VO(X,2)/82.05/VO(X,0))
350 LR=K1*F*XLAMBDA[3*VO(X,3)/VO(X,2)/VO(X,0)
360 LD=K2*XLAMBDA*(VO(X,0)/MW)[.5
370 SUM=0
    :FORY=4TO13
    :SUM=SUM+VO(X,Y)*Q1(Y)*VO(X,0)/2000
    :NEXTY
380 LQ=K3*XLAMBDA[2/(VO(X,0)[.5)/VO(X,2)*SUM
390 VO(X,1)=SQR(LOG(2))*(LN+LL+LR+LQ)/LD
400 PRINT"VOIGT a = ";VO(X,1)
    :FORJ=1TO2000
    :NEXTJ
405 LPRINT"% AIR FOR ";CS$;" = ";X*10
    :LPRINTVO(X,0);LN;LL;LR;LQ;LD;VO(X,1)
410 NEXTX
420 REM SAVE THE CALCULATED PARAMETERS AS A FILE 'VOIGT'+CHEM
ICAL SYMBOL FOR METAL SPECIE
430 REM FILE TO CONTAIN THE TEMPERATURE,VOIGT a,TOTAL NO. OF
MOLES AND MOLES OF METAL.
440 CLS
    :PRINT
    :PRINT
    :PRINT"ENTER THE NUMBER IDENTIFIER FOR THE CASE"
450 J$=CS$+"NO3"
460 PRINT
    :PRINT"  1 - 40% MG  55% ";J$;" 5% BINDER"
470 PRINT"  2 - 50% MG  45% ";J$;" 5% BINDER"
```

```
480 PRINT"  3 - 60% MG  35% ";J$;" 5% BINDER"
485 PRINT"  4 - SPECIAL CASE"
490 PRINT
    :PRINT"ENTER THE NUMBER BY THE CASE IN PROGRESS";
500 A$=INKEY$
    :IFVAL(A$)<1ORVAL(A$)>4THEN500ELSEIFA$=""THEN500
502 IFVAL(A$)=4THENLINEINPUT"ENTER THE SPECIAL CASE IDENTIFIE
R";ID$
    :GOTO520
510 ID$="VOIGT"+CS$+A$+":1"
520 OPEN"O",1,ID$
530 FORX=0TO9
    :FORY=0TO3
    :PRINT#1,VO(X,Y)
    :NEXTY,X
540 CLOSE
600 GOTO100
1000 MW=22.9898
    :XL=5892.95
    :SIGMA(3)=60E-16
    :MU=1
    :F=.982
    :A21=.65E8
    :RETURN
1010 MW=39.10
    :XL=7681.95
    :SIGMA(3)=60E-16
    :MU=1.7
    :F=1.021
    :A21=.39E8
    :RETURN
1020 MW=6.939
    :XL=6707.837
    :SIGMA(3)=45E-16
    :MU=.302
    :F=.753
    :A21=.37E8
    :RETURN
1030 MW=85.48
    :XL=7873.95
    :SIGMA(3)=75E-16
    :MU=3.718
    :F=.997
    :A21=.36E8
    :RETURN
1040 MW=132.91
    :XL=8732.5
    :SIGMA(3)=90E-16
```

```
5 REM PHISLOPE/BAS
10 CLEAR100
     :DIM L1(5,1),WL(75),SL(75),IN(75),CC(75)
     :DEFINTA,N,Q
     :N=1
     :ONERRORGOTO5000
100 CLS
     :PRINT"LINEAR REGRESSION - 2 VARIABLES"
102 INPUT"ENTER THE CHEMICAL SYMBOL OF THE METAL";ID$
103 LPRINT"VOIGT FUNCTION SLOPES AND INTERCEPTS FOR ";ID$
104 LPRINT" "
     :LPRINT"WAVELENGTH";TAB(15)"SLOPE";TAB(30)"INTERCEPT";TA
B(45)"CORR. COEFF."
110 P$="###.##"
120 PRINT
     :PRINT"ENTER - INDEPENDENT VARIABLE FIRST."
125 FORX=1TO5
     :PRINT"ENTER POINT NO.";X;"  ";
     :INPUTL1(X,0)
126 NEXT
130 QQ=QQ+1
     :INPUT"ENTER THE WAVELENGTH";WL(QQ)
135 FORY=1TO5
     :PRINT"ENTER VOIGT VALUE NO. ";Y;"  ";
     :INPUTL1(Y,1)
140 NEXT
145 N=5
     :GOSUB 150
     :GOTO 190
150 CLS
155 G=0
     :FOR A=1 TO N
160 F=A-2*INT((A-1)/2)
165 PRINTTAB(25*(F-1))A;"-";L1(A,0);",";L1(A,1);
170 IF F>=2 THEN PRINT
175 IF A>=30+G*30 THEN INPUT"PRESS ENTER TO CONTINUE LIST-";
A$
     :G=G+1
180 NEXT A
     :IF A/2=INT(A/2) THEN PRINT
185 RETURN
190 INPUT"DO YOU WANT TO CHANGE, DELETE, OR ADD DATA (Y/N)";
A$
195 IF A$="Y" THEN 500
200 C=2
     :GOTO230
205 PRINT
     :PRINT"DATA CAN BE ANALYZED AS ONE OF THE FOLLOWING:"
210 PRINTTAB(25)"1. LINEAR - LINEAR"
```

```
215 PRINTTAB(25)"2. LOG - LOG"
220 PRINTTAB(25)"3. LOG - LINEAR"
225 PRINT
     :INPUT"ENTER THE NUMBER BY THE DESIRED CHOICE";C
230 ONCGOTO 250 , 235 , 245
235 FORQ=1TON
     :L=LOG(L1(Q,0))
     :L1(Q,0)=L
     :L=LOG(L1(Q,1))
     :L1(Q,1)=L
240 NEXTQ
     :GOTO 250
245 FORQ=1TON
     :L=LOG(L1(Q,0))
     :L1(Q,0)=L
     :NEXTQ
     :GOTO 250
250 FOR A=1 TO N
     :X1=X1+L1(A,0)
     :Y1=Y1+L1(A,1)
     :X2=X2+L1(A,0)*L1(A,0)
     :Y2=Y2+L1(A,1)*L1(A,1)
     :Z=Z+L1(A,0)*L1(A,1)
     :NEXT A
255 X3=X1/N
     :Y3=Y1/N
     :S1=X2-X1*X3
     :S2=Y2-Y1*Y3
     :S=Z-X1*Y3
260 B=S/S1
     :B1=Y3-B*X3
     :S3=S2-B*S
265 IF N>2 THEN S4=S3/(N-2)
270 PRINT"NUMBER = ";N
275 PRINT "MEAN OF X = ";X3," OF Y = ";Y3
280 PRINT"SLOPE = ";B,"Y - INTERCEPT = ";B1
285 PRINT
     :PRINT"SUM OF SQUARES","TOTAL";Y2
290 PRINT"MEAN = ";Y3*Y1;"     SLOPE = ";B*S
295 PRINT"RESIDUAL = ";S3
300 PRINT
     :PRINT"STANDARD DEVIATIONS"
305 PRINT"X= ";SQR(S1/(N-1)),"Y = ";SQR(S2/(N-1))
310 IF S4<0 THEN PRINT
     :PRINT
     :GOTO 325
315 PRINT"ERROR = ";SQR(S4),"Y-BAR = ";SQR(S4/N)
320 PRINT"SLOPE = ";SQR(S4/S1),"Y-INTER. = ";SQR(S4*(1/N+X3*
```

```
X3/S1))
325 PRINT
    :IF S4<>0 THENPRINT"F-RATIO FOR SLOPE = ";B*S/S4
330 PRINT"CORR. COEFF. = ";S/SQR(S1*S2)
335 X1=0
    :Y1=0
    :X2=0
    :Y2=0
    :Z=0
338 INPUT"  PRESS ENTER TO CONT.-";A$
340 LPRINTWL(QQ);TAB(15)B;TAB(30)B1;TAB(45)S/SQR(S1*S2)
342 SL(QQ)=B
    :IN(QQ)=B1
    :CC(QQ)=S/SQR(S1*S2)
344 GOTO480
355 CLS
    :PRINT@475,"WORKING"
    :MX(1,1)=0
    :MX(1,0)=0
360 MN(1,1)=L1(1,1)
    :MN(1,0)=L1(1,0)
    :FOR A=1 TO N
    :IF L1(A,0)<MN(1,0) THEN MN(1,0)=L1(A,0)
365 IF L1(A,1)<MN(1,1) THEN MN(1,1)=L1(A,1)
370 NEXTA
375 FOR A=1 TO N
    :IF L1(A,0)>MX(1,0) THEN MX(1,0)=L1(A,0)
380 IF L1(A,1)>MX(1,1) THEN MX(1,1)=L1(A,1)
385 NEXTA
390 H1=40/(MN(1,1)-MX(1,1))
    :J1=-MX(1,1)*H1
395 H2=100/(MX(1,0)-MN(1,0))
    :J2=27-MN(1,0)*H2
400 CLS
    :FOR A=0 TO 40
    :SET(26,A)
    :NEXTA
    :FOR A=0 TO 30 STEP 10
    :SET(27,A)
    :NEXT A
405 FOR A=26 TO 127
    :SET(A,41)
    :NEXTA
    :FOR A=51 TO 126 STEP 25
    :SET(A,40)
    :NEXT A
410 IFC=1THENPRINT@448,"Y";
    :PRINT@930,"X";
```

```
415 IFC=2THENPRINT@448,"LOG Y";
    :PRINT@930,"LOG X";
420 IFC=3THENPRINT@448,"Y";
    :PRINT@930,"LOG X";
425 FOR A=1 TO N
    :SET(L1(A,0)*H2+J2,L1(A,1)*H1+J1)
    :NEXTA
430 PRINT@837,"";
    :PRINT USING P$;MN(1,1);
    :PRINT@5,"";
    :PRINT USING P$;MX(1,1);
435 PRINT@908,"";
    :PRINT USING P$;MN(1,0);
    :PRINT@954,"";
    :PRINT USING P$;MX(1,0);
440 FOR A=27 TO 125
    :E=(((A-J2)/H2)*B+B1)*H1+J1
445 IF E<0 THEN 455
450 SET(A,E)
455 NEXT A
460 PRINT@960,"SLOPE=";B;"INTER.=";B1;"CORR. COEFF.";S/SQR(S
1*S2)
465 INPUT"  PRESS ENTER TO CONT.-";A$
470 K=0
    :W=31+G*30
    :G=G+1
    :RETURN
475 GOSUB 605
    :FORQ=1TON
    :L=L1(Q,0)
    :L1(Q,0)=L1(Q,1)
    :L1(Q,1)=L
    :NEXTQ
    :GOSUB 150
    :GOTO 190
480 ONCGOTO 500 , 485 , 495
485 FORQ=1TON
    :L=EXP(L1(Q,0))
    :L1(Q,0)=L
    :L=EXP(L1(Q,1))
    :L1(Q,1)=L
490 NEXTQ
    :GOTO 500
495 FORQ=1TON
    :L=EXP(L1(Q,0))
    :L1(Q,0)=L
    :NEXTQ
    :GOTO 500
```

```
500 PRINT"ENTER A COMMAND TO ADD - DELETE - CHANGE - SWAP -
RERUN - END"
505 INPUT"COMMAND";B$
510 A$=LEFT$(B$,1)
515 IF A$="A" THEN 550
520 IF A$="D" THEN 555
525 IF A$="C" THEN 580
530 IF A$="S" THEN 475
535 IF A$="R"THENGOSUB 605
     :GOTO 205
540 IF A$="E" THEN 100
541 IFA$="Q"THEN130
545 PRINT"ILLEGAL COMMAND; ENTER AGAIN"
     :GOTO 500
550 N=N+1
     :GOSUB 605
     :GOTO 135
555 GOSUB 150
     :PRINT"ENTER PAIR NUMBER TO BE DELETED";
     :INPUT D
560 GOSUB 605
565 IF D>N THEN PRINT"PAIR ";D;" NOT FOUND "
     :GOTO 500
570 PRINT"PAIR ";D;" FOUND AND DELETED"
575 FOR A=D TO N
     :L1(A,0)=L1(A+1,0)
     :L1(A,1)=L1(A+1,1)
     :NEXT A
     :N=N-1
     :GOTO 190
580 GOSUB 150
     :INPUT"ENTER THE DATA PAIR NUMBER TO BE CHANGED";D
585 GOSUB 605
590 IF D>N THEN PRINT"PAIR ";D;" NOT FOUND-"
     :GOTO 500
595 PRINT"PAIR ";D;" FOUND - ENTER NEW VALUES FOR BOTH";
     :INPUT X,Y
600 L1(D,0)=X
     :L1(D,1)=Y
     :GOTO 190
605 X1=0
     :X2=0
     :X3=0
     :Y1=0
     :Y2=0
     :Y3=0
     :Z=0
     :S=0
```

```
     :S1=0
     :S2=0
     :S3=0
     :S4=0
     :B=0
     :B1=0
610 RETURN
1000 CLS
     :INPUT"ENTER THE NUMBER OF WAVELENGTHS";NN
1005 OPEN"O",1,"PHI"+ID$+":1"
     :PRINT#1,NN
1010 FORQQ=1TONN
     :PRINT#1,WL(QQ),SL(QQ),IN(QQ),CC(QQ)
     :NEXT
1020 CLOSE1
1030 STOP
2000 OPEN"I",1,"PHI"+ID$+":1"
2010 FORQQ=6TO55
     :INPUT#1,WL(QQ),SL(QQ),IN(QQ),CC(QQ)
     :NEXT
2020 CLOSE1
2030 STOP
5000 PRINT"ERROR NO. ";ERR/2+1;" IN LINE ";ERL
5005 RESUMENEXT
```

Table C- 1
Voigt Function Parameters for Lithium

WAVELENGTH	SLOPE	INTERCEPT	CORR. COEFF.
5850.74	1.000020	-19.5003	1.000010
5950.49	0.999992	-19.2190	0.999980
6050.40	1.000000	-18.9020	1.000040
6100.36	0.999978	-18.7282	1.000040
6200.21	1.000010	-18.3366	1.000100
6300.68	1.000010	-17.8633	0.999948
6400.77	1.000000	-17.2675	0.999989
6450.13	0.999982	-16.9916	1.000020
6500.27	1.000020	-16.4534	1.000010
6525.15	1.000000	-16.1903	1.000040
6550.22	1.000010	-15.9874	0.999996
6575.40	1.000010	-15.[illegible]302	1.000040
6600.95	0.999992	-15.0950	1.000030
6610.79	0.999985	-14.8988	0.999999
6620.66	0.999976	-14.6810	0.999989
6630.57	0.999979	-14.4368	1.000020
6640.50	0.999992	-14.1584	1.000030
6650.47	0.999960	-13.8350	0.999999
6660.46	0.999947	-13.4489	1.000040
6670.48	0.999928	-12.9700	1.000020
6680.54	1.000570	-12.3403	1.000050
6690.62	0.999622	-11.4122	1.000010
6695.69	0.999258	-10.7127	1.000030
6700.73	0.997816	-9.6284	1.000010
6702.25	0.996479	-9.1449	1.000010
6704.28	0.991127	-8.2280	1.000000
6705.81	0.970020	-7.0643	0.999944
6706.82	0.827408	-5.4637	0.997953
6707.83	-.780611	-1.5533	-.998902
6708.34	0.239457	-3.7738	0.996188
6708.85	0.861987	-5.6329	0.998698
6709.36	0.949721	-6.5328	0.999830
6709.86	0.972973	-7.1287	0.999954
6710.88	0.988310	-7.9501	0.999988
6715.45	0.998140	-9.7844	1.000000
6720.04	0.999277	-10.7225	1.000020
6730.24	0.999789	-11.9341	1.000010
6740.48	0.999894	-12.6830	1.000010
6750.74	0.999951	-13.2265	1.000040
6760.01	0.999973	-13.6146	1.000040
6770.33	0.999970	-13.9724	1.000030
6780.69	0.999995	-14.2760	0.999983
6790.04	0.999982	-14.5145	1.000100
6800.46	0.999973	-14.7501	0.999986
6820.34	0.999989	-15.1331	0.999977
6840.34	0.999998	-15.4544	1.000040
6860.45	0.999995	-15.7311	0.999983
6880.69	0.999982	-15.9742	1.000020
6899.97	1.000010	-16.1801	0.999999
6950.82	0.999992	-16.6350	1.000030
7000.22	0.999982	-16.9909	1.000020
7050.33	1.000010	-17.2929	0.999996
7100.02	1.000020	-17.5499	1.000110
7150.42	1.000000	-17.7775	1.000090
7200.37	1.000010	-17.9774	0.999948
7299.98	1.000020	-18.3183	1.000060
7399.91	0.999998	-18.6030	1.000090
7500.09	1.000010	-18.8464	0.999952
7600.40	0.999998	-19.0503	1.000090
7700.75	0.999998	-19.2451	0.999986

Table C- 2
Voigt Function Parameters for Sodium

WAVELENGTH	SLOPE	INTERCEPT	CORR. COEFF.
4920.02	1.002140	-21.3014	0.999994
4950.53	1.000010	-21.2204	1.000000
4999.98	1.000020	-21.0926	0.999937
5025.51	0.999994	-21.0243	1.000020
5075.61	0.999994	-20.8853	0.999983
5100.15	1.000000	-20.8146	1.000100
5199.82	1.000040	-20.5069	1.000063
5300.62	0.999984	-20.1836	1.000010
5400.46	1.000010	-19.7464	1.000000
5500.03	1.000080	-19.2370	1.000070
5600.16	1.000020	-18.6309	1.000040
5700.69	1.000020	-17.7500	1.000010
5750.64	1.000010	-17.1265	1.000070
5800.34	0.999994	-16.2408	1.000020
5819.77	0.999960	-15.7556	1.000010
5840.00	0.999964	-15.0867	1.000050
5850.13	0.999946	-14.6451	1.000030
5860.04	0.999937	-14.0917	1.000060
5870.48	0.999801	-13.2707	1.000030
5880.22	0.999208	-11.9611	0.999996
5882.17	0.998737	-11.5386	0.999997
5884.13	0.997756	-10.9918	0.999987
5886.08	0.994783	-10.2121	1.000020
5888.04	0.977779	-8.8278	0.999934
5889.02	0.903169	-7.3328	0.998843
5889.99	-.829329	-1.9485	-.999608
5890.48	0.738936	-6.1016	0.989796
5891.22	0.950485	-7.9759	0.999715
5892.20	0.985157	-9.0205	0.999974
5893.18	0.990755	-9.3905	1.000010
5894.16	0.978914	-9.0846	0.999958
5895.14	0.873870	-7.6152	0.997987
5895.87	-.833186	-2.6232	-.999642
5896.61	0.826910	-7.3464	0.996145
5897.10	0.942898	-8.4979	0.999617
5898.08	0.984292	-9.6730	0.999964
5899.06	0.992985	-10.3447	1.000000
5900.04	0.996111	-10.8160	1.000010
5902.01	0.998324	-11.4724	1.000000
5904.22	0.999117	-11.9875	0.999996
5908.16	0.999575	-12.6362	0.999982
5909.88	0.999683	-12.8589	1.000020
5920.00	0.999896	-13.8035	1.000030
5940.10	0.999960	-14.8993	1.000000
5960.73	0.999993	-15.6109	1.000020
5980.04	0.999981	-16.1014	1.000040
6000.70	0.999998	-16.5170	1.000020
6049.87	1.000000	-17.2478	0.999956
6099.85	1.000020	-17.7818	1.000080
6199.73	1.000020	-18.5343	1.000010
6300.25	1.000010	-19.0674	0.999997
6399.92	1.000020	-19.4729	1.000080
6499.93	1.000010	-19.8013	1.000080
6600.17	1.000020	-20.0760	0.999974
6700.50	0.999998	-20.3107	1.000130
6749.50	1.000020	-20.4139	1.000120
6800.79	0.999998	-20.5149	0.999988
6849.69	1.000000	-20.6054	0.999992
6900.91	0.999045	-20.6930	0.999993
7000.70	0.999109	-20.8541	0.999947

Table C- 3
Voigt Function Parameters for Potassium

WAVELENGTH	SLOPE	INTERCEPT	CORR. COEFF.
5099.35	0.999987	-23.7072	0.999926
5300.32	1.000010	-23.4675	1.000050
5599.86	1.000000	-23.0880	1.000050
5800.43	1.000000	-22.8144	0.999994
5999.11	1.000020	-22.5231	1.000060
6300.23	1.000000	-22.0272	1.000050
6501.40	1.000020	-21.6500	1.000070
6701.06	1.000010	-21.2169	1.000000
6800.61	1.000010	-20.9710	1.000020
6999.71	0.999979	-20.3975	0.999989
7100.69	1.000010	-20.0450	1.000020
7200.67	1.000020	-19.6353	1.000100
7299.95	1.000020	-19.1368	0.999989
7400.02	1.000010	-18.4870	1.000060
7449.42	0.999998	-18.0751	0.999970
7500.62	1.000010	-17.5409	1.000090
7525.35	0.999980	-17.2229	1.000040
7550.25	1.000020	-16.8431	1.000030
7575.31	0.999967	-16.3701	0.999980
7600.54	0.999950	-15.7412	1.000040
7615.53	0.999912	-15.2394	0.999999
7630.57	0.999807	-14.5506	1.000030
7639.86	0.999645	-13.9489	1.000020
7650.34	0.998860	-12.8998	1.000010
7655.01	0.997547	-12.1367	0.999997
7659.68	0.990517	-10.8234	0.999996
7662.02	0.970105	-9.5566	0.999791
7663.19	0.866638	-8.1746	0.997609
7664.36	-.858621	-2.3687	-.999485
7665.53	-.823367	-2.5666	-.998868
7666.70	0.873049	-8.2819	0.997852
7667.87	0.965560	-9.6032	0.999839
7670.21	0.990869	-10.8661	0.999983
7674.90	0.997675	-12.0985	0.999992
7680.77	0.999093	-12.7883	1.000020
7683.12	0.999160	-12.8791	0.999990
7689.01	0.998013	-12.5721	0.999986
7692.54	0.994344	-11.8699	1.000020
7696.08	0.964627	-10.2384	0.999843
7697.26	0.868071	-8.8875	0.997629
7698.44	-.853384	-3.0957	-.999400
7699.62	-.830306	-3.2257	-.999001
7700.80	0.872111	-8.9582	0.997811
7701.98	0.965541	-10.2843	0.999860
7704.34	0.990984	-11.5401	0.999992
7710.26	0.998227	-12.9864	1.000030
7715.00	0.999174	-13.6230	0.999985
7719.75	0.999522	-14.0772	0.999989
7730.44	0.999817	-14.7808	1.000080
7739.98	0.999893	-15.2200	0.999980
7750.73	0.999931	-15.6049	1.000080
7760.32	0.999960	-15.8866	1.000030
7769.92	0.999941	-16.1292	0.999989
7779.56	0.999958	-16.3429	1.000040
7790.42	0.999979	-16.5569	1.000030
7800.10	0.999969	-16.7283	1.000020
7819.54	1.000020	-17.0305	0.999989
7840.30	0.999893	-17.3062	0.999980
7859.94	0.999998	-17.5343	1.000010
7879.68	1.000010	-17.7383	1.000020
7899.51	0.999998	-17.9229	0.999970
7949.54	0.999979	-18.3204	0.999951
8000.22	1.000030	-18.6513	1.000040
8099.59	1.000030	-19.1650	1.000070
8200.13	1.000010	-19.5681	1.000020
8300.45	1.000010	-19.8950	1.000020
8400.45	1.011130	-20.1946	1.000010
8500.00	1.000010	-20.4032	1.000020
8603.42	1.000010	-20.6158	1.000030
8799.45	1.000000	-20.9547	0.999967
8999.23	1.000020	-21.2374	1.000040
9202.68	1.000010	-21.4789	0.999974
9403.77	0.999988	-21.6832	1.000010
9601.60	0.999995	-21.8585	0.999960
9801.54	1.000010	-22.0149	1.000050

Table C- 4
Voigt Function Parameters for Rubidium

WAVELENGTH	SLOPE	INTERCEPT	CORR. COEFF.
5899.79	1.000010	-23.6497	1.000060
6000.60	1.000020	-23.5004	0.999960
6199.43	1.000020	-23.2966	1.000070
6399.31	1.000030	-22.0833	1.000080
6601.04	1.000020	-22.5173	1.000070
6799.65	1.000000	-22.1970	1.000020
6999.83	1.000010	-21.6222	1.000030
7099.98	0.999995	-21.3377	1.000040
7150.25	1.000060	-21.1482	1.000070
7200.32	1.000000	-21.0145	1.000004
7300.50	1.000020	-20.6396	0.999980
7400.63	1.000000	-20.1894	1.000020
7500.58	1.000000	-19.6204	0.999994
7550.45	0.999993	-19.2651	1.000040
7600.23	0.999986	-18.8342	1.000010
7625.37	0.999988	-18.5748	1.000010
7650.67	0.999995	-18.2733	1.000010
7675.37	0.999995	-17.9250	1.000070
7700.23	0.999995	-17.4957	1.000010
7725.25	0.999968	-16.9361	0.999987
7750.43	0.999927	-16.1343	1.000000
7760.70	0.999900	-15.6782	0.999987
7770.22	0.999833	-15.1322	1.000010
7780.54	0.999596	-14.2912	1.000030
7790.10	0.998349	-12.9559	1.000020
7796.49	0.986903	-10.9082	0.999985
7797.29	0.977697	-10.3868	0.999943
7798.09	0.952881	-9.6025	0.999709
7798.89	0.837686	-8.3454	0.996294
7799.69	-.729243	-2.8967	-.995991
7800.48	-.879289	-2.1671	-.999712
7801.29	0.807663	-7.9718	0.994377
7802.09	0.944953	-9.4322	0.999582
7805.29	0.993337	-11.5670	1.000010
7820.53	0.999509	-14.3432	1.000010
7850.39	0.999927	-16.0325	1.000010
7875.58	0.999955	-16.5303	1.000000
7900.11	0.999934	-16.3601	0.999994
7920.67	0.999779	-15.4990	1.000030
7940.51	0.996345	-12.9016	0.999980
7944.66	0.976541	-11.0690	0.999949
7945.48	0.950002	-10.3150	0.999667
7946.32	0.825088	-8.9399	0.995550
7947.15	-.795601	-3.3338	-.998242
7947.97	-.840975	-3.1100	-.999209
7948.81	0.816105	-8.8269	0.994977
7949.63	0.947345	-10.2429	0.999622
7955.45	0.997031	-13.1071	1.000000
7960.45	0.998910	-14.0896	1.000010
7970.45	0.999671	-15.2189	1.000000
7980.49	0.999853	-15.9158	1.000030
7990.54	0.999907	-16.4142	1.000010
8000.63	0.999941	-16.7994	0.999987
8010.74	0.999961	-17.1112	1.000010
8020.03	0.999541	-17.3466	0.999950
8030.18	0.999995	-17.5788	1.000040
8040.37	0.999995	-17.7770	0.999987
8050.57	0.999995	-17.9527	1.000070
8075.36	1.000000	-18.3103	1.000050
8100.29	0.999988	-18.6015	1.000030
8150.62	1.000010	-19.0620	1.000080
8200.69	1.000020	-19.4168	1.000090
8299.99	1.000940	-19.9521	1.000100
8350.09	1.000010	-20.1666	1.000050
8400.80	1.000020	-20.3597	1.000070
8450.25	1.000010	-20.5286	1.000000
8500.29	1.000020	-20.6837	1.000030
8600.21	1.000000	-20.9557	0.999940
8699.20	1.000010	-21.1868	1.000050
8799.81	0.999988	-21.3919	1.000010
9001.08	1.000010	-21.7364	1.000000
9200.63	1.000020	-22.0153	1.000040
9401.48	1.000020	-22.2512	1.000120
9599.17	1.000010	-22.4507	1.000000
9801.14	1.000010	-22.6284	1.000000

Table C- 5
Voigt Function Parameters for Cesium

WAVELENGTH	SLOPE	INTERCEPT	CORR. COEFF.
6850.59	1.000000	-23.6451	0.999939
7000.91	0.999779	-23.5345	0.999973
7200.53	1.000010	-23.2336	1.000050
7399.70	1.000020	-22.8985	1.000010
7599.22	1.000020	-22.5139	1.000060
7800.14	1.000020	-22.0525	1.000040
7899.70	1.000020	-21.7823	1.000100
7999.79	0.997582	-21.4693	0.999875
8074.90	1.000010	-20.9628	1.000020
8100.38	1.000020	-20.9030	1.000050
8149.95	1.000010	-20.7625	1.000040
8200.13	0.999995	-20.5759	1.000010
8250.27	0.999995	-20.3236	1.000010
8300.39	0.999995	-19.9619	0.999984
8350.45	0.999995	-19.4991	0.999984
8400.45	0.999974	-18.8586	1.000030
8419.95	0.999985	-18.5260	1.000060
8440.21	0.999980	-18.0980	0.999996
8460.57	0.999948	-17.5347	0.999979
8480.34	0.999911	-16.7561	1.000010
8500.21	0.999588	-15.4259	0.999979
8505.02	0.999313	-14.9021	1.000010
8510.52	0.998218	-14.0597	0.999997
8515.34	0.994583	-12.8324	0.999997
8517.41	0.986357	-11.9191	0.999974
8519.48	0.923459	-10.1076	0.998733
8520.17	0.752444	-8.5977	0.986015
8520.86	-.876647	-2.8563	-.999603
8521.55	-.690673	-3.7027	-.994637
8522.24	0.796687	-9.0388	0.991528
8522.93	0.935091	-10.3636	0.999129
8530.53	0.997975	-13.8278	0.999997
8550.64	0.999779	-16.1002	1.000010
8600.25	0.999983	-17.9611	1.000010
8650.46	0.999995	-18.6833	1.000070
8700.52	0.999998	-18.8914	1.000000
8750.45	1.000000	-18.7445	1.000010
8800.22	0.999985	-18.3012	0.999953
8850.55	0.999780	-17.5008	0.999990
8899.96	0.999999	-16.0018	1.000010
8920.33	0.999578	-14.7386	1.000000
8940.04	0.998667	-10.8738	0.999936
8941.56	0.931388	-9.5710	0.999005
8942.31	0.778985	-8.1716	0.989582
8943.08	-.774160	-2.6396	-.997596
8943.84	-.831450	-2.3748	-.998932
8944.59	0.763583	-8.0163	0.987614
8945.36	0.936450	-9.5071	0.998699
8947.64	0.986759	-11.2499	0.999963
8949.92	0.994634	-12.1528	1.000010
8955.25	0.998414	-13.3719	1.000010
8960.59	0.999255	-14.1216	0.999987
8970.52	0.999705	-15.0361	1.000000
8980.48	0.999837	-15.6600	1.000020
8990.45	0.999936	-16.1341	0.999979
9000.45	0.999937	-16.5164	1.000000
9020.51	0.999958	-17.1111	1.000010
9040.66	0.999969	-17.5666	1.000000
9060.13	0.999980	-17.9223	0.999990
9080.45	0.999985	-18.2334	0.999995
9100.09	0.999990	-18.4913	0.999979
9125.34	0.999990	-18.7772	1.000000
9149.94	1.000020	-19.0183	0.999984
9175.47	0.999980	-19.2382	0.999947
9200.34	1.000000	-19.4292	1.000010
9225.35	1.000000	-19.6023	0.999969
9250.49	0.999995	-19.7607	0.999984
9260.26	0.999990	-19.8105	1.000000
9300.91	1.000000	-20.0404	0.999993
9400.63	1.000010	-20.4869	1.000090
9499.65	1.000010	-20.8371	1.000050
9600.77	0.999981	-21.1315	1.000000
9800.48	1.000010	-21.5914	1.000110
9999.16	1.000010	-21.9456	0.999974
%10199.50	1.000020	-22.2354	1.000060

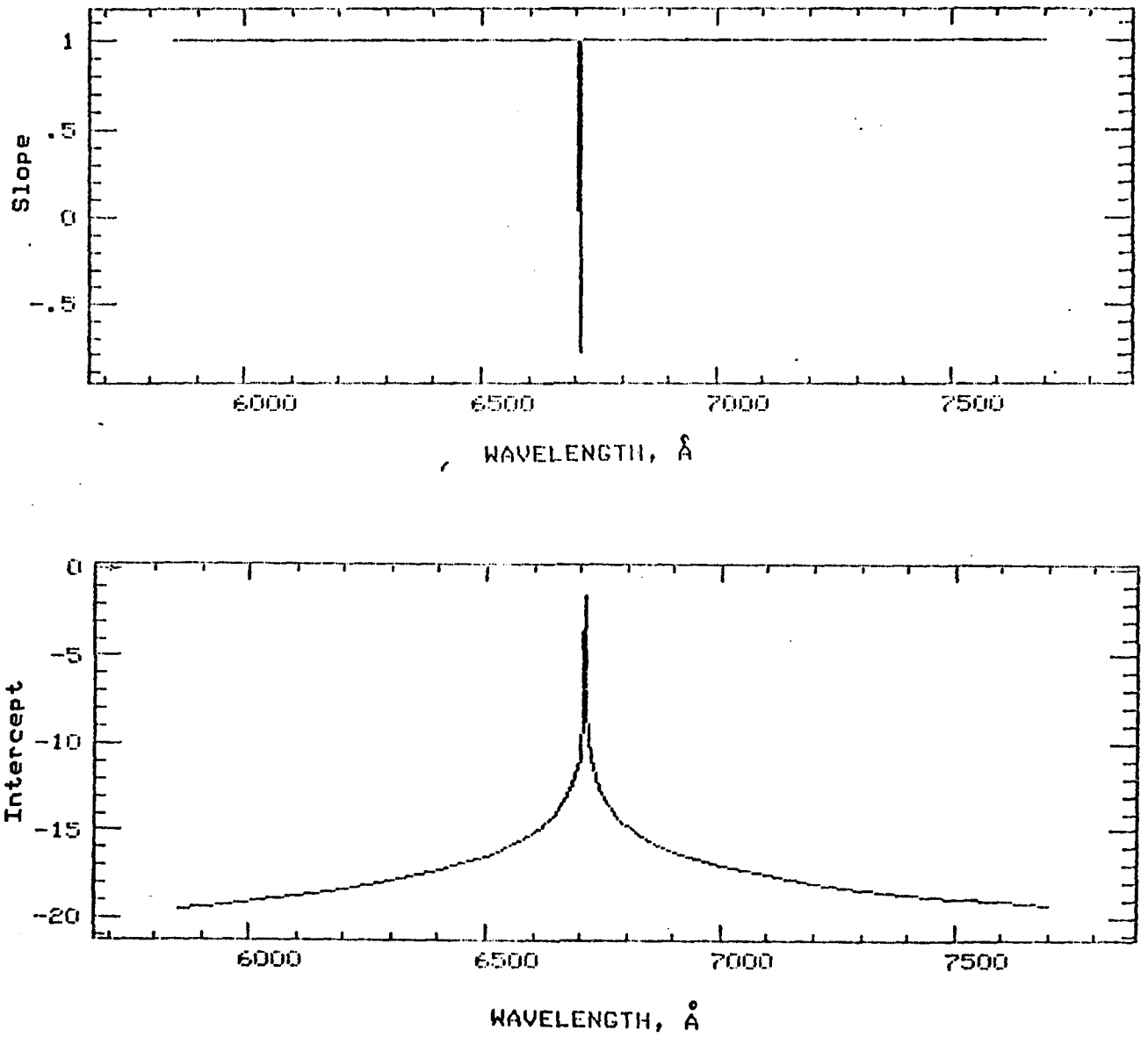

Figure C-1
Slope and Intercept for Lithium Voigt Function

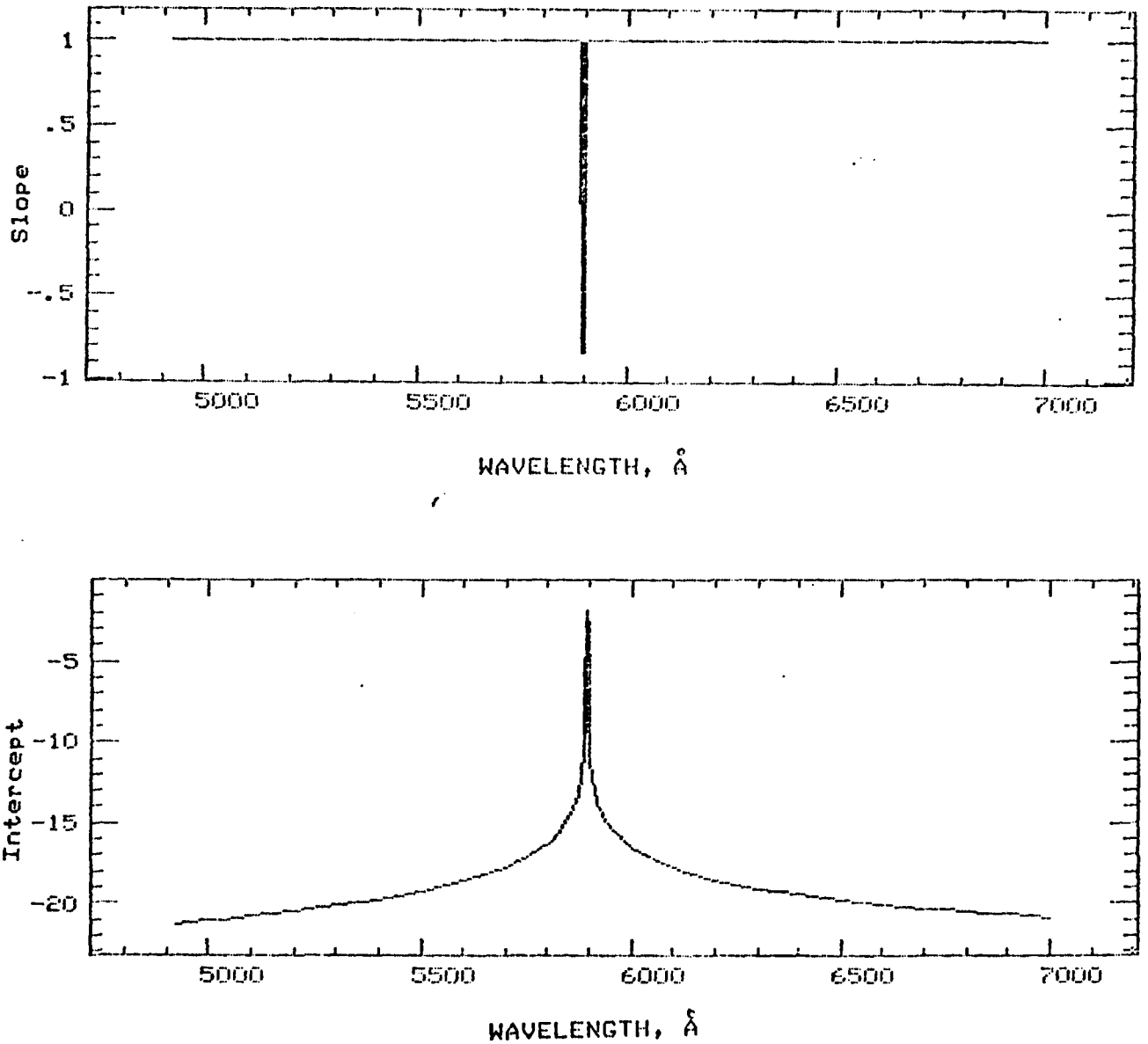

Figure C-2
Slope and Intercept for Sodium Voigt Function

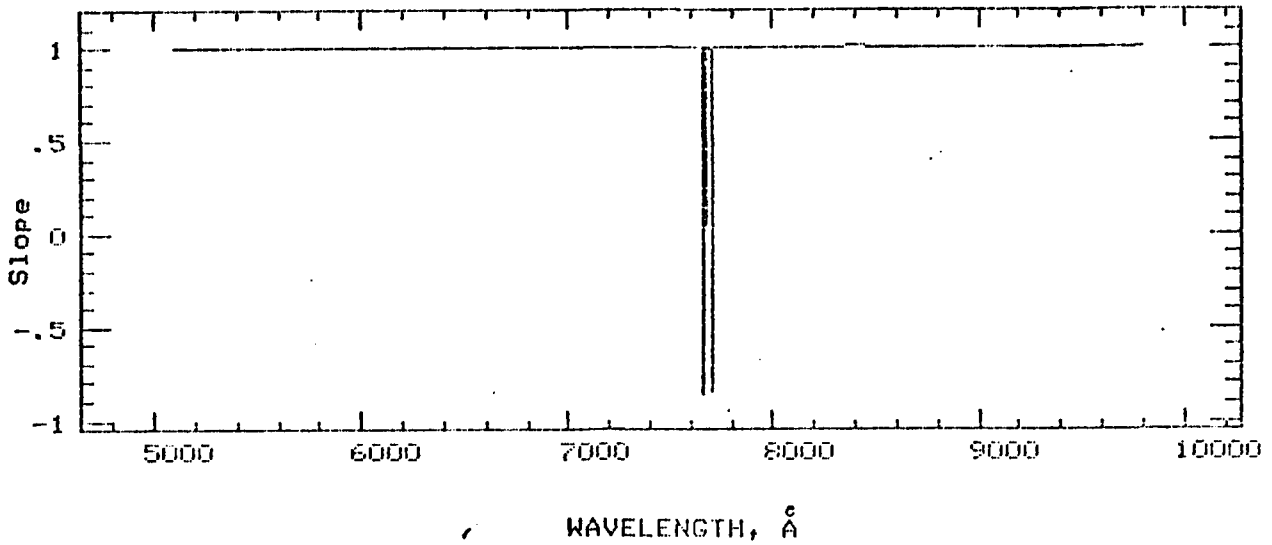

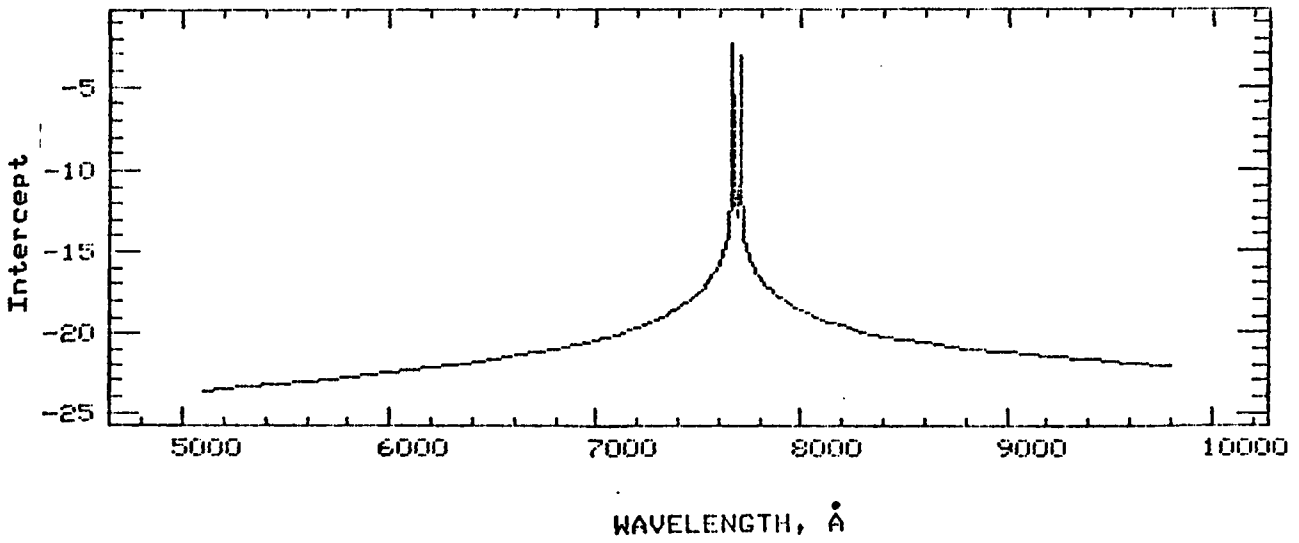

Figure C-3
Slope and Intercept for Potassium Voigt Function

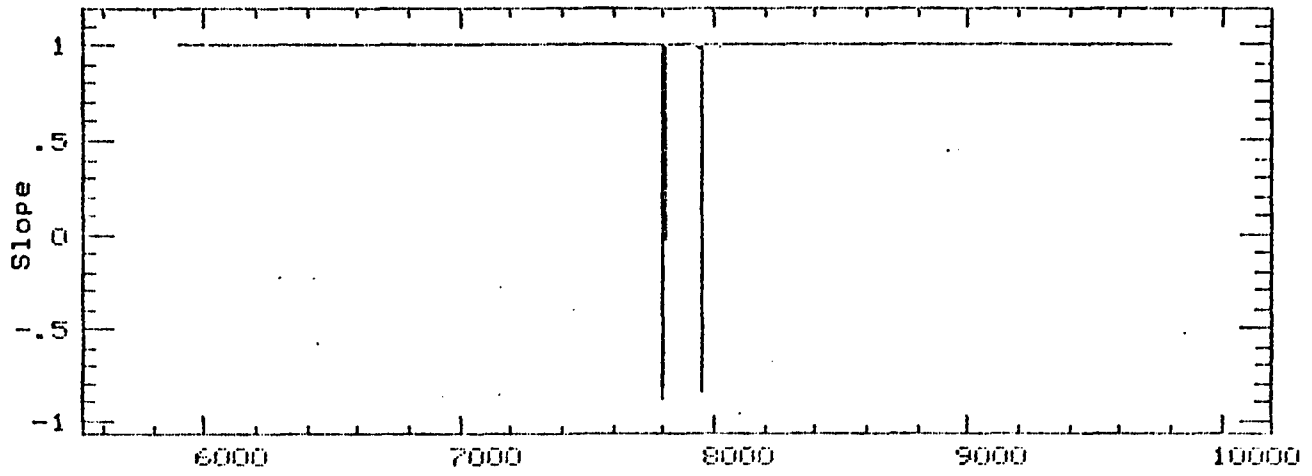

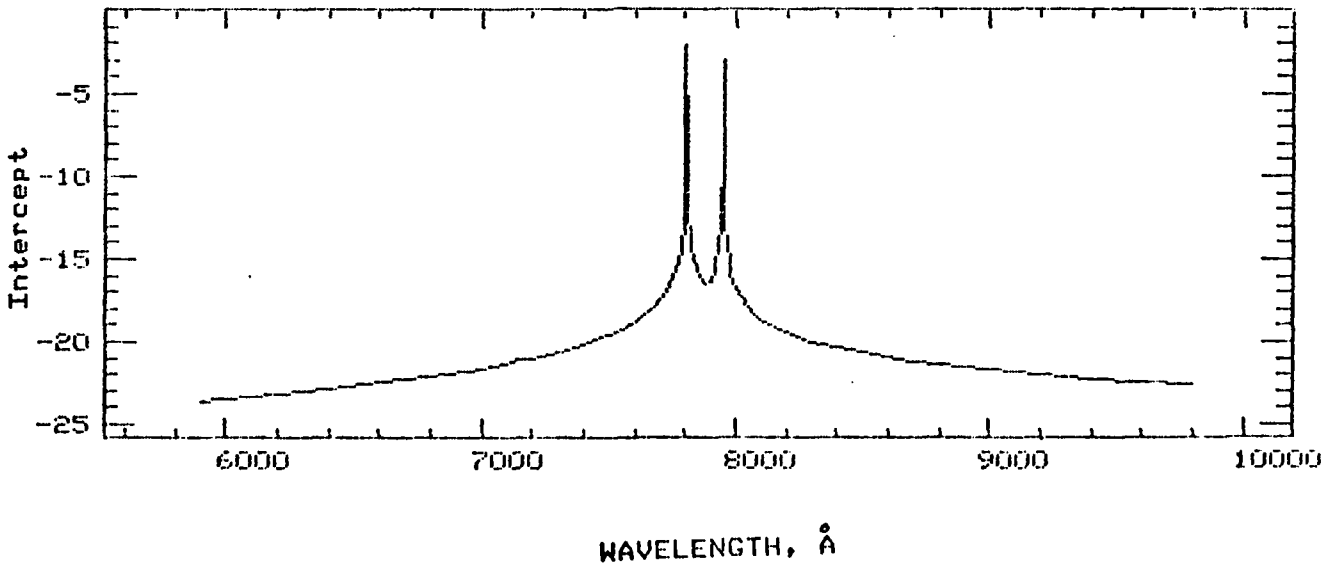

Figure C-4
Slope and Intercept for Rubidium Voigt Function

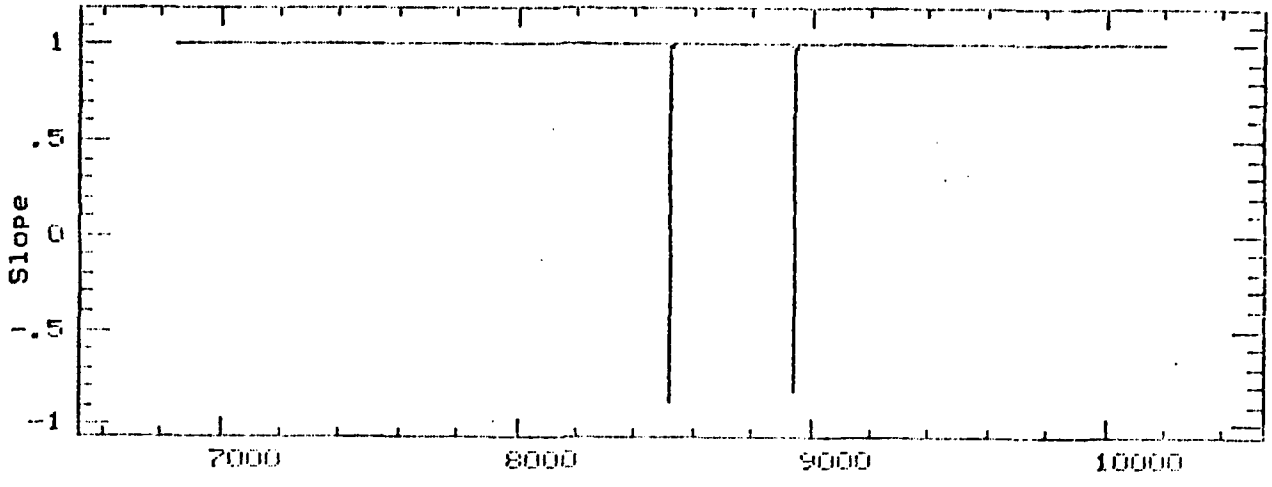

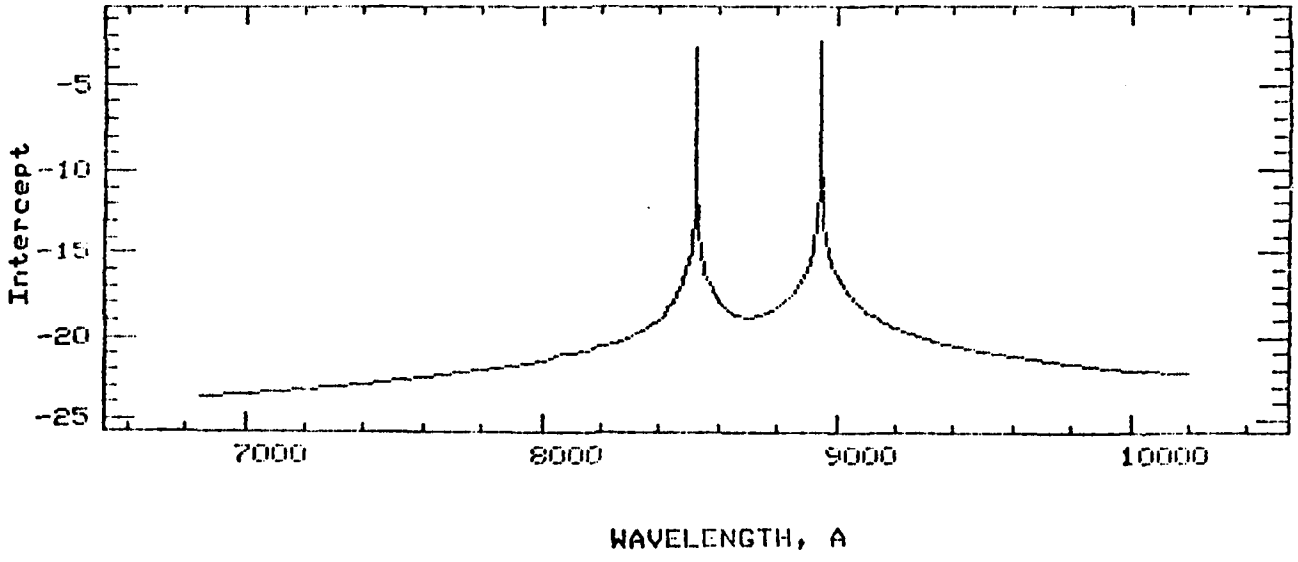

Figure C-5
Slope and Intercept for Cesium Voigt Function